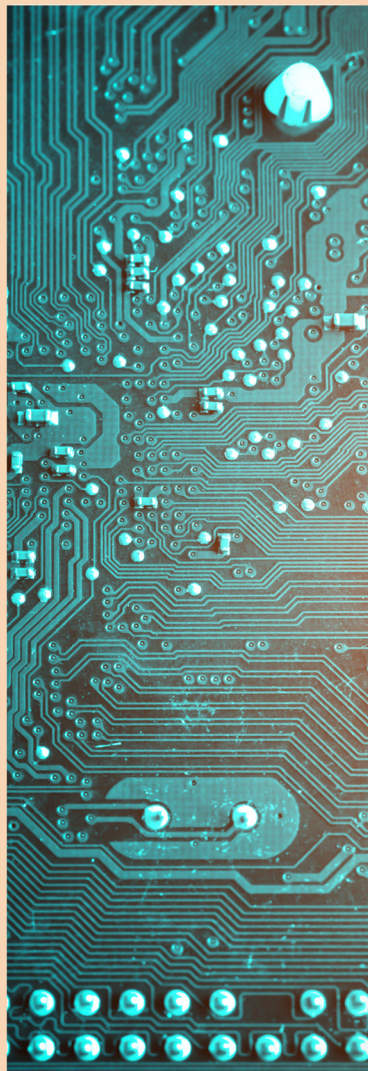




**Technology
Center**

COLLECTIVE MONOGRAPH



INNOVATIVE MATERIALS AND TECHNOLOGIES IN FUNCTIONAL ENGINEERING SYSTEMS

INNOVATIVE MATERIALS AND TECHNOLOGIES IN FUNCTIONAL ENGINEERING SYSTEMS

Collective monograph

UDC 621

164

Published in 2023
by TECHNOLOGY CENTER PC
Shatylova dacha str., 4, Kharkiv, Ukraine, 61165

164

Authors:

Sergiy Luniov, Yuliia Udovyt'ska, Vitalii Kashyts'kyi, Mykola Khvyshchun, Yurii Koval, Sergiy Moroz, Maryna Zhal'dak, Olena Mokrousova, Anna Bondarieva, Nina Merezhko, Taras Karavaiev, Halyna Mykhailova, Valentyna Halushko, Sergiy Kolesnichenko, Kostiantyn Polianskyi, Oleksandr Slipych, Denis Uvarov, Oksana Kliui, Mykola Dron', Andrii Dreus, Ludmila Dubovik, Olena Kositsyna
Innovative materials and technologies in functional engineering systems: collective monograph. — Kharkiv: TECHNOLOGY CENTER PC, 2023. — 145 p.

Collective monograph highlights the results of systematic scientific research devoted to some innovative technological solutions in materials science. The practical application of the results of these studies covers electronic equipment, light industry, construction, and rocketry.

The monograph is intended for researchers dealing with the problems of obtaining materials and applying coatings, as well as improving the properties of materials and structures for various operational applications.

Figures 79, Tables 31, References 143 items.

All rights reserved. No part of this book may be reprinted or reproduced or utilised in any form or by any electronic, mechanical, or other means, now known or hereafter invented, including photocopying and recording, or in any information storage or retrieval system, without permission in writing from the authors. This book contains information obtained from authentic and highly regarded sources. Reasonable efforts have been made to publish reliable data and information, but the author and publisher cannot assume responsibility for the validity of all materials or the consequences of their use. The authors and publishers have attempted to trace the copyright holders of all material reproduced in this publication and apologize to copyright holders if permission to publish in this form has not been obtained. If any copyright material has not been acknowledged please write and let us know so we may rectify in any future reprint.

The publisher, the authors and the editors are safe to assume that the advice and information in this book are believed to be true and accurate at the date of publication. Neither the publisher nor the authors or the editors give a warranty, express or implied, with respect to the material contained herein or for any errors or omissions that may have been made.

Trademark Notice: product or corporate names may be trademarks or registered trademarks, and are used only for identification and explanation without intent to infringe.

DOI: 10.15587/978-617-7319-96-1

ISBN 978-617-7319-96-1 (on-line)

Cite as: *Innovative materials and technologies in functional engineering systems (2023)*. Kharkiv: TECHNOLOGY CENTER PC, 176. doi: <https://doi.org/10.15587/978-617-7319-96-1>



Copyright © 2023 Authors
This is an open access paper under the Creative Commons CC BY license


AUTHORS

CHAPTER 1

SERGIY LUNIOV

Doctor of Physical and Mathematical Sciences, Associate Professor

Department of Physics and Higher Mathematic
Lutsk National Technical University

 ORCID ID: <https://orcid.org/0000-0003-0737-8703>

YULIYA UDovytska

PhD, Teacher of Professional Disciplines


Department of Informatics and Computer Engineering
Volyn Professional College of National University of Food Technologies

 ORCID ID: <https://orcid.org/0000-0003-4707-6363>

VITALII KASHYTSKYI

PhD, Professor

Department of Materials Science
Lutsk National Technical University

 ORCID ID: <https://orcid.org/0000-0003-2346-912X>

MYKOLA KHVYSHCHUN

PhD, Associate Professor


Department of Electronics and Telecommunications
Lutsk National Technical University

 ORCID ID: <https://orcid.org/0000-0002-3918-4527>

YURII KOVAL

PhD, Associate Professor


Department of Physics and Higher Mathematic
Lutsk National Technical University

 ORCID ID: <https://orcid.org/0000-0002-4570-8024>

SERGIY MOROZ

PhD, Associate Professor

Department of Electronics and Telecommunications
Lutsk National Technical University


 ORCID ID: <https://orcid.org/0000-0003-4677-5170>

CHAPTER 2

MARYNA ZHALDAK

PhD, Associate Professor


Department Commodity Science and Customs Affairs
State University of Trade and Economics / Kyiv National University of Trade and Economics

 ORCID ID: <https://orcid.org/0000-0002-4490-8673>

OLENA MOKROUSOVA

Doctor of Technical Sciences, Professor

Department Commodity Science and Customs Affairs
State University of Trade and Economics / Kyiv National University of Trade and Economics

 ORCID ID: <https://orcid.org/0000-0003-1943-8048>

ANNA BONDARIEVA

PhD

Director

Omnichannel LLC "Epicenter K"

 ORCID ID: <https://orcid.org/0000-0002-3241-2726>

NINA MEREZHKO

Doctor of Technical Sciences, Professor, Head of Department

Department Commodity Science and Customs Affairs
State University of Trade and Economics / Kyiv National University of Trade and Economics

 ORCID ID: <https://orcid.org/0000-0003-3077-9636>

TARAS KARAVAIIEV

Doctor of Technical Sciences, Professor

Department Commodity Science and Customs Affairs
State University of Trade and Economics / Kyiv National University of Trade and Economics

 ORCID ID: <https://orcid.org/0000-0003-4429-2474>

HALYNA MYKHAILOVA

Doctor of Technical Sciences, Associate Professor

Department of Commodity Science and Customs Affairs
State University of Trade and Economics / Kyiv National University of Trade and Economics

 ORCID ID: <https://orcid.org/0000-0002-1083-5875>

CHAPTER 3

VALENTYNA HALUSHKO

Doctor of Technical Sciences, Associate Professor

Department of Building Structures, Buildings and Structures
Donbas National Academy of Civil Engineering and Architecture

 ORCID ID: <https://orcid.org/0000-0001-5744-0486>


SERGIY KOLESNICHENKO

Doctor of Technical Sciences, Associate Professor

Department of Building Structures, Buildings and Structures
Donbas National Academy of Civil Engineering and Architecture

 ORCID ID: <https://orcid.org/0000-0001-5087-8354>

KOSTIANTYN POLIANSKYI

PhD, Senior Lecturer
Department of Automobile Roads
Donbas National Academy of Civil Engineering and
Architecture
 ORCID ID: <https://orcid.org/0000-0002-2615-3975>

OLESANDR SLIPYCH

PhD
Director
INDUSTRIAL CONSTRUCTION GROUP LLC
 ORCID ID: <https://orcid.org/0000-0002-3458-007X>


DENIS UVAROV

Graduate Student
Department of Construction Production Technology
Odesa State Academy of Construction and Architecture
 ORCID ID: <https://orcid.org/0000-0002-3591-342X>

OXSANA KLIUI

Graduate Student
Industrial Construction Group
 ORCID ID: <https://orcid.org/0009-0003-2332-2803>


ANDRII DREUS

Doctor of Technical Sciences, Professor, Head of
Department
Department of AeroHydro Mechanics and Energy and
Mass Transfer
Oles Honchar Dnipro National University
 ORCID ID: <https://orcid.org/0000-0003-0598-9287>

LUDMILA DUBOVIK


Senior Researcher
Scientific Research Institute of Power
Oles Honchar Dnipro National University
 ORCID ID: <https://orcid.org/0000-0003-1178-9281>

OLENA KOSITSYNA

PhD, Associate Professor, Head of Department
Department of Analytical Chemistry and Chemical
Technology
Oles Honchar Dnipro National University
 ORCID ID: <https://orcid.org/0000-0003-0857-831X>

CHAPTER 4

MYKOLA DRON'

Doctor of Technical Sciences, Professor
Department of Rocket Space and Innovative Technologies
Oles Honchar Dnipro National University
 ORCID ID: <https://orcid.org/0000-0003-0682-8004>

ABSTRACT

Collective monograph highlights the results of systematic scientific research devoted to some innovative technological solutions in materials science. The practical application of the results of these studies covers electronic equipment, light industry, construction, and rocketry.

Chapter 1 examines the problem of obtaining radiation-protective coatings based on epoxy composites for electronic equipment materials. Dependences of the electron concentration, specific conductivity, and Hall EMF on the induction of external magnetic field for the n-Si and n-Ge single crystals, irradiated by the fast electrons, coated with a layer of ED-20 epoxy resin, have been obtained. The composite layer was without fillers and with iron and aluminum powders as fillers. It has been shown that the presence of such a coating layer increases the radiation resistance of n-Si and n-Ge single crystals, and the greatest radiation resistance is achieved by silicon and germanium single crystals coated with an epoxy composite with an iron powder filler. The determined presence of the residual magnetization of the iron powder filler and the corresponding induced additional Hall EMF may be of practical importance in the development of energy storage systems based on irradiated n-Ge and n-Si single crystals covered with a layer of epoxy resin with iron powder filler.

Chapter 2 is devoted to the development of nanopigments based on modified montmorillonite for the formation of polymer-mineral decoration of natural leather. An algorithm for obtaining nanopigments by successive modification of aqueous dispersions of montmorillonite with cationically active and anionically active compounds has been proposed. The composition of coating compositions with the use of nanopigments has been optimized and rational ratios of the components of the coating composition have been obtained, which ensure the formation of a polymer-mineral coating with the required level of operational properties. It has been proven that the use of nanopigments in the composition of coating compositions allows to reduce the consumption of coating paint for decoration, the thickness of the coating film and to obtain a coating with high quality indicators in terms of adhesion to dry and wet skin, resistance of the coating to multiple bends, dry and wet friction.

Chapter 3 analyzes the modern level of the technology of coating processes on a vertical surface, which actualizes the study of the problem of improving the operational properties of an anti-corrosion coating. The dependence of the effective application of anti-corrosion coatings and their physical and mechanical properties on the technological parameters has been determined. An automated unit for applying protective anti-corrosion coatings and removable nozzles to it for performing work in hard-to-reach places has been proposed. The practical significance of the obtained results lies in the determination of specific technological parameters and cleaning modes, when applying a film coating on a vertical surface, in particular in hard-to-reach places.

In Chapter 4, the possibility of using polymers as a structural material for creating the bodies of launch vehicles, as well as solid fuel for rocket engines is considered. Research is related to the

development of a new type of ultralight launch vehicles: combustible or autophagic launch vehicles. The thermophysical and mechanical characteristics of various types of polymers have been analyzed from the point of view of the possibility of their use as structural materials for the bodies of ultralight missile carriers. The results of theoretical and experimental studies of thermal destruction of polymer materials under aerodynamic heating conditions are presented. It is shown that polymer materials, in particular polyethylene, under suitable conditions, can be used to make fuel tanks for solid-fuel rockets that use a new principle of burning the structure during flight. The development of such launch vehicles and the commercialization of scientific research in this area will allow domestic companies in the aerospace industry to occupy a niche in the market for launching small satellites.

KEYWORDS

Epoxy composite coatings, Hall effect, radiation resistance, magnetic sensitivity, single crystals of silicon and germanium, metal powder fillers, montmorillonite, anionic dyes, nanopigment, polymer film former, polymer-mineral coating compositions, anti-corrosion coatings, polymer bodies, polymer fuel.

CIRCLE OF READERS AND SCOPE OF APPLICATION

The monograph is intended for researchers dealing with the problems of obtaining materials and applying coatings, as well as improving the properties of materials and structures for various operational applications.

The monograph is also useful for practitioners – designers and technologists who implement modern solutions in the field of materials science and technologies of applying protective coatings and are interested in improving the operational properties of their products.

CONTENTS

List of Tables	ix
List of Figures.....	xi
Introduction.....	1
1 Development of radiation-protective coatings based on epoxy composites for materials of electronic equipment	3
1.1 Total energy losses of electrons when passing through the polymer composite	4
1.2 The method of increasing the radiation resistance of n-Ge and n-Si single crystals to streams of high-energy electron irradiation.....	15
1.3 Magnetic sensitivity of electron-irradiated n-Ge and n-Si single crystals coated with an epoxy composite layer	21
Conclusions	30
References.....	31
2 Nanopigments and polymer-mineral decoration of natural leathers	34
2.1 Innovative materials and technologies for finishing natural leather	37
2.2 Nano pigments-based on modified montmorillonite	45
2.3 Application of nano pigments for polymer-mineral leather decorations.....	59
Conclusions	68
References.....	70
3 Modern technologies of repair and restoration works of buildings in use	73
3.1 Analysis of the technical and economic nature of the problem	75
3.2 Theoretical aspects of the influence of technological parameters of film coating processes on improving their quality.....	81
3.3 Designs of the device on the technology of applying film coatings in the conditions of buildings that are in use.....	94
3.4 Methodology of comprehensive assessment of the economic efficiency of film coating	103
Conclusions	106
References.....	107
4 Thermodynamic assessment of the possibility of using polymeric materials in promising launch vehicles.....	110

4.1	Experimental studies of thermodynamic processes during the thermal destruction of polymeric materials.....	118
4.1.1	Analysis of the physicochemical properties of polymeric materials as structural materials of ultralight LV.....	118
4.1.2	Methodology of experimental studies of thermodynamic processes during the thermal destruction of polymer materials by methods of thermal analysis	126
4.1.3	Research results of thermodynamic processes of destruction of polymeric materials during heating	129
4.2	Analytical study of the destruction rate of thermoplastic polymers under the influence of high-speed gas flows	133
4.2.1	Physical models of thermal destruction of thermoplastic materials under the influence of high-temperature and high-speed gas flow.....	133
4.2.2	Development of a method for determining the speed of thermal destruction of thermoplastic materials under the influence of high-temperature and high-speed gas flow	136
	References.....	141

LIST OF TABLES

1.1	Elemental composition of the PC	5
1.2	Concentration of radiation defects in irradiated silicon single crystals coated with an epoxy composite layer	20
1.3	Concentration of radiation defects in irradiated germanium samples coated with epoxy composite layer	21
1.4	Approximation polynomials for calculation of Hall EMF and magnetic sensitivity at $T=300$ K for irradiated germanium samples coated with a protective layer of epoxy resin	27
1.5	Approximation polynomials for the calculation of Hall EMF and magnetic sensitivity at $T=240$ K for irradiated germanium samples coated with a protective layer of epoxy resin	27
1.6	Approximation polynomials for the calculation of Hall EMF and magnetic sensitivity at $T=190$ K for irradiated germanium samples coated with a protective layer of epoxy resin	28
1.7	Approximation polynomials for the calculation of Hall EMF and magnetic sensitivity at $T=290$ K for unirradiated and irradiated silicon single crystals coated with a protective layer of epoxy resin	28
1.8	Approximation polynomials for the calculation of Hall EMF and magnetic sensitivity at $T=200$ K for irradiated silicon single crystals coated with a protective layer of epoxy resin	29
2.1	The share of finished leather of various types of decoration in the world in 2022	37
2.2	Ranking of importing countries in the world	38
2.3	Leading export countries in the world	39
2.4	Basic physical and chemical characteristics of the research objects	46
2.5	Indicators of structural changes of montmorillonite	50
2.6	Physicochemical characteristics of dyes	51
2.7	Change in optical densities in the spectra of modified montmorillonite	56
2.8	Chemical composition of nanopigments for leather decoration	58
2.9	Properties of nanopigments for leather decoration	59
2.10	Characteristics of the experimental plan	63
2.11	Indicators of the quality of leather covering	67
2.12	Indicators of quality of covering and finished leathers	68
3.1	Effect of preparation of the vertical surface on the service life of the film coating	81
3.2	Types of methods when applying an anti-protective coating to a vertical surface	82

3.3	Dependence of the strength of the film coating and the amount of mixture loss on the speed of the jet exit	90
3.4	Dependence of the film coating strength and the amount of mixture loss from the distance of the nozzle to the vertical surface	92
3.5	Results of experiment No. 1	98
3.6	Technical characteristics of spray nozzles for paint and varnish materials	100
3.7	Results of the experiment No. 2	101
4.1	Enthalpy of the formation of some combustion products	115
4.2	Physical and mechanical properties of polyethylene and polypropylene	121
4.3	Thermophysical and thermal properties of polyethylene and polypropylene	123
4.4	Research results	132

LIST OF FIGURES

1.1	Specific ionization losses of fast electrons in the polymer composite	7
1.2	Specific radiation losses of fast electrons in the polymer composite	9
1.3	Dependence of total specific energy losses of fast electrons in the studied polymer composite on the kinetic energy of electrons	10
1.4	Dependence of the average electron path in the polymer composite on its initial kinetic energy in the energy range from 0 to 1 MeV	10
1.5	Dependence of the average electron path in the polymer composite on its initial kinetic energy in the energy range from 0 to 10 MeV	11
1.6	Geometry of the process of passing fast electrons through a polymer composite	12
1.7	Transmittance by the number of electrons at different angles of incidence	12
1.8	Energy transmittance of electrons at different angles of incidence	13
1.9	Transmittance of the number of electrons at normal incidence on the composite for different initial electron energies	13
1.10	Energy transmittance at normal incidence on the composite for different initial electron energies	14
1.11	Comparison of transmittances by number of particles and energy at normal incidence on the composite	14
1.12	Concentration vs temperature dependences of generated radiation defects in irradiated n-Ge specimens coated with a layer of epoxy composite	17
1.13	Temperature dependences of specific conductivity for n-Ge single crystals, coated with a layer of epoxy composite	18
1.14	Temperature dependences of electron concentration for irradiated n-Si single crystals coated with a layer of epoxy composite	18
1.15	Temperature dependences of specific conductivity for irradiated n-Si single crystals coated with a layer of epoxy resin	19
1.16	Dependences of Hall voltage on induction of external magnetic field at T=300 K for irradiated n-Ge single crystals with different type of outer coating layer	23
1.17	Dependences of Hall voltage on induction of external magnetic field at T=240 K for irradiated n-Ge single crystals with different type of outer coating layer	23
1.18	Dependences of Hall voltage on induction of external magnetic field at T=190 K for irradiated n-Ge single crystals with different type of outer coating layer	24
1.19	Dependence of $U_x(t)$ when field magnetized B=0.5 T for irradiated n-Ge single crystals coated with a layer of epoxy composite with an iron powder filler	25
1.20	Dependences of Hall EMF on the induction of an external magnetic field at T=290 K for irradiated n-Si single crystals coated with a layer of epoxy resin	25

1.21	Dependences of Hall EMF on the induction of an external magnetic field at $T=200$ K for irradiated n-Si single crystals coated with a layer of epoxy resin	26
1.22	Dependence of Hall EMF during field magnetization $B=0.5$ T on time for irradiated n-Si single crystals coated with a layer of epoxy resin with an iron powder filler	26
2.1	Features of the montmorillonite structure	45
2.2	Distribution of montmorillonite particles in an aqueous dispersion: a – native, b – modified with sodium carbonate, c – sodium pyrophosphate	48
2.3	Diffractograms of native and modified forms of montmorillonite	49
2.4	Effect of pH on the ζ -potential of montmorillonite MMT- Cr^{3+}	50
2.5	Adsorption isotherm on MMT- Cr^{3+} dyes: a – anionic black, b – anionic dark green (curve 1) and anionic blue (curve 2)	52
2.6	Influence of medium pH on the level of adsorption of anionic black on MMT- Cr^{3+}	53
2.7	Absorption spectra of MMT- Cr^{3+} montmorillonite, black nanopigment and anionic black dye	54
2.8	Absorption spectra of MMT- Cr^{3+} montmorillonite, dark green nanopigment and anionic dark green dye	54
2.9	Mechanism of interaction of modifiers with montmorillonite	57
2.10	The scheme of obtaining nanopigments	58
2.11	Changes in the physical and mechanical properties of polymer films as a result of the addition of black (a , b) and green (c , d) nanopigments at elongation 100 % – 1, 300 % – 2, and break – 3	60
2.12	Mechanism of polymer matrix structuring by nanopigment	62
2.13	Generalized desirability function	65
2.14	The range of optimal values of the initial variables: Y_1 – modulus of elasticity at 100 % elongation, MPa; Y_2 – tensile strength, MPa; Y_3 – relative elongation at break, %; Y_4 – adhesion of the covering to the leather N/m; Y_5 – covering resistance to wet friction, rotation	66
3.1	Classification of contamination types of vertical surfaces	76
3.2	Classification of priming application methods	76
3.3	Classification of methods of applying paint to a vertical surface	76
3.4	Classification of paint and varnish materials	77
3.5	Examples of types of materials	79
3.6	Photo fragment of the method of applying the primer with a brush	83
3.7	Photo fragment of the method of applying the primer with a roller	83
3.8	The device for performing works on strengthening the foundations of soils and foundations and performing pile foundations for strengthening slopes	84
3.9	General view of the device on a vertical surface	86
3.10	Device for intensification of the liquid mixture injection	87
3.11	Device (nozzle) for spraying the fluid mixture	88

LIST OF FIGURES

3.12	Nozzle section	89
3.13	Schemes of the formation of a separate strip of the material layer: <i>a</i> – perpendicular-rectilinear; <i>b</i> – perpendicular-circular; <i>c</i> – inclined-rectilinear	90
3.14	Graphs of the coating strength dependence on the speed of feeding the film mixture and the amount of rebound	91
3.15	Graph of the dependence of the number of losses on the distance to the vertical surface	92
3.16	Graph of the dependence of the mixture strength and the amount of losses on the angle of inclination of the nozzle to the vertical surface	93
3.17	General appearance of the device	95
3.18	Supporting frame, view from a-a	96
3.19	General view of the proposed device	97
3.20	Spot size	97
3.21	Graph of dependence of costs of film coating on a vertical surface	99
3.22	Graph of the dependence of the torch diameter on the distance from the surface to the nozzle	99
3.23	Schemes for selecting parameters for applying a film coating on a vertical surface	99
3.24	Scheme of selecting the optimal distance from the vertical surface to the nozzle	101
3.25	Graph of dependence of the film coating on the torch diameter	102
3.26	Graph of the dependence of the torch on the distance	102
3.27	Fragment of film coating application	102
4.1	A variant of the forced-feed autophane motor	114
4.2	The theoretical specific thrust impulse I_{spec}^+ , his increase I_{spec}^+ and decrease I_{spec}^- vs. the filler (η) and condensate mass content (z) in combustion products: <i>a</i> – for polyethylene – oxygen propellant; <i>b</i> – for polyethylene – hydrogene peroxide (98 %) propellant; 1 – max ($I_{spec}^+ - I_{spec}^-$) area	117
4.3	Dependence of yield strength on temperature for HDPE, PP [49, 50]	124
4.4	Dependence of Young's modulus on temperature for HDPE, PP [49, 50]	125
4.5	Scheme of a thermoanalytical device	127
4.6	General view of the STA-6000 analyzer	127
4.7	Experimental sample	128
4.8	Schematic view of TA curves	129
4.9	Example of a thermogram for heating a sample of high molecular weight polyethylene	130
4.10	Example of a thermogram for heating a sample of low molecular weight polyethylene	130
4.11	An example of a thermogram for heating a polypropylene sample	131
4.12	An example of a thermogram for heating a sample of white polypropylene	132
4.13	Schemes of destruction of a heat-protective coating with a polymer filler: <i>a</i> – a filler with high thermal resistance; <i>b</i> – a filler with low thermal resistance	135
4.14	Scheme of destruction of polymer material	135

4.15	Flight parameters of a polymer rocket in the atmospheric section accepted for calculation	139
4.16	Temperature distribution at different time points in: <i>a</i> – polyethylene shell; <i>b</i> – polypropylene shell	140

INTRODUCTION

Traditional notions regarding the division of materials according to certain characteristics have been somewhat transformed in modern conditions in the direction of blurring the boundaries between different materials. Modern technological knowledge allows combining different materials, obtaining new composite materials with fundamentally new properties for various fields of application. Therefore, it is expedient today to define materials according to the principle of their innovativeness, bearing in mind the fundamentally new properties and possibilities of their application for various material objects.

Thus, for electronic equipment, it is important to obtain radiation-protective coatings and a reasoned choice of composites for materials and to identify new patterns that will allow obtaining the expected effects. Such effects can be related, for example, to energy, in energy storage systems.

The search for new innovative solutions based on the development of nanopigments for the light industry can contribute to the development of new coating compositions, which is important in leather technologies.

Problems of anti-corrosion protection of equipment parts and structures are always relevant. Therefore, the issues of forming materials and technologies for applying such coatings need development. In this perspective, it is especially important to note the construction field, where it is far from always possible to ensure the high-quality formation of an anti-corrosion layer due to the complexity of the profile and placement of surfaces that need protection, as well as sometimes difficult accessibility to these surfaces.

Polymers, as one of the most promising materials, require in-depth attention due to the possibility of various applications thanks to the purposeful regulation of their properties. In particular, it is of interest to use them in the rocket industry as a structural material for creating the bodies of launch vehicles, as well as solid fuel for rocket engines.

The results of theoretical and experimental research presented in this monograph reflect the aforementioned trends in the innovativeness of materials. Thus, the determined presence of the residual magnetization of the iron powder filler and the corresponding induced additional Hall EMF can be of practical importance in the development of energy storage systems based on irradiated n-Ge and n-Si single crystals covered with a layer of epoxy resin with iron powder filler.

The optimized composition of coating compositions using nanopigments based on modified montmorillonite and the rational ratio of coating composition components ensure the formation of a polymer-mineral coating with the required level of operational properties in leather technology.

Specific technological parameters and regimes of surface cleaning during the application of a film coating, in particular in hard-to-reach places, allow to increase the anti-corrosion resistance of construction structures. It also allows creating new innovative solutions in terms of technical and automated means of coating.

The results of determining the thermal destruction of polymeric materials under aerodynamic heating conditions allow us to justify new applications of such materials, in particular, polyethylene, which under certain conditions can be used to make fuel tanks for solid-fuel rockets that use a new principle of burning the structure during flight.

It is clear that these are only some areas of application of innovative materials and related technologies reflected in this monograph. Therefore, the further development of scientific research in this direction is promising and should be covered in other monographs on this topic in order to expand the understanding of modern innovative materials and provide practice with new opportunities.

CHAPTER 1

DEVELOPMENT OF RADIATION-PROTECTIVE COATINGS
BASED ON EPOXY COMPOSITES FOR MATERIALS OF
ELECTRONIC EQUIPMENT

CHAPTER 1

ABSTRACT

The basics of the theory of electron energy loss when passing through a composite material are presented. This made it possible to explain the influence of the metal filler on the amount of such losses. Dependences of the electron concentration, specific conductivity, and Hall EMF on the induction of external magnetic field for the n-Si and n-Ge single crystals, irradiated by the fast electrons, coated with a layer of ED-20 epoxy resin, were obtained. The composite layer was without fillers and with iron and aluminum powders as fillers. The presence of such a coating layer increases the radiation resistance of n-Si and n-Ge single crystals. Silicon and germanium single crystals coated with epoxy composite with iron powder filler have the highest radiation resistance. Obtained dependences of the Hall EMF on the induction of magnetic field for the investigated n-Si and n-Ge samples are linear. Only the silicon and germanium single crystals coated with epoxy with iron powder filler exhibit slight deviation from linearity at magnetic fields below 0.3 T. Residual magnetization, which induced the additional EMF Hall, was detected for the germanium and silicon single crystals, coated with a layer of epoxy resin with the iron powder filler. The presence of residual magnetization of the iron powder filler and the corresponding induced additional Hall EMF can be of practical importance in the development of energy storage systems based on irradiated n-Ge and n-Si single crystals coated with a layer of epoxy resin with the iron powder filler.

The chapter for a wide range of specialists with the radiation physics of solids is designed. It will be useful also for graduate students and students of physical and physical-technical specialties.

KEYWORDS

Epoxy composite coatings, Hall effect, radiation defects, radiation resistance, magnetic sensitivity, silicon and germanium single crystals, radiation losses, metal powder fillers.

Currently, there is a growing need for new materials with specific properties or known materials with improved properties [1–6]. Advances in some fields of technology are largely determined

by the ability of such materials to function in extreme conditions, such as elevated levels of radiation, temperature, chemical activity, mechanical and tribotic loads. The modern development of the nuclear industry, nuclear energy, military, and space technology is in dire need of the development of a new generation of electronic equipment based on these materials. The design of such devices is relevant to ensure the safety of work at nuclear and space plants, the disposal of nuclear waste, and work in radioactively contaminated areas. In addition, high-radiation physical experiments performed on charged particle accelerators at CERN require semiconductor devices capable of providing long-term dosimetric control in the internal tracks of nuclear installations. Devices with such performance are not available worldwide and cannot be designed using traditional semiconductor materials technologies, such as monocrystalline silicon and germanium technologies. Also, the use of already known materials and products to solve such problems creates the need not only to assess their radiation resistance in order to determine the limits of applicability but also the ability to use radiation as a technological tool to improve the properties of these materials. The problem of protection of semiconductor electronics elements from radiation can be solved by applying local radiation protection, the essence of which is to use special coatings that are directly applied to the surface of such elements. Promising in this direction is the development and application of polymer composite coatings based on epoxy resins, which have a number of advantages over other reactive polymers due to high manufacturability, adhesive strength, hardness, wear resistance, corrosion resistance, and resistance to rapidly changing temperature fields. Also, such coatings are lighter and cheaper compared to metal cases. Therefore, the development of a set of physical-mechanical and operational properties of epoxy composites and, accordingly, obtaining protective coatings for silicon and germanium single crystals from the aggressive action of radiation, environment, and other high-energy physical fields will allow creating of fundamentally new elements and devices of extreme electronics.

1.1 TOTAL ENERGY LOSSES OF ELECTRONS WHEN PASSING THROUGH THE POLYMER COMPOSITE

During the operation of spacecraft in the Earth's radiation belts, materials located on the outer surface area exposed to electron flows with a wide energy spectrum. Thermalizing in dielectric materials, these particles are able to create an uncompensated electric charge, i.e. to cause radiation electrification, which can significantly change the electrophysical properties of dielectrics [7]. Therefore, one of the main reasons that lead to the failure of electronic and electrical equipment of the spacecraft is the electrical breakdown of dielectrics. In the orbits of spacecraft, where there are intense flows of high-energy electrons, the absorbed dose of radiation inside is mainly determined not by electrons but by their radiation. It is known that in a geostationary orbit the absorbed radiation dose from hard electromagnetic radiation under radiation protection in 11 mm aluminum is more than two thousand times higher than the radiation dose from the electrons that generate this radiation. For polymers, this problem is less relevant, as they weakly generate

inhibitory X-rays caused by exposure to the protective material of high-energy corpuscular radiation. In addition, the polymeric materials have a lower density, which reduces the weight of the protective material at the initial level of protection. To use a new polymer composite in space, it is necessary to mathematically model the effect of electron radiation on it. In [7], a polymer composite (PC) synthesized on the basis of impact-resistant polystyrene and organosiloxane methylpolysiloxane xerogel filler (MPS) was selected. The elemental composition of the PC is presented in **Table 1.1**. It was previously found that this composition is optimal for use in space. The temperature interval of polystyrene composite operation is from +160 °C to –170 °C, it is resistant to VUV radiation and atomic oxygen.

• **Table 1.1** Elemental composition of the PC

The content of the MPS, wt. %	The content of elements in the composite, wt. %			
	Si	O	H	C
60	24	17.633	6.750	51.617

Consider a polymeric, completely amorphous composite material with a density $\rho = 1.159 \text{ g/cm}^3$. To study the ionization energy losses during the passage of electrons through the investigated polymer composite material, let's use the formula [8]:

$$\left(-\frac{dE}{dx} \right)_{col} = K \rho \frac{Z}{A} \frac{1}{2\beta^2} \left[\ln \left(\frac{m_e c^2 E_k}{I^2 \frac{\beta^2}{2(1-\beta^2)}} \right) - \frac{2\sqrt{1-\beta^2} - 1 + \beta^2}{1-\beta^2} \ln 2 + \frac{1}{8} (1 - \sqrt{1-\beta^2})^2 \right], \quad (1.1)$$

where $K = 4\pi \cdot r_e^2 m_e c^2 N_A = 0.307 \text{ MeV/g/cm}^2$;

$m_e c^2 = 0.511 \text{ MeV}$ – the rest energy of the electron;

$r_e = e^2 / m_e c^2 = 2.8 \cdot 10^{-13} \text{ cm}$ – classical electron radius;

$N_A = 6 \cdot 10^{23} \text{ 1/mol}$;

ρ – the density of the substance;

I – the average ionization potential of the atom of the substance of the medium;

$\beta = \sqrt{1 - \frac{(m_e c^2)^2}{(m_e c^2 + E_k)^2}}$ – Lorentz factor of an electron with kinetic energy E_k .

The studied composite material consists of atoms of different grades, each of which will contribute to the ionization energy loss of electrons. Then the formula will be:

$$\left(-\frac{dE}{dx}\right)_{cal} = \sum_i \left(-\frac{dE}{dx}\right)_i, \quad (1.2)$$

where $(-dE/dx)_i$ is the density and contribution of the i -th element in the complex substance and the ionization losses of the electron.

Rewrite expression (1.1) in a more convenient form for analysis:

$$\left(-\frac{dE}{dx}\right)_{cal} = \rho \frac{Z}{A} F(E_k, I), \quad (1.3)$$

$$F(E_k, I) = \frac{K}{2\beta^2} \left[\ln \left(\frac{m_e c^2 E_k}{I^2} \frac{\beta^2}{2(1-\beta^2)} \right) - (2\sqrt{1-\beta^2} - 1 + \beta^2) \ln 2 + \right. \\ \left. 1 - \beta^2 + \frac{1}{8} (1 - \sqrt{1-\beta^2})^2 \right]. \quad (1.4)$$

In this case, the contribution of each element to the total ionization losses is as follows:

$$\left(-\frac{dE}{dx}\right)_{cal}^C = \rho_C \frac{Z_C}{A_C} F(E_k, I_C), \quad (1.5a)$$

$$\left(-\frac{dE}{dx}\right)_{cal}^{Si} = \rho_{Si} \frac{Z_{Si}}{A_{Si}} F(E_k, I_{Si}), \quad (1.5b)$$

$$\left(-\frac{dE}{dx}\right)_{cal}^O = \rho_O \frac{Z_O}{A_O} F(E_k, I_O), \quad (1.5c)$$

$$\left(-\frac{dE}{dx}\right)_{cal}^H = \rho_H \frac{Z_H}{A_H} F(E_k, I_H). \quad (1.5d)$$

The average ionization potentials of atoms have the following values:

$$I_C \approx 785V, I_{Si} \approx 1735V, I_O \approx 955, I_H \approx 19.25V. \quad (1.6)$$

Given (1.5a–c), the ionization energy loss of electrons in the studied composite material is written in the form:

$$\left(-\frac{dE}{dx}\right)_{col} = \rho_C \frac{Z_C}{A_C} F(E_k, I_C) + \rho_{Si} \frac{Z_{Si}}{A_{Si}} F(E_k, I_{Si}) + \rho_O \frac{Z_O}{A_O} F(E_k, I_O) + \rho_H \frac{Z_H}{A_H} F(E_k, I_H). \quad (1.7)$$

Fig. 1.1 presents the curves constructed on the basis of expressions (1.3–1.7), showing the total ionization losses of electrons in the polymer composite (thicker curve) and the separate contribution of each chemical element of the composite to the ionization losses. From **Fig. 1.1** it follows that a greater contribution to the ionization losses is made by the carbon component while taking into account the low density of the composite, energy losses are quite high.

In addition to ionization losses, there are also radiation energy losses of electrons when passing through the investigated polymer composite material. Radiation energy losses of the electron in the matter are equal:

$$\left(-\frac{dE}{dx}\right)_{rad} = p \frac{Z^2 K \alpha \varepsilon}{A 4\pi m} G(E_k), \quad (1.8)$$

where $F(x) = \int_0^x \frac{\ln(1+y)}{y} dy$; $\varepsilon = E_k + m_e c^2$ – total electron energy; p – electron momentum.

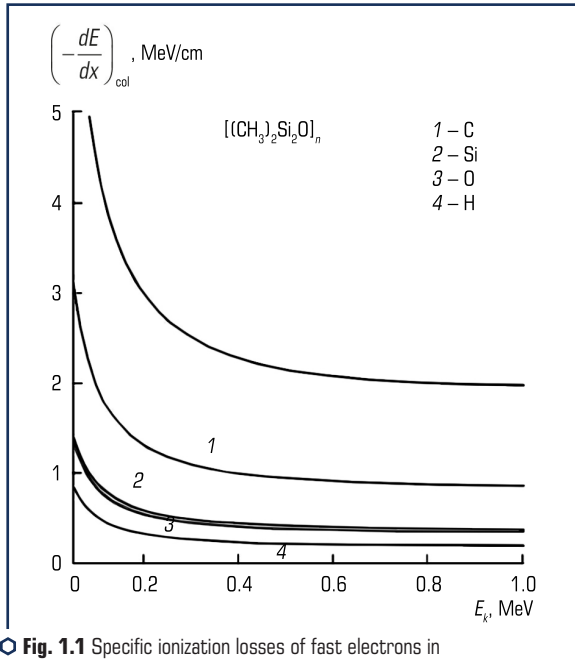


Fig. 1.1 Specific ionization losses of fast electrons in the polymer composite

$$G(E_k) = \frac{K\alpha}{4\pi} \frac{\varepsilon}{m} \left[\frac{12\varepsilon^2 + 4m_e^2 c^4}{3\varepsilon p} \ln\left(\frac{\varepsilon + p}{m_e c^2}\right) - \frac{(8\varepsilon + 6p)m_e^2 c^4}{3\varepsilon p^2} \left(\ln\left(\frac{\varepsilon + p}{m_e c^2}\right)\right)^2 - \right. \\ \left. - \frac{4}{3} + \frac{2m_e^2 c^4}{\varepsilon p} F\left(\frac{2p(\varepsilon + p)}{m_e^2 c^4}\right) \right]. \quad (1.9)$$

Since the studied polymer composite consists of several elements, the contribution of each to the radiation losses of the fast electron is determined by the expressions:

$$\left(-\frac{dE}{dx}\right)_{rad}^C = \rho_C \frac{Z_C^2}{A_C} G(E_k), \quad (1.10a)$$

$$\left(-\frac{dE}{dx}\right)_{rad}^{Si} = \rho_{Si} \frac{Z_{Si}^2}{A_{Si}} G(E_k), \quad (1.10b)$$

$$\left(-\frac{dE}{dx}\right)_{rad}^O = \rho_O \frac{Z_O^2}{A_O} G(E_k), \quad (1.10c)$$

$$\left(-\frac{dE}{dx}\right)_{rad}^H = \rho_H \frac{Z_H^2}{A_H} G(E_k), \quad (1.10d)$$

Then the total energy loss of the electron to radiation

$$\left(-\frac{dE}{dx}\right)_{rad} = \left(\rho_C \frac{Z_C^2}{A_C} + \rho_{Si} \frac{Z_{Si}^2}{A_{Si}} + \rho_O \frac{Z_O^2}{A_O} + \rho_H \frac{Z_H^2}{A_H} \right) G(E_k). \quad (1.11)$$

Fig. 1.2 presents the curves constructed on the basis of expressions (1.9) and (1.11), which show the total losses of fast electron radiation in the polymer composite (thicker curve) and the separate contribution of each chemical element of the composite to these losses. **Fig. 1.2** follows that the silicon component makes a greater contribution to radiation losses. Given the low density of the composite, the radiation energy losses are quite high, but they are small in comparison with the ionization losses at the considered electron energy values. In the general case, the energy losses of electrons in the studied polymer composite are determined by the sum of ionization and radiation losses (**Fig. 1.3**).

From **Fig. 1.3** it follows that at the considered values of electron energy, interesting from the point of view of electronic protection of the equipment in space, losses of energy of electron are generally defined by ionization of atoms.

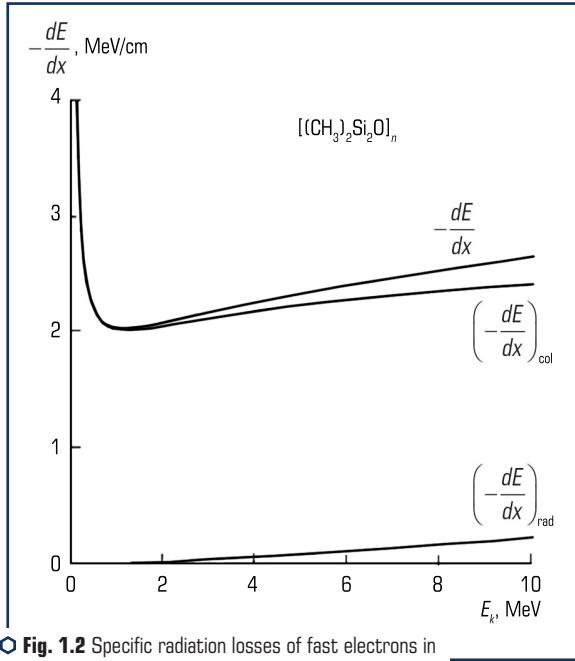


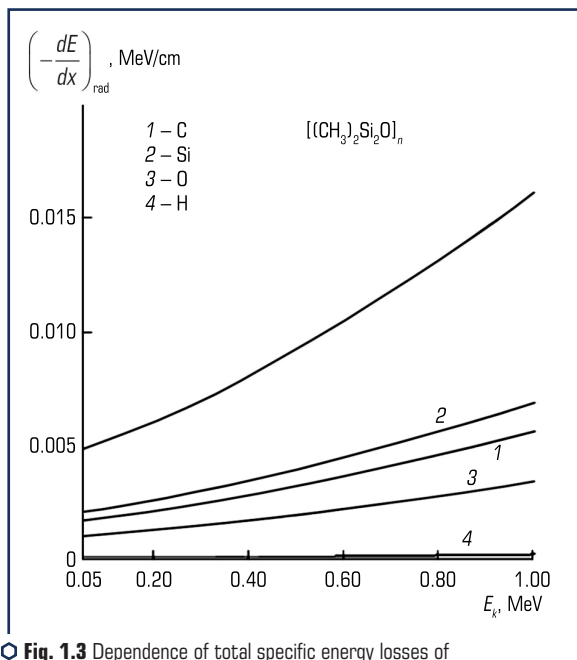
Fig. 1.2 Specific radiation losses of fast electrons in the polymer composite

Since the electron is "inhibited" by losses, let's find the average distance, which determines the average path length that the particle would travel in the process of deceleration in an unlimited and homogeneous medium, provided that it continuously loses energy along the entire path according to braking ability ($-dE/dx$). Real runs are random numbers and distributed around the average run. The average mileage is calculated by the formula:

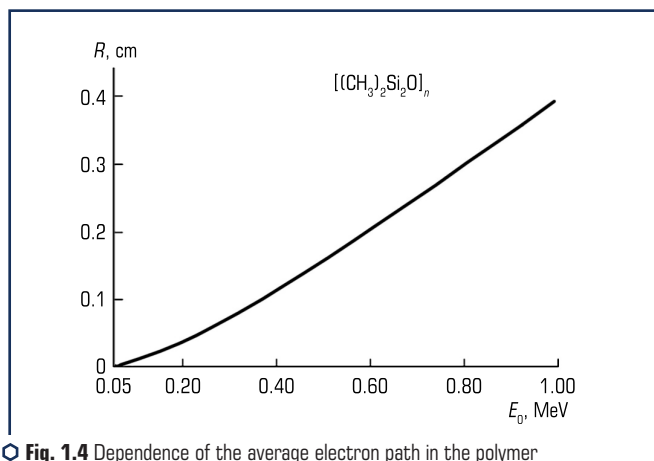
$$R(E_0) = \int_0^{E_0} \frac{dE_k}{\left(-\frac{dE}{dx}\right)}, \quad (1.12)$$

$$\text{where } \left(-\frac{dE}{dx}\right) = \left(-\frac{dE}{dx}\right)_{col} + \left(-\frac{dE}{dx}\right)_{rad}.$$

Fig. 1.4 and 1.5 show the dependences of the average electron path in the composite on its initial kinetic energy. The curves are constructed in different energy ranges.



○ **Fig. 1.3** Dependence of total specific energy losses of fast electrons in the studied polymer composite on the kinetic energy of electrons



○ **Fig. 1.4** Dependence of the average electron path in the polymer composite on its initial kinetic energy in the energy range from 0 to 1 MeV

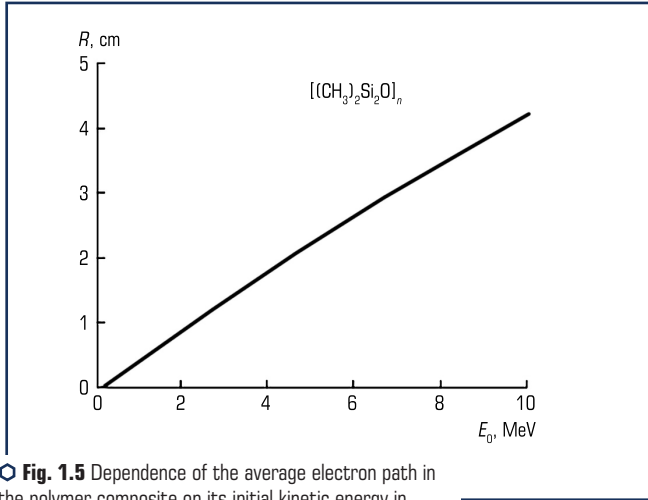


Fig. 1.5 Dependence of the average electron path in the polymer composite on its initial kinetic energy in the energy range from 0 to 10 MeV

Calculations show that the average electron path in the studied composite is quite small in a wide range of the initial energy of the electron, which indicates the prospects of its use to protect against the effects of electrons in outer space. Since fast electrons in outer space have a wide energy range and different orientations of the initial velocity, it is also necessary to investigate the electron transmission coefficients of this polymer composite.

Let's consider the transmittance of the number of particles and the energy of electrons incident on the material at an angle ϕ relative to the normal to its surface and pass a layer of matter with a thickness of x (**Fig. 1.6**):

$$T_N(x) = \frac{N(x)}{N_0}, \quad (1.13)$$

$$T_{E_x}(x) = \frac{E(x)}{N_0 E_0}. \quad (1.14)$$

Here N_0 and E_0 are the numbers of incident electrons and their kinetic energy. The Monte Carlo statistical method was used to simulate the process of electron transmission through the studied polymer composite.

Fig. 1.7–1.11 graphically present the results of modeling the dependence of the transmission coefficients on the number of particles and energy on the thickness of the composite for the angles and initial energies presented in the figures.

It is possible to make a conclusion about the high stability of the investigated composite in relation to a stream of fast electrons in the general case of their falling at various angles concerning normal to a target surface. A layer of such a composite, $x > 2$ cm thick, can completely shield the elements of electronic equipment from electron flows with energies up to 5 MeV.

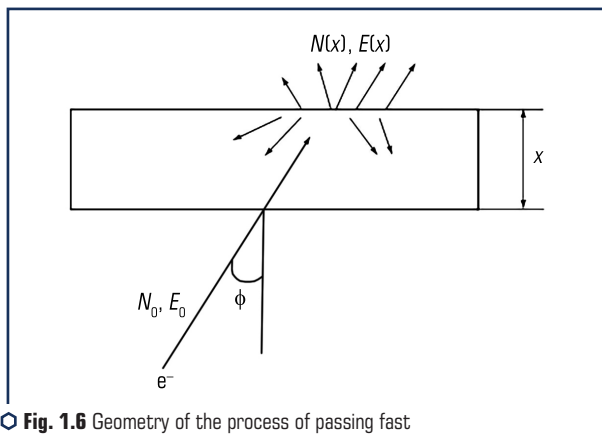


Fig. 1.6 Geometry of the process of passing fast electrons through a polymer composite

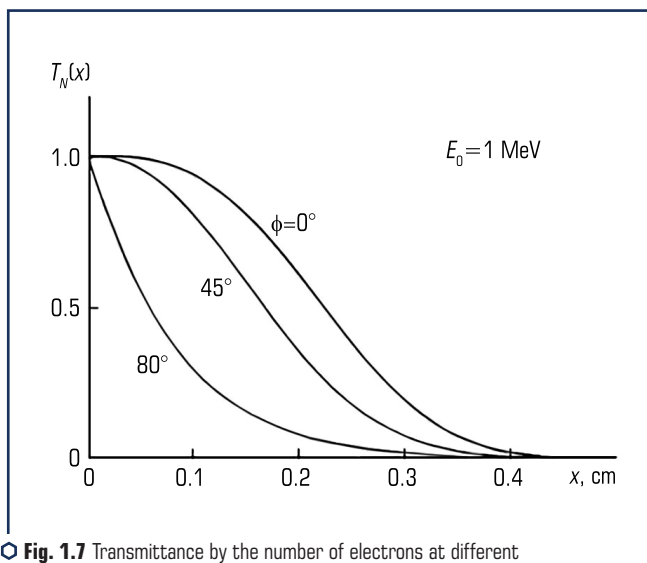


Fig. 1.7 Transmittance by the number of electrons at different angles of incidence

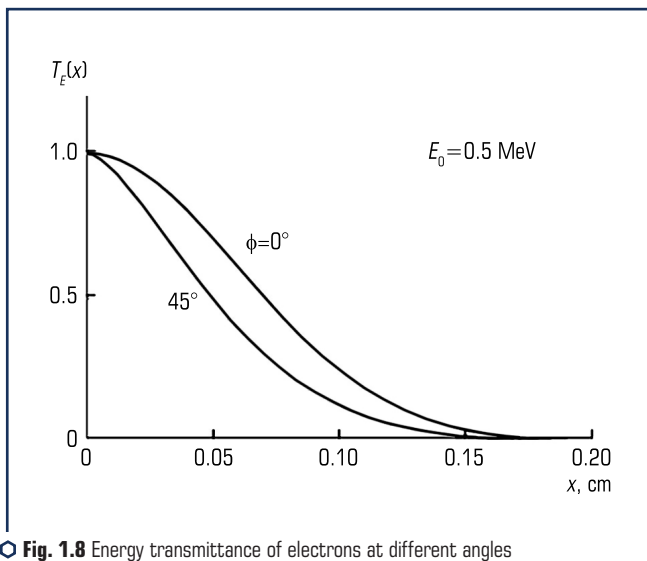


Fig. 1.8 Energy transmittance of electrons at different angles of incidence

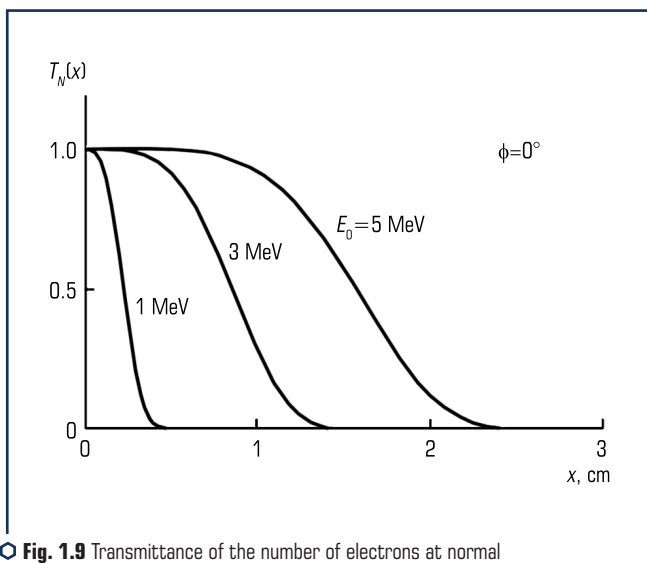


Fig. 1.9 Transmittance of the number of electrons at normal incidence on the composite for different initial electron energies

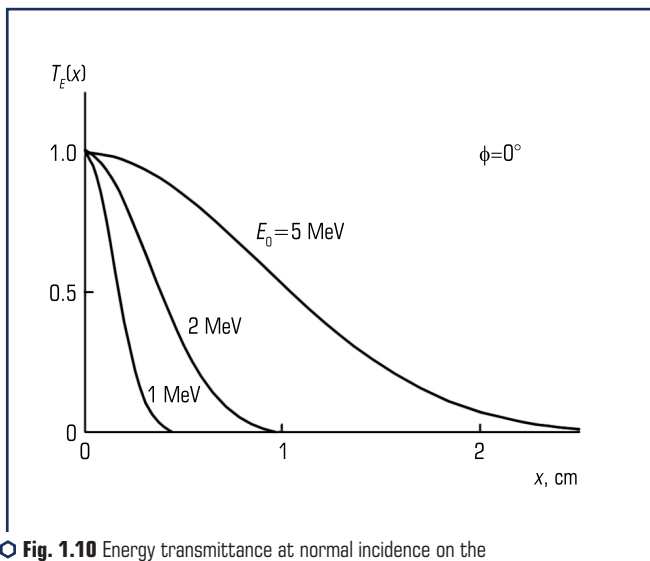


Fig. 1.10 Energy transmittance at normal incidence on the composite for different initial electron energies

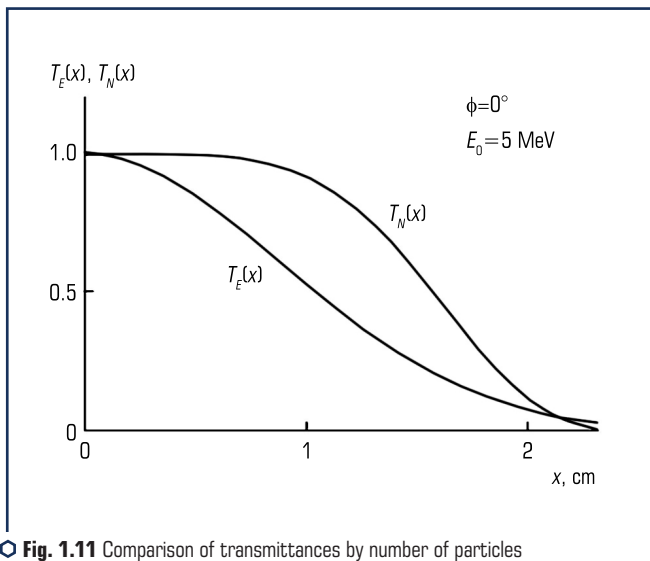


Fig. 1.11 Comparison of transmittances by number of particles and energy at normal incidence on the composite

1.2 THE METHOD OF INCREASING THE RADIATION RESISTANCE OF N-GE AND N-SI SINGLE CRYSTALS TO STREAMS OF HIGH-ENERGY ELECTRON IRRADIATION

Virtually all materials from which various structural units and working parts of nuclear and thermonuclear installations and spacecraft are made are exposed to radiation during their operation. Since, for example, the duration of nuclear reactors and designed thermonuclear devices must be at least 10 years (otherwise they will be economically unprofitable), at the same time must continuously "work" and structural materials [9, 10]. Reactor radiation, affecting the materials, changes their structure, and hence their strength, electrical and other properties. Radiation defects that are formed under such irradiations are mainly formed defects of the crystal structure (vacancies, between nodal atoms or their complexes with other impurities) [11, 12]. The energy transferred to a solid can lead to the rupture of interatomic bonds and the displacement of atoms with the formation of a primary radiation defect such as the Frenkel pair (vacancies and inter-nodal atom). Electromagnetic radiation (optical photons, γ -quanta, X-rays) directly disrupts the electronic system of the crystal, and only at the next stage are the various mechanisms of atomic displacement activated. The formation of radiation defects in the transfer of energy to electrons is possible in dielectrics and semiconductors. In metals, energy, quanta, or particles of radiation are usually spent on the excitation of atomic electrons and converted into heat without creating structural defects. The types and concentration of the formed stable radiation defects are determined both by the radiation conditions and by the properties of the solids themselves. In this case, the formation of stable point defects (isolated vacancies or internodal atoms, divacancies, complexes of Frenkel vapor components with impurity atoms) is most characteristic of light particles and photons of not very high energies.

The main criterion to which it is customary to pay attention when considering the behavior of materials in radiation fields is their ability to resist the action of radiation and retain their original properties. This characteristic of the material is called radiation resistance. Substances and materials differ significantly in their radiation resistance. This is due to differences in their physical and chemical properties: elemental composition, phase state, chemical and electronic state of molecules, structural defects. Radiation resistance significantly depends on the radiation environment, type of radiation, dose rate, ambient temperature, operating conditions. The first human-observed changes in materials under the influence of radiation were harmful, so the term "radiation damage to materials" appeared. Now, however, it is possible with the help of fast particles to purposefully change the structure of materials under certain conditions, thereby controlling their macroscopic properties. This opens wide opportunities for the application of radiation technologies in the production of, for example, crystals, and sometimes finished products from them with specially defined properties.

Semiconductor materials are widely used as various radiation detectors. Silicon or germanium diodes are used similarly to gas-filled ionization chambers to measure the spectral distribution of radiation quanta. The advantage of semiconductor detectors is that their ionization current is ten times greater than that of gases. Due to the higher density, the semiconductor absorbs much

more energy than gases. However, germanium and silicon detectors must be cooled to a temperature close to 200 °C and also use electronic pulse conversion circuits with low intrinsic noise. Currently, the task of ensuring the high performance of devices and equipment in the conditions of radiation exposure (electrons, protons, heavy charged particles, X-rays, and gamma radiation) is quite acute [13–17].

Radiation resistance of the equipment determines the term of its active use and trouble-free operation. This is especially true for electronic systems that are part of the onboard equipment of spacecraft [15]. Widespread use in the electronic equipment of the spacecraft of semiconductor devices and integrated circuits sensitive to the action of ionizing radiation of outer space, as well as increasing the service life of space objects requires ensuring the radiation resistance of micro-electronic elements for a given radiation environment.

Today, such methods of increasing the radiation resistance of silicon and germanium as nucleolar doping, pre-radiation heat treatment, doping with isovalent and electrically inactive impurities are used [18–20].

One of the promising areas of development of radiation-resistant equipment is the use of local protection methods, in particular the creation of special cases and coatings with integrated radiation shields [17]. These technologies allow the use of chips of commercial and industrial classes instead of radiation-resistant chips, which makes it possible to reduce the cost of onboard equipment and expand the range of components used. In this regard, it is practically and commercially advantageous to create protective screens, coatings, or shells of epoxy composite materials, which are more technological, lighter, and cheaper compared to metal cases. This requires detailed studies of the effect of radiation on the shielding capacity of such materials, especially when irradiated with high-energy particles.

In [21–23], the shielding ability of the epoxy composite coating layer from the effects of high-energy electron irradiation are investigated. This layer, 5 mm thick, which was an epoxy-diane resin brand ED-20 with PEPA hardener (12 parts by weight per 100 parts by weight of epoxy resin) without fillers and with fillers of iron and aluminum powders (30 parts by weight per 100 parts by weight of epoxy resin), was applied to the samples germanium and silicon. The investigated n-Ge and n-Si single crystals were grown by the Czochralski method and in the process of cultivation were doped with impurities of antimony and phosphorus, concentrations of $5 \cdot 10^{14} \text{ cm}^{-3}$ and $2.2 \cdot 10^{16} \text{ cm}^{-3}$, respectively.

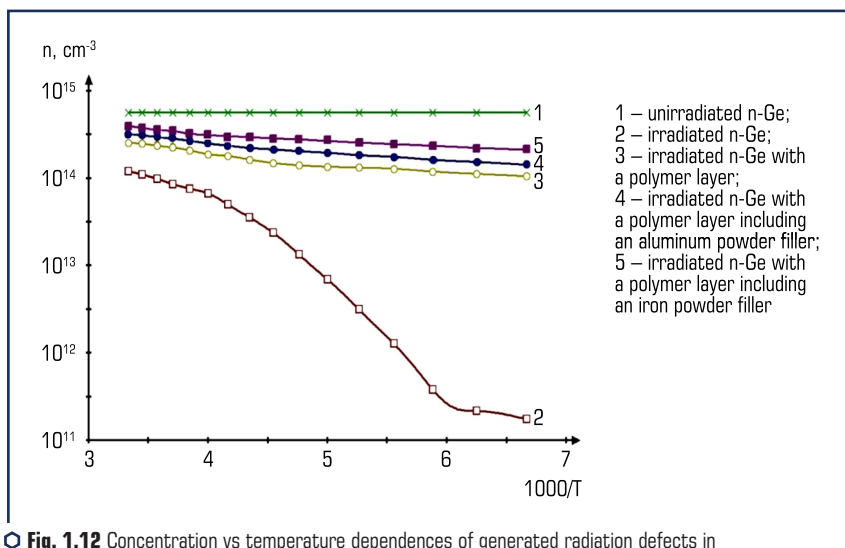
The method of obtaining samples of semiconductors and epoxy composites is described in detail in paragraph 1.2.

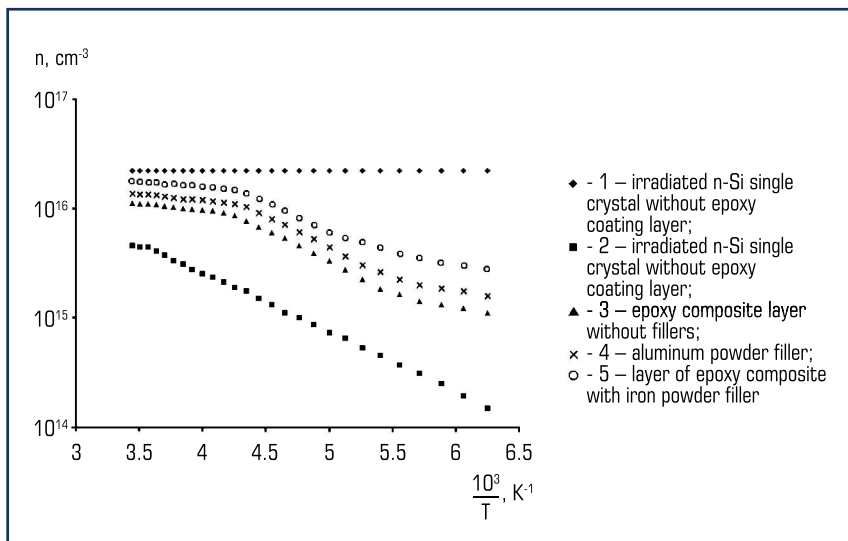
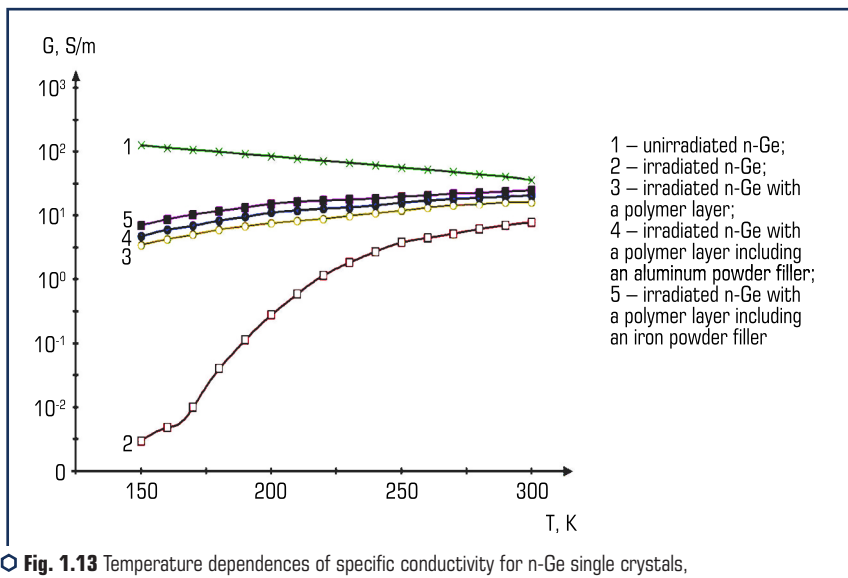
According to the experimental data of the authors [24], the dependence of the absorbed electron irradiation dose on the thickness of the polymer composite sample is extreme. The presence of a maximum for this dependence is associated with the development of the ionization process in the mass of the composite, which is caused by incident electrons and an increase in the ionization density of the medium due to the backscattering of secondary electrons at great depths. This leads to an increase in the absorbed radiation dose. It was also shown that with increasing energy of

the incident electron beam, this maximum expands and shifts in proportion to the thickness of the polymer composite. Therefore, as follows from these results, to reduce the transmittance of the electron irradiation flow, it is necessary to use either a very thick layer of polymer composite (for electron energy of 10 MeV it must be at least 50 mm) for the thickness at which the maximum is observed on the dependence of the absorbed dose. Therefore, in our research, let's choose the optimal coating layer of epoxy-diane resin with a thickness of 5 mm.

To study the shielding ability of such a layer of epoxy coating from electron irradiation, the temperature dependencies of electrical conductivity and Hall constant were measured for electron-irradiated electrons with energy 10 MeV and flow $\Omega=5 \cdot 10^{15}$ el./cm² n-Ge single crystals and irradiated electrons with energy 12 MeV and $\Omega=1 \cdot 10^{17}$ el./cm² n-Si single crystals coated with a layer of epoxy resin. In [25, 26], the temperature dependences of the electron concentration (Hall constant) for the same n-Si and n-Ge single crystals were obtained, irradiated with different streams of electrons.

As follows from these dependences, for electron irradiation flows $\Omega > 5 \cdot 10^{16}$ el./cm² and $\Omega > 5 \cdot 10^{16}$ el./cm² there is a significant decrease in the radiation resistance of the studied single crystals of silicon and germanium. With this in mind, it is chosen the above energies and electron irradiation flows of these single crystals. The temperature dependences of the concentration and specific electrical conductivity of the n-Si and n-Ge single crystals irradiated with electrons are presented in **Fig. 1.12–1.15**.





As follows from these dependencies, the electron concentration, specific conductivity, and, accordingly, radiation resistance increase for single crystals of germanium and silicon coated with a layer of epoxy-diane resin. The highest radiation resistance is achieved for n-Ge and n-Si samples coated with a layer of epoxy composite with an iron powder filler. According to the results of theoretical calculations, the average electron path in the polymer composite, in the first place, will be inversely proportional to the values of

$$B = \sum_{i=1}^n \rho_i \frac{Z_i}{A_i} \text{ and } C = \sum_{i=1}^n \rho_i \frac{Z_i^2}{A_i}.$$

Here ρ_i – the densities of the i -th chemical element, which is part of the macromolecule of the polymer composite, or filler, Z_i and A_i that respectively, their charge and mass numbers.

The values for $B_i = \rho_i \frac{Z_i}{A_i}$ and for $C_i = \rho_i \frac{Z_i^2}{A_i}$ the iron powder filler are larger than for the aluminum powder filler.

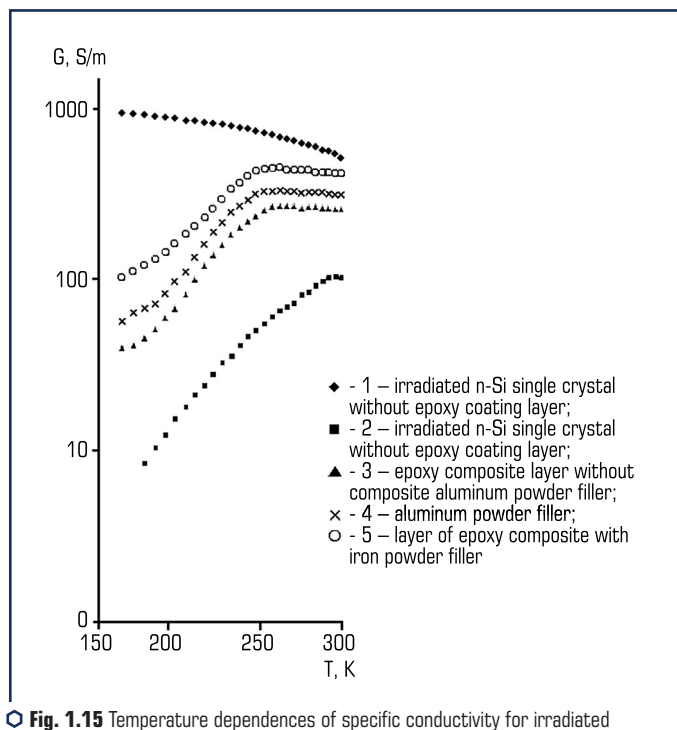


Fig. 1.15 Temperature dependences of specific conductivity for irradiated n-Si single crystals coated with a layer of epoxy resin

Therefore, the transmittance of the electron beam for a layer of epoxy composite with a filler of iron powder is less than for a layer of epoxy coating with a filler of aluminum powder. This explains the correspondingly higher radiation resistance of germanium samples coated with a layer of epoxy resin with iron powder filler than samples of germanium with a protective layer of epoxy resin filled with aluminum powder. A significant increase in the content of metallic filler in the epoxy polymer will reduce the densities of the chemical elements that are part of it, and in accordance with the weakening of the shielding capacity of the epoxy coating layer from radiation. Therefore, in our studies, let's choose the content of fillers of iron and aluminum powders, not exceeding 30 wt. including when this effect will be little noticeable. The increase in electron concentration and specific conductivity for irradiated n-Ge and n-Si single crystals coated with an epoxy coating layer is associated with a decrease in the concentration of radiation defects with deep acceptor levels in such single crystals due to attenuation of electron beam energy during epoxy composition. In [25] based on the measurements of infrared Fourier spectroscopy, Hall effect, and tenso-Hall effect, the nature and concentration of the main types of radiation defects for n-Si single crystals were determined. It was found that the main radiation defects formed by electron irradiation are A-centers (VO_i complexes), complexes containing internodal carbon (C_iO_i complexes), and VO_iP complexes (A-center modified with phosphorus). Irradiation of n-Ge samples with electron flows with an energy of 10 MeV leads to the formation of both point defects belonging to the VO_iI_2 complexes (A-center – two internodal germanium atoms) and order regions [27, 28]. The decrease in the concentration and specific conductivity of these samples with decreasing temperature is explained by the deionization of the deep acceptor level of $E_c-0.27$ eV belonging to the A-center. To quantify the level of defects in the studied single crystals of silicon and germanium, calculations of the concentration of formed radiation defects were performed. To do this, as shown in [25, 26], a system of equations of electroneutrality was solved. The results of such calculations are presented in **Tables 1.2 and 1.3**.

● **Table 1.2** Concentration of radiation defects in irradiated silicon single crystals coated with an epoxy composite layer single crystals coated with an epoxy composite layer

Sample type	Irradiated single crystal n-Si (without coating with a layer of epoxy composite)	Irradiated n-Si single crystal covered with a layer of epoxy composite	Irradiated n-Si single crystal coated with a layer of epoxy composite with aluminum powder filler	Irradiated n-Si single crystal coated with a layer of epoxy composite with iron powder filler
Concentration of complexes VO_iP_i , cm^{-3}	$1 \cdot 10^{16}$	$8.5 \cdot 10^{15}$	$6.6 \cdot 10^{15}$	$4.2 \cdot 10^{15}$
Concentration of complexes VO_iN_2 , cm^{-3}	$2.5 \cdot 10^{14}$	$1.7 \cdot 10^{14}$	$1.3 \cdot 10^{14}$	$7.1 \cdot 10^{13}$
Concentration of complexes $\text{C}_i\text{O}_i\text{N}_3$, cm^{-3}	$7.4 \cdot 10^{15}$	$2.3 \cdot 10^{15}$	$1.6 \cdot 10^{15}$	$2.9 \cdot 10^{13}$

• **Table 1.3** Concentration of radiation defects in irradiated germanium samples coated with epoxy composite layer

Sample type	Irradiated n-Ge single crystal (without epoxy composite layer coating)	Irradiated n-Ge single crystal covered with a layer of epoxy composite	Irradiated n-Ge single crystal covered with a layer of epoxy composite	Irradiated n-Ge single crystal coated with a layer of epoxy composite with iron powder filler
Concentration of A-centers N , cm^{-3}	$2.8 \cdot 10^{14}$	$2.3 \cdot 10^{14}$	$1.9 \cdot 10^{14}$	$1.6 \cdot 10^{14}$

As follows from **Tables 1.2 and 1.3**, the presence of a protective layer of epoxy composite leads to a decrease in the concentration of radiation defects in n-Si and n-Ge single crystals, especially when this protective layer contains an iron powder filler. In this case, for the irradiated n-Si, the concentration of the formed radiation defects corresponding to the VO_2P and VO_2 complexes decreases several times, and the C_2O_2 complexes decrease by more than two orders of magnitude.

A similar situation is observed for irradiated n-Ge single crystals. Therefore, the presence of a protective layer of epoxy composite significantly increases the radiation resistance of n-Si and n-Ge single crystals. The introduction into the polymer matrix of fillers of aluminum and iron powders leads to an increase in the shielding ability of such a layer from radiation. The obtained layer of epoxy-diane resin brand ED-20 with PEPA hardener (12 parts by weight) (without fillers) and with fillers of iron and aluminum powders (30 parts by weight) can be a promising material for creating cheap protective coatings for semiconductor electronics, which made on the basis of silicon and germanium, from the aggressive action of high-energy electron irradiation.

1.3 MAGNETIC SENSITIVITY OF ELECTRON-IRRADIATED N-GE AND N-SI SINGLE CRYSTALS COATED WITH AN EPOXY COMPOSITE LAYER

Interest in magnetic field sensors has not waned for several decades, due to the development of a large number of electronic devices that work on the basis of measurements of magnetic field parameters [29]. These include non-contact DC meters and switches, pipeline diagnostics and information input systems, motion meters in automotive and aerospace products, tomographs in medicine, Hall sensors for nuclear, thermonuclear energy, and research [30, 31]. Such a wide scope of operation of magnetic field sensors puts forward a number of requirements for them: increase of radiation resistance and range of operating temperatures; reduction of power consumption; size reduction; placement on one crystal of all elements that simultaneously measure different components of the magnetic field. In particular, in charged particle accelerators, nuclear and thermonuclear reactors, the magnetic field is measured under radiation conditions, so the efficiency and reliability of magnetic field sensors depend on the stability of their characteristics. This puts forward the requirements of increased radiation resistance to semiconductor materials,

on the basis of which the sensitive elements of Hall sensors are made [32]. Materials such as Si are used to make semiconductor Hall sensors; Ge; HgTe; HgSe; GaAs; InSb; InAs and others. In this respect, monocrystalline silicon and germanium occupy advanced positions due to their unique properties, commercial availability, and well-developed cultivation technology [33]. In the practical use of Hall sensors, there are two types of tasks. In one case, it is necessary to obtain the maximum, at a given scattering power, the EMF Hall, and the input resistance of the circuit can be arbitrarily large. In the second case, the goal is to get the maximum power in the Hall circuit. To implement the optimal in its parameters Hall sensors, working on the first principle, it is necessary to make them from a material having a low concentration of charge carriers of one sign, i.e. a large value of the Hall constant. In the second case, to match the sensor with the device, the material must meet two conditions: the resistance of the sample should not be too small and the mobility of the charge carriers should be high enough. When operating Hall sensors in conditions of radiation exposure, along with high radiation resistance, it is necessary to ensure their protection from the aggressive effects of the environment and various physical fields. One way to solve this complex problem is to develop simple, lightweight, relatively inexpensive, and technological protective coatings for the magnetically sensitive element of the Hall sensor. In this sense, epoxy composites are promising materials, given the above characteristics.

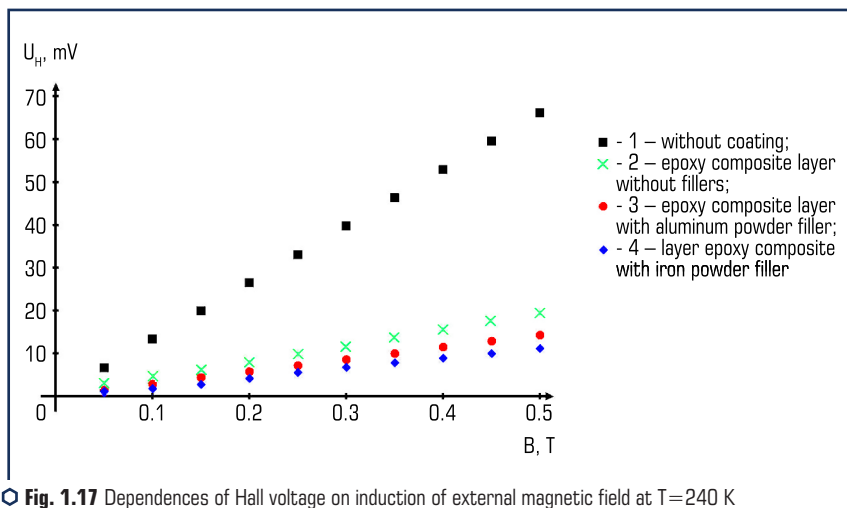
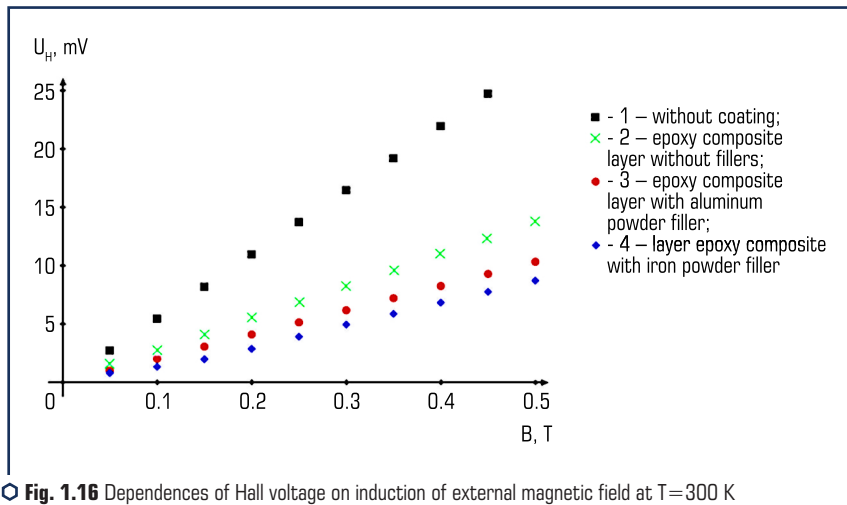
Therefore, it is interesting from a practical point of view to develop protective coatings based on epoxy-composite materials for silicon single crystals, which can be used to design a magnetically sensitive element of Hall sensors operating in conditions of high radiation.

In [23, 34], the magnetic sensitivity of electron-irradiated n-Ge and n-Si single crystals coated with a layer of epoxy resin (without fillers and with fillers of aluminum and iron powders) are researched. The conditions of electron irradiation, characteristics of the studied single crystals of silicon and germanium, epoxy coating layer, and methods of preparation of samples for research, experimental measurements were the same as in studies of radiation resistance of these single crystals. In [34], the effect of electron irradiation with an energy of 10 MeV and a flow $\Omega = 5 \cdot 10^{15}$ el./cm² on the magnetic sensitivity of n-Ge single crystals coated with an epoxy composite layer was investigated. As a result of measurements of the Hall effect, the dependences of the Hall voltage U_H on the induction of the magnetic field B at different temperatures were obtained.

As follows from these figures, the dependences $U_H = f(B)$ are linear for germanium single crystals coated with a layer of epoxy resin without filler and with a filler of aluminum powder in the entire range of the studied magnetic fields. These dependencies indicate a secondary role of the magnetoresistance effect, which can be manifested for germanium single crystals with oxygen-containing complexes at higher values of magnetic fields [35]. For germanium samples coated with a layer of epoxy composite with an iron powder filler, there is a slight deviation from the linearity of the dependence $U_H = f(B)$ at magnetic fields up to 0.3 T (**Fig. 1.16–1.18, curves 4**).

This can be explained by the fact that when such samples are placed in a magnetic field, the iron powder is magnetized, the magnetic field of which additionally affects the germanium sample

and thus changes the EMF of Hall. Confirmation of the existence of an additional magnetic field is the presence of residual magnetization, which creates an EMF Hall, after the "exclusion" of the external magnetic field.



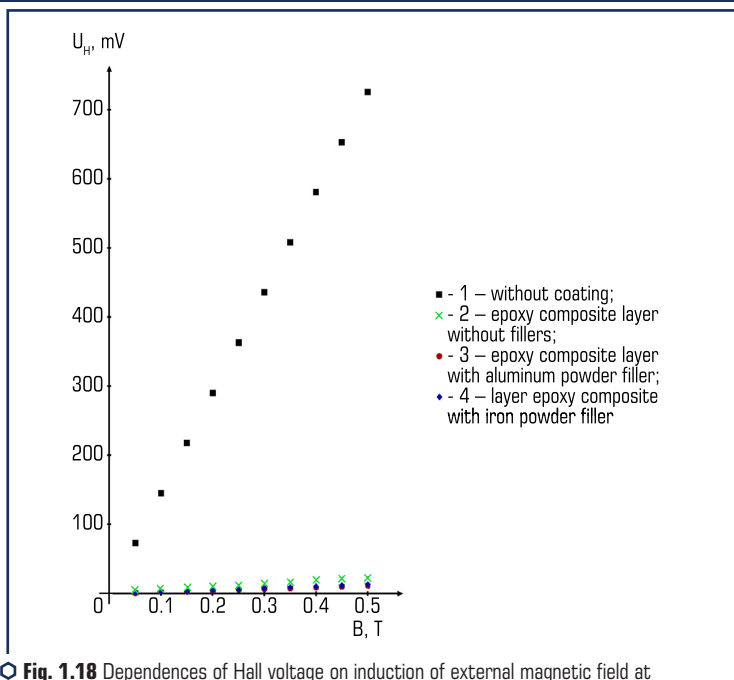


Fig. 1.18 Dependences of Hall voltage on induction of external magnetic field at $T=190$ K for irradiated n-Ge single crystals with different type of outer coating layer

The dependences of the Hall EMF on time in the absence of an external magnetic field for different temperatures are shown in Fig. 1.19.

As follows from Fig. 1.19, the residual magnetization of iron powder, which is a filler for epoxy resin, creates a Hall EMF of 2.123 mV, 1.967 mV and 1.552 mV at temperatures of 190 K, 240 K, and 300 K, respectively. The EMF of Hall decreases most rapidly (more than 10 times in 2 hours) at $T=300$ K (Fig. 1.4, curve 3). This is due to the fact that the increase in temperature leads to a decrease in the degree of directional orientation of the magnetic fields of individual domains of iron powder [36]. Similar dependences of the Hall EMF on the induction of an external magnetic field at temperatures $T=290$ K and $T=200$ K (Fig. 1.20 and 1.21) were obtained for n-Si single crystals in [23].

These dependencies are linear with the exception of silicon single crystals coated with a layer of epoxy composite with an iron powder filler, for which, as for n-Ge single crystals, there is a slight deviation from the linearity of the dependence $U_H=f(B)$ at magnetic fields up to 0.3 T (Fig. 1.21, curve 5), which is explained by the presence of additional magnetization of iron powder, which changes the EMF of Hall.

The dependencies of the EMF Hall on time in the absence of an external magnetic field for n-Si samples coated with a layer of epoxy resin with iron powder filler are shown in Fig. 1.22.

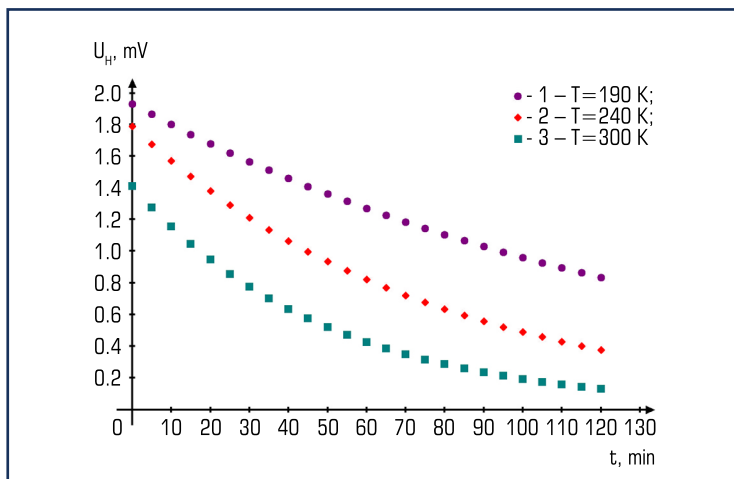


Fig. 1.19 Dependence of $U_x(t)$ when field magnetized $B=0.5$ T for irradiated n-Ge single crystals coated with a layer of epoxy composite with an iron powder filler

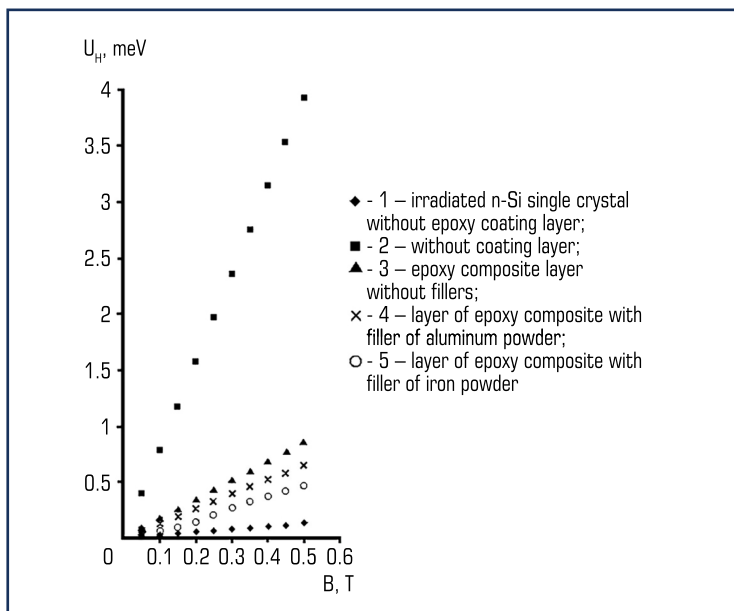


Fig. 1.20 Dependences of Hall EMF on the induction of an external magnetic field at $T=290$ K for irradiated n-Si single crystals coated with a layer of epoxy resin

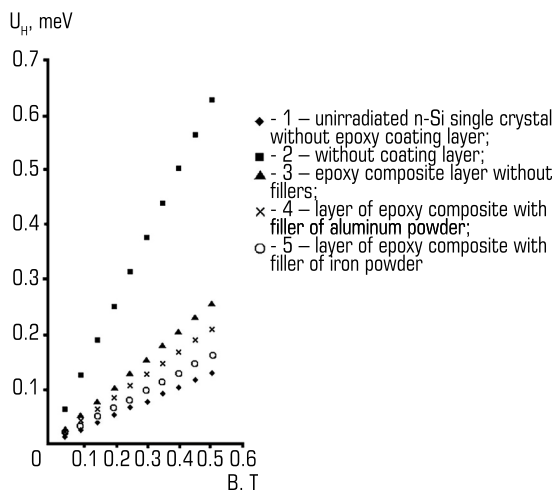


Fig. 1.21 Dependences of Hall EMF on the induction of an external magnetic field at $T=200$ K for irradiated n-Si single crystals coated with a layer of epoxy resin

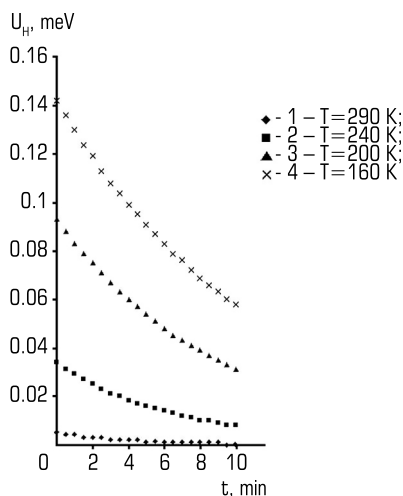


Fig. 1.22 Dependence of Hall EMF during field magnetization $B=0.5$ T on time for irradiated n-Si single crystals coated with a layer of epoxy resin with an iron powder filler

As for germanium single crystals, for silicon single crystals the residual magnetization of iron powder increases with decreasing temperature. At a temperature $T=290$ K, the additionally induced Hall EMF is only $5 \mu\text{V}$ (**Fig. 1.22, curve 1**), so it does not affect the linearity of the dependence $U_H=f(B)$ (**Fig. 1.20, curve 5**). To calculate the magnetic sensitivity of the studied n-Ge and n-Si single crystals, the analytical dependences of the EMF Hall on the induction of an external magnetic field were obtained using the least-squares method. Approximation polynomials for the calculation of such dependencies are presented in **Tables 1.4–1.8**.

● **Table 1.4** Approximation polynomials for calculation of Hall EMF and magnetic sensitivity at $T=300$ K for irradiated germanium samples coated with a protective layer of epoxy resin

Sample type	Dependence of EMF Hall U_H (meV) on the induction of an external magnetic field B (T)	Dependence of magnetic sensitivity $\beta=\delta U_H/\delta B$ (meV/T) on the induction of an external magnetic field B (T)
Irradiated n-Ge single crystal without a protective layer of epoxy coating	$U_H=55V$	55
Irradiated n-Ge single crystal covered with a layer of epoxy resin	$U_H=27.51V$	27.51
Irradiated n-Ge single crystal coated with an epoxy layer with aluminum powder filler	$U_H=20.75V$	20.75
Irradiated n-Ge single crystal coated with a layer of epoxy resin with an iron powder filler	$U_H = \begin{cases} 28.89V^2 + 6.659V + 0.43, & V < 0.3; \\ 18.92V, & V \geq 0.3 \end{cases}$	$\beta = \begin{cases} 57.78V + 6.659, & V < 0.3; \\ 18.92, & V \geq 0.3 \end{cases}$

● **Table 1.5** Approximation polynomials for the calculation of Hall EMF and magnetic sensitivity at $T=240$ K for irradiated germanium samples coated with a protective layer of epoxy resin

Sample type	Dependence of EMF Hall U_H (meV) on the induction of an external magnetic field B (T)	Dependence of magnetic sensitivity $\beta=\delta U_H/\delta B$ (meV/T) on the induction of an external magnetic field B (T)
1	2	3
Irradiated n-Ge single crystal without a protective layer of epoxy coating	$U_H=132V$	132
Irradiated n-Ge single crystal covered with an epoxy layer	$U_H=38.9V$	38.9
Irradiated n-Ge single crystal coated with a layer of epoxy resin with aluminum powder filler	$U_H=28.44V$	28.44

• Continuation of Table 1.5

1	2	3
Irradiated n-Ge single crystal coated with a layer of epoxy resin with iron powder filler	$U_H = \begin{cases} 30,12V^2 + 12,6V + 0,276, \\ V < 0,3; \\ 22,08V, \\ V \geq 0,3 \end{cases}$	$\beta = \begin{cases} 60,24V + 12,6, \\ V < 0,3; \\ 22,08, \\ V \geq 0,3 \end{cases}$

• Table 1.6 Approximation polynomials for the calculation of Hall EMF and magnetic sensitivity at T=190 K for irradiated germanium samples coated with a protective layer of epoxy resin

Sample type	Dependence of EMF Hall U_H (meV) on the induction of an external magnetic field B (T)	Dependence of magnetic sensitivity $\beta = \delta U_H / \delta B$ (meV/T) on the induction of an external magnetic field B (T)
Irradiated n-Ge single crystal without a protective layer of epoxy coating	$U_H = 1452V$	1452
Irradiated n-Ge single crystal covered with an epoxy layer	$U_H = 52.7V$	52.7
Irradiated n-Ge single crystal coated with a layer of epoxy resin with aluminum powder filler	$U_H = 36.5V$	36.5
Irradiated n-Ge single crystal coated with a layer of epoxy resin with iron powder filler	$U_H = \begin{cases} 32,85V^2 + 13,55V + 0,54, \\ V < 0,3; \\ 26,74V, \\ V \geq 0,3 \end{cases}$	$\beta = \begin{cases} 65,7V + 13,55, \\ V < 0,3; \\ 26,74, \\ V \geq 0,3 \end{cases}$

• Table 1.7 Approximation polynomials for the calculation of Hall EMF and magnetic sensitivity at T=290 K for unirradiated and irradiated silicon single crystals coated with a protective layer of epoxy resin

Sample type	Dependence of EMF Hall U_H (meV) on the induction of an external magnetic field B (T)	Dependence of magnetic sensitivity $\beta = \delta U_H / \delta B$ (meV/T) on the induction of an external magnetic field B (T)
1	2	3
Irradiated n-Si single crystal without a protective layer of epoxy coating	$U_H = 1.257V$	1.257
Irradiated n-Si single crystal coated with a layer of epoxy resin	$U_H = 0.509V$	0.509
Irradiated n-Si single crystal coated with an epoxy layer with aluminum powder filler	$U_H = 0.42V$	0.42

● Continuation of Table 1.7

1	2	3
Irradiated n-Si single crystal coated with a layer of epoxy resin and filled with iron powder	$U_H = 0.32V$	0.32
Non-irradiated n-Si single crystal without a protective layer of epoxy coating	$U_H = 0.257V$	0.257

As follows from the tables, the magnetic sensitivity of single crystals of silicon and germanium increases with decreasing temperature, as the concentration of electrons in the conduction band of silicon decreases and the Hall constant increases, which determines the value of magnetic sensitivity. For n-Ge and n-Si single crystals coated with a layer of epoxy resin without fillers and with aluminum powder filler, the magnetic sensitivity does not depend on the induction of an external magnetic field, and for the case of such single crystals coated with a layer of epoxy resin with iron powder filler, increases linearly with increasing magnetic field to 0.3 T. The least-squares approximation polynomials obtained for the calculation of Hall EMF and magnetic sensitivity can be used in the construction of radiation-resistant magnetically sensitive elements for Hall sensors based on germanium and silicon single crystals coated with a layer of epoxy resin.

● **Table 1.8** Approximation polynomials for the calculation of Hall EMF and magnetic sensitivity at $T = 200$ K for irradiated silicon single crystals coated with a protective layer of epoxy resin

Sample type	Dependence of EMF Hall U_H (mV) on the induction of an external magnetic field B (T)	Dependence of magnetic sensitivity $\beta = \delta U_H / \delta B$ (mV/T) on the induction of an external magnetic field B (T)
Irradiated n-Si single crystal without a protective layer of epoxy coating	$U_H = 7.85V$	7.85
Irradiated n-Si single crystal coated with a layer of epoxy resin	$U_H = 1.717V$	1.717
Irradiated n-Si single crystal coated with an epoxy layer with aluminum powder filler	$U_H = 1.303V$	1.303
Irradiated n-Si single crystal coated with a layer of epoxy resin and filled with iron powder	$U_H = \begin{cases} 2,757V^2 - 0,054V + 0,041, & V < 0,3; \\ 0,928V, & V \geq 0,3 \end{cases}$	$\beta = \begin{cases} 5,514V - 0,054, & V < 0,3; \\ 0,928, & V \geq 0,3 \end{cases}$
Non-irradiated n-Si single crystal without a protective layer of epoxy coating	$U_H = 0.257V$	0.257

The epoxy coating layer will also provide additional protection of the magnetosensitive element from moisture, vibration, rapidly changing temperature fields, and electromagnetic radiation, which will allow the use of such Hall sensors in harsher operating conditions.

The presence of residual magnetization of the iron powder filler and the corresponding induced additional Hall EMF can be of practical importance in the development of energy storage systems based on irradiated n-Ge and n-Si single crystals coated with a layer of epoxy resin with iron powder filler.

CONCLUSIONS

1. It is established that the most radiation-resistant to high-energy electron irradiation are n-Ge and n-Si single crystals covered with a layer of epoxy coating with an iron powder filler containing 30 parts by weight on 100 parts by weight including the epoxy resin. This is due to the fact that for iron filler there is an optimal ratio between its density, mass, and charge numbers, due to which the average electron path in the polymer composite will be the lowest compared to the layer of the epoxy composite without fillers and aluminum powder filler.

2. The dependences of the EMF Hall on the induction of an external magnetic field at different temperatures for electron-irradiated n-Ge single crystals (energy 10 MeV and flow $\Omega = 5 \cdot 10^{15}$ el./cm²) and n-Si (energy 12 MeV and flow $\Omega = 1 \cdot 10^{17}$ el./cm²) coated with a layer of epoxy-diane resin brand ED-20 with the content of PEPA hardener 12 parts by weight on 100 parts by weight including epoxy resin, both without fillers and with fillers of iron and aluminum powders with mass fractions of 30 %.

From the analysis of these dependencies it follows that they are linear for single crystals of germanium and silicon, coated with a layer of epoxy resin without fillers and with fillers of aluminum powder in the whole range of the studied magnetic fields.

For n-Ge and n-Si samples coated with a layer of epoxy resin with iron powder filler, there is a slight deviation from the linearity of such dependences at magnetic fields up to 0.3 T, which is explained by additional magnetization of iron powder.

The presence of residual magnetization can be used to develop on the basis of data from single crystals of energy storage systems.

3. It was established that the residual magnetization of the iron powder filler in the epoxy coating layer leads to the emergence of Hall EMF in n-Ge and n-Si single crystals. This will be able to find its practical use in the development of energy storage systems based on such single crystals.

4. Experimental researches of radiation resistance of n-Ge and n-Si single crystals can be used in the development and modeling based on epoxy resin with fillers of aluminum and iron powders of relatively cheap, light, and technological protective coatings of sensitive elements sensors made on the basis of silicon and germanium, or cases of semiconductor devices for nuclear and thermonuclear energy, aerospace industry, scientific research.

CONFLICT OF INTEREST

The authors declare that they have no conflict of interest in relation to this research, whether financial, personal, authorship or otherwise, that could affect the research and its results presented in this paper.

REFERENCES

1. Klym, H., Ingram, A., Shpotyuk, O., Filipecki, J., Hadzaman, I. (2007). Extended positron-trapping defects in insulating MgAl_2O_4 spinel-type ceramics. *Physica status solidi (c)*, 4 (3), 715–718. doi: <https://doi.org/10.1002/pssc.200673735>
2. Klym, H., Karbovnyk, I., Luchechko, A., Kostiv, Y., Pankratova, V., Popov, A. I. (2021). Evolution of Free Volumes in Polycrystalline BaGa_2O_4 Ceramics Doped with Eu^{3+} Ions. *Crystals*, 11 (12), 1515. doi: <https://doi.org/10.3390/cryst11121515>
3. Karbovnyk, I., Borshchysyn, I., Vakhula, Ya., Lutsyuk, I., Klym, H., Bolesta, I. (2016). Impedance characterization of Cr^{3+} , Y^{3+} and Zr^{4+} activated forsterite nanoceramics synthesized by sol-gel method. *Ceramics International*, 42 (7), 8501–8504. doi: <https://doi.org/10.1016/j.ceramint.2016.02.075>
4. Luniov, S. V., Burban, O. V., Nazarchuk, P. F. (2015). Electron scattering in the Δ_1 model of the conduction band of germanium single crystals. *Semiconductors*, 49 (5), 574–578. doi: <https://doi.org/10.1134/s1063782615050140>
5. Luniov, S. V., Nazarchuk, P. F., Burban, O. V. (2013). Parameters of the high-energy Δ_1 -minimum of the conduction band in n-Ge. *Journal of Physical Studies*, 17 (3). doi: <https://doi.org/10.30970/jps.17.3702>
6. Fedosov, A. V., Luniov, S. V., Fedosov, S. A. (2011). Influence of uniaxial deformation on the filling of the level associated with A-center in n-Si crystals. *Ukrainian Journal of Physics*, 56 (1), 69–73. doi: <https://doi.org/10.15407/ujpe56.1.69>
7. Pavlenko, V. I., Edamenko, O. D., Cherkashina, N. I., Noskov, A. V. (2014). Total energy losses of relativistic electrons passing through a polymer composite. *Journal of Surface Investigation. X-Ray, Synchrotron and Neutron Techniques*, 8 (2), 398–403. doi: <https://doi.org/10.1134/s1027451014020402>
8. Storm, L., Israel, H. I. (1970). Photon cross sections from 1 keV to 100 MeV for elements $Z=1$ to $Z=100$. *Atomic Data and Nuclear Data Tables*, 7 (6), 565–681. doi: [https://doi.org/10.1016/s0092-640x\(70\)80017-1](https://doi.org/10.1016/s0092-640x(70)80017-1)
9. Smirnov, L. S. (Ed.) (1980). *Voprosy radiatsionnoi tekhnologii poluprovodnikov*. Novosibirsk: Nauka.
10. Koshkin, V. M., Volovichev, I. N., Gurevich, Yu. G., Gal'chinet'skiy, L. P., Rarenko, I. M. (2006). *Materialy i ustroystva s gigantskim radiatsionnym resursom. Materialy stcintilliatcionnoi tekhniki*, 60.

11. Uglov, V. V. (2007). Radiatsionnye efekty v tverdykh telakh. Minsk: BSU, 167.
12. Brudny, V. N. (2005). Radiatsionnye efekty v poluprovodnikakh. Vestnik Tomskogo gosudarstvennogo universiteta, 285, 95–102.
13. Bagatin, M., Gerardin, S. (2016). Ionizing radiation effects in electronics: from memories to imagers. CRC press, 412. doi: <https://doi.org/10.1201/b19223>
14. Schrimpf, R. D. (2007). Radiation Space Environment. Radiation Effects in Microelectronics. Springer, 11–29.
15. Novikov, L. S. (2010). Radiatsionnye vozdeystviia na materialy kosmicheskikh apparatov. Moscow: Universitetskaya kniga, 192.
16. Vasilenkov, N., Maksimov, A., Grabchikov, S., Lastovskiy, S. (2015). Special-Propose Radiation Protective Packages for Microelectronics Devices. Electronics: Science, Technology, Business, 4, 50–56. Available at: <https://www.electronics.ru/journal/article/4657>
17. Zeynali, O., Masti, D., Gandomkar, S. (2012). Shielding protection of electronic circuits against radiation effects of space high energy particles. Advances in Applied Science Research, 3 (1), 446–451.
18. Barabash, L. I., Vishnevsky, I. M., Groza, A. A., Karpenko, A. Ya., Litovchenko, P. G., Starchik, M. I. (2007). Modern methods of the increase of the semiconductor materials radiation hardness. Problems of Atomic Science and Technology, 2, 182–189.
19. Dezillie, B., Li, Z., Eremin, V., Chen, W., Zhao, L. J. (2000). The effect of oxygen impurities on radiation hardness of FZ silicon detectors for HEP after neutron, proton and gamma irradiation. IEEE Transactions on Nuclear Science, 47 (6), 1892–1897. doi: <https://doi.org/10.1109/23.914465>
20. Litovchenko, P. G., Barabash, L. Y., Berdnyichenko, S. V., Varnyina, V. Y., Groza, A. A., Dolgolenko, O. P. (2009). Influence of impurities on the radiation stability of the silicon. Voprosy atomnoi nauki i tekhniki, 2 (93), 39–42.
21. Udovyt'ska, Yu. A., Maslyuk, V. T. (2020). Development of epoxy composite protective coatings for increasing the radiation stability of n-Ge single crystals. Functional Materials, 27 (1), 24–28. doi: <https://doi.org/10.15407/fm27.01.24>
22. Udovyt'ska, Yu. A., Luniov, S. V., Kashytskyi, V. P., Khvyshchun, M. V., Tsy, A. I., Maslyuk, V. T. (2020). Vykorystannia epoksykompozytiv dlia pidvyshchennia radiatsiinoi stiiokosti monokrystaliv n-Ge. Relaksatsiino, nelineino, akustooptychni protsesy i materialy. Luts'k, 101–103.
23. Udovyt'ska, Yu. A., Luniov, S. V., Kashytskyi, V. P., Maslyuk, V. T. (2021). Effect of Epoxy Composite Coatings on Radiation Stability and Magnetic Sensitivity of n-Si Single Crystals. Surface Engineering and Applied Electrochemistry, 57 (2), 222–227. doi: <https://doi.org/10.3103/s1068375521020125>
24. Pavlenko, V. I., Yastrebinskiy, R. N., Edamenko, O. D., Tarasov, D. G. (2010). Affecting of high-power bunches of rapid electrons polymeric radiation-protective kompozity. Problems of atomic science and technology, 1 (65), 129–134. Available at: https://vant.kipt.kharkov.ua/ARTICLE/VANT_2010_1/article_2010_1_129.pdf

25. Luniov, S., Zimych, A., Khvyshchun, M., Yevsiuk, M., Maslyuk, V. (2018). Specific features of defect formation in the nSi <P> single crystals at electron irradiation. *Eastern-European Journal of Enterprise Technologies*, 6 (12 (96)), 35–42. doi: <https://doi.org/10.15587/1729-4061.2018.150959>
26. Luniov, S. V., Zimych, A. I., Nazarchuk, P. F., Maslyuk, V. T., Megela, I. G. (2016). Radiation defects parameters determination in n-Ge single crystals irradiated by high-energy electrons. *Nuclear Physics and Atomic Energy*, 17 (1), 47–52. doi: <https://doi.org/10.15407/jnpae2016.01.047>
27. Luniov, S. V., Zimych, A. I., Nazarchuk, P. F., Maslyuk, V. T., Megela, I. G. (2015). The impact of radiation defects on the mechanisms of electron scattering in single crystals n-Ge. *Journal of Physical Studies*, 19 (4). doi: <https://doi.org/10.30970/jps.19.4704>
28. Luniov, S. V., Khvyshchun, M. V., Tsy, A. I., Maslyuk, V. T. (2021). Influence of Electron Irradiation and Annealing on the IR Absorption of Germanium Single Crystals. 2021 IEEE 12th International Conference on Electronics and Information Technologies (ELIT), 18–22. doi: <https://doi.org/10.1109/ELIT53502.2021.9501152>
29. Tumanski, S. (2013). Modern magnetic field sensors: a review. *Przeglad elektrotechniczny*, 10, 1–12.
30. Ripka, P. (2010). Electric current sensors: a review. *Measurement Science and Technology*, 21 (11), 112001. doi: <https://doi.org/10.1088/0957-0233/21/11/112001>
31. Darbar, R., Sen, P. K., Dash, P., Samanta, D. (2016). Using Hall Effect Sensors for 3D Space Text Entry on Smartwatches. *Procedia Computer Science*, 84, 79–85. doi: <https://doi.org/10.1016/j.procs.2016.04.069>
32. Bolshakova, I. A., Kulikov, S. A., Konopleva, R. F., Chekanov, V. A., Vasilevskii, I. S., Shurygin, F. M. et al. (2014). Application of reactor neutrons to the investigation of the radiation resistance of semiconductor materials of Group III–V and sensors. *Physics of the Solid State*, 56 (1), 157–160. doi: <https://doi.org/10.1134/s1063783414010089>
33. Claes, C., Simoen, E. (2007). *Germanium-Based Technologies*. Oxford: Elsevir. doi: <https://doi.org/10.1016/b978-0-08-044953-1.x5000-5>
34. Udovyt'ska, Yu. A., Luniov, S. V., Kashytskyi, V. P., Maslyuk, V. T., Megela, I. G. (2019). Development of protective coatings based on epoxy composite materials for germanium single crystals from the influence of magnetic field and radiation. *Sensor Electronics and Microsystem Technologies*, 16 (4), 53–65. doi: <https://doi.org/10.18524/1815-7459.2019.4.178074>
35. Babich, V. M., Baranskii, P. I., Shershel, V. A. (1970). The influence of oxygen and impurity-oxygen complexes on magnetoresistance of N-Ge in strong magnetic fields. *Physica Status Solidi (b)*, 42 (1), K23–K27. doi: <https://doi.org/10.1002/pssb.19700420152>
36. Zhang, S., Zhao, D. (2017). *Advances in magnetic materials: processing, properties, and performance*. CRC press. doi: <https://doi.org/10.4324/9781315371573>

CHAPTER 2

NANOPIGMENTS AND POLYMER-MINERAL DECORATION OF
NATURAL LEATHERS

ABSTRACT

The work is devoted to the development of nanopigments based on modified montmorillonite for the formation of polymer-mineral decoration of natural leather.

The covering takes the main place among the processes of manufacturing natural leather and provides the leather with high operational and aesthetic properties. A promising direction of resource-saving and ecological leather production is the development of nanopigments on a mineral basis – modified montmorillonite, and their use for polymer-mineral finishing of leather.

An algorithm for obtaining nanopigments by successive modification of aqueous dispersions of montmorillonite with cationically active and anionically active compounds is proposed. Dispersion of montmorillonite particles with sodium carbonate and modification with hydroxochromic complexes provides a change in surface chemistry and is accompanied by structural transformations of the mineral. A high level of adsorption of anionic black and dark green dyes on the surface of particles of modified montmorillonite was established. The formation of chemical and physicochemical interactions between the dye and exchangeable cations of montmorillonite has been proven. The composition of nanopigments based on colored dispersions of montmorillonite, which are characterized by high hiding power and stability over time, has been developed.

The influence of nanopigments at a consumption of 1.5–2.0 % of montmorillonite on the physical and mechanical properties of polymer films was established, which was confirmed by a three-fold increase in the modulus of elasticity and strength limit, as well as a decrease by 11.5 % in elongation at break for polymer films. The increase in the physical and mechanical properties of polymer films is the result of physical adsorption and is associated with the formation of relatively strong coordination bonds of the polymer with the active functional centers of the montmorillonite surfaces. The mineral in the composition of nanopigments increases the physical and mechanical properties of covering films, plasticizes and structures the polymer composition, contributes to the production of leathers with high organoleptic characteristics of the front surface, namely, the volume of the network, graininess, pleasant fingerboard.

Using the method of simplex-lattice planning, the composition of covering compositions was optimized using nanopigments, rational ratios of the components of the covering composition were

obtained, which ensure the formation of a polymer-mineral covering with the required level of operational properties, which is characterized by high adhesion to the leather, resistance to dry and wet friction, elasticity and strength.

The use of nanopigments in the composition of covering compositions allows to reduce the cost of covering paint for decoration, the thickness of the covering film and obtain a covering with high quality indicators in terms of the level of adhesion to dry and wet leather, resistance of the covering to repeated bending, dry and wet friction.

KEYWORDS

Leather, montmorillonite, modification, anionic dyes, nanopigment, polymer film former, polymer-mineral covering, decoration, covering compositions, quality, properties, composition optimization.

The modern assortment of leather materials, which are widely used for the manufacture of shoes, clothes, haberdashery, furniture, and interior upholstery of cars and airplanes, includes natural leather – face with covering decoration and pile. Depending on the quality of the front surface of the leather, it can be made with a natural front surface by covering it by applying a thin protective polymer film, sometimes transparent and colorless. However, the presence of defects on the front surface requires partial polishing of the front surface, the formation of a multi-layer colored covering and the production of leathers with an artificial front surface, the share of which is almost 60 % of the total output.

Finishing takes the main place among the processes of manufacturing natural leather and provides the leather with high aesthetic properties: uniform color over the entire area, good appearance, gloss or matte covering, a variety of imaginative combinations of several shades of colors. Also, the leather acquires the necessary operational properties: high adhesion of the covering to the leather, resistance to dry and wet friction, to stretching, to multiple bends, to the action of water, light, high and low temperatures, organic solvents used during chemical cleaning. Hygienic properties are also extremely important: vapor and air permeability of the leather and covering film.

The covering, which is applied to decorate the front surface of the leather in the form of a covering composition, has a composition: a polymer film former that forms a covering film; pigment concentrate or pigment that colors the covering film in the required color; wax emulsion, which gives the covering gloss and hydrophobicity; plasticizer to reduce the stiffness of the covering film or increase frost resistance; a dispersant or emulsifier that stabilizes the covering composition. The largest mass fraction in the covering composition belongs to the film-former (50–60 wt. parts) and pigment or pigment concentrate (10–15 wt. parts), which determines their crucial importance for the formation of a high-quality covering finish on the leather.

The range of polymer film-formers for covering leathers is quite wide and includes polyurethane, polyacrylate, nitrocellulose, and a mixture of film-formers of different nature is used to ensure sufficient operational properties of leathers.

To give the necessary color or shade to natural leather, pigment concentrates are used, which contain a pigment, a binder or thickener, a dispersant, a plasticizer, an antiseptic, and a solvent. Among the binders, the most common are casein, methylcellulose, or synthetic acrylic thickeners. In the case of manufacturing casein pigment concentrates, phenolic antiseptics are used to extend their shelf life.

Modern requirements for leather products due to changes in fashion trends and design solutions require constant and rapid updating of the range of leather, which is ensured by finishing the front surface in a wide color spectrum, forming a multi-colored covering with complex effects of embossing, cutting or imitating various textures.

Providing the required color or shade is the most difficult task for leather production, since the color range of existing pigment concentrates is quite limited, which is due to the complexity of their production and chemical basis. This situation is complicated by the fact that food protein – casein is mainly used as a binder to obtain pigment concentrate. Casein pigment concentrate has a number of disadvantages – low aggregative stability during storage, low covering ability, rots without an antiseptic, is characterized by a narrow range of colors.

A promising direction of resource-saving and ecological finishing of leather is obtaining nanopigments on a mineral basis – modified montmorillonite, and using them for finishing leather. The unlimited amount of the mineral in Ukraine, the ability of montmorillonite dispersions to be modified will make it possible to obtain environmentally friendly nanopigments of a wide color range, saturated color with improved technological properties (strength, elasticity, covering ability), and will also allow to exclude casein pigment concentrates and other auxiliary substances from the composition of covering compositions substances. The high dispersity of montmorillonite, the ability to thixotropy will lead to obtaining nanopigments stable over time, and the use of a mineral base in the covering composition will contribute to the structuring of the polymer and the improvement of the operational properties of the covering for leather.

Therefore, the development of nanopigments and parameters of polymer decoration of natural leather with their application is an urgent task.

The aim of this study is the development and application of nanopigments based on modified montmorillonite for polymeric leather decoration.

The object of the study is the modification of montmorillonite to obtain nanopigments and the parameters of their application for polymer finishing of leather.

The subject is the properties of nanopigments based on modified montmorillonite and the quality indicators of leather with a polymer finish.

To achieve this aim, the following objectives have been set:

- to investigate the effect of gradual modification of montmorillonite with compounds of anionic and cationic nature on the change in the structural properties of the mineral;

- to investigate the nature of the interaction of modified montmorillonite with anionic dyes, develop the composition and evaluate the properties of the nanopigment;
- to establish the influence of the mineral component on the formation of the structure of the polymer matrix for leather decoration;
- to establish the parameters of polymer structuring with nanopigment, physico-mechanical and chemical properties of covering compositions for finishing leather;
- to optimize the composition of the covering composition for decoration;
- to investigate the physical and mechanical properties and quality of leather covering.

2.1 INNOVATIVE MATERIALS AND TECHNOLOGIES FOR FINISHING NATURAL LEATHER

Leather production is an important component in the structure of the light industry of the countries of the world. In Ukraine, the light industry includes more than 10,000 enterprises, of which 1,500 specialize in the production of leather materials and leather shoes [1].

In the conditions of the war in Ukraine, caused by the aggression of the occupying country, the loss of a significant share of domestic and foreign markets is observed, the problem of stable activity of national product manufacturers, in particular leather and footwear production, is worsening. Today, one of the most important tasks of the state is the support of industrial production, domestic and foreign markets of light industry products [2].

The study of global prospects for the development of the leather industry and the production of multi-functional leather goods revealed a wide interrelationship between the projected dynamics of the development of raw materials and the technological support of leather production, taking into account the environmental and economic policies of the international environment.

According to the analysis of indicators of Ukraine's foreign trade activity for hides of various finishing methods [1], it was established that the main share of imports and exports of both the world and Ukraine is provided by hides with a natural surface (**Table 2.1**).

● **Table 2.1** The share of finished leather of various types of decoration in the world in 2022

Leather	Cost, million USD		Share, %	
	export	import	export	import
1	2	3	4	5
In general, all types of leathers	18091.6	18870.6	–	–
Hides from raw cattle				
additionally processed after tanning	8226.4	7872.2	45.47	41.72
with a natural front surface (whole)	3191.4	2760.7	17.64	14.63
with natural front surface (halves)	2126.4	2093.8	11.75	11.10

• Continuation of Table 2.1

1	2	3	4	5
with a polished front surface	1609.5	1375.6	8.90	7.29
Other				
Goat, pig, reptile and antelope leathers, additionally processed after tanning	831.9	775.9	4.60	4.11
Sheep leathers treated after tanning	596.3	532.9	3.30	2.82
Suede, including combined suede	423.1	352.41	2.34	1.87

The share of world imports for leathers with a configuration in the form of whole leathers with a natural front surface is much smaller than the corresponding indicator for half leathers. Indicators of foreign trade activity of Ukraine point to the 7th place in the world import for hides with a natural front surface and halves, and only 20 for polished hides. The total volume of exports for hides with a natural front surface (whole and halves) significantly outweighs imports (Table 2.2).

• Table 2.2 Ranking of importing countries in the world

Leather

with a natural front surface (whole)		with natural front surface (halves)		with polished front surface (not whole)	
Importing country	Cost, million USD	Importing country	Cost, million USD	Importing country	Cost, million USD
World	2760.7	World	2093.8	World	1375.6
1. China	223.2	1. China	369.6	1. Vietnam	362.6
2. Italy	197.4	2. Vietnam	335.4	2. Indonesia	226.6
3. Mexico	174.3	3. Hong Kong, China	178.5	3. China	96.8
4. Vietnam	194.2	4. France	77.9	4. Thailand	84.7
5. Hong Kong, China	167.9	5. Italy	64.6	1. Italy	55.9
44. Ukraine	6.4	7. Ukraine	63.9	20. Ukraine	14.2

According to indicators of foreign trade activity, Ukraine ranked 17th in world exports in 2022 (Table 2.3) for leathers with a natural face surface, and for leathers with a natural face surface (whole) and polished leathers – only 47 and 48, respectively.

The share of export of polished hides is half as much as the total export volume of hides with a natural front surface (whole and half).

● **Table 2.3** Leading export countries in the world

Leather					
with a natural front surface (whole)		with natural front surface (halves)		with polished front surface (not whole)	
Exporting country	Cost, million USD	Exporting country	Cost, million USD	Exporting country	Cost, million USD
World	3191.4	World	2126.4	World	1609.5
1. Italy	1324.6	1. China	330.5	1. Thailand	401.9
2. Brazil	549.3	2. Italy	324.8	2. Italy	366.3
3. Austria	198.3	3. Republic of Korea	267.0	3. China	233.2
4. Germany	173.2	4. Hong Kong, China	190.2	4. Vietnam	131.9
5. Hong Kong, China	125.3	5. Brazil	121.9	5. India	77.2
47. Ukraine	1.0	17. Ukraine	30.2	48. Ukraine	0.6

This indicates the significant interest of the international community in leathers with a natural facial surface, which is due to their competitiveness and significant advantages in terms of functional and hygienic properties [1].

The formation of the quality of natural leathers of various finishes is determined by the choice and characteristics of leather raw materials, the intended purpose of the finished leathers and is ensured at the stages of the technological process [3], which include:

- stage of preparatory processes: formation of a capillary-porous structure of the dermis with a clear separation of intertwined collagen fibers with different sizes of structural elements;
- stage of tanning processes: fixation and stabilization of the collagen structure of the dermis;
- finishing stage: complex formation of the volume of the dermis, hygienic, aesthetic and operational properties of the leather.

To obtain high-quality leathers, it is important to achieve an optimal state of the dermis structure at each stage of technological processing.

In the preparatory processes, sufficiently aggressive chemical compounds are used, including alkalis, acids, inorganic salts, as well as enzymes. The use of such compounds is due to the need to prepare the structure of the dermis for the main tanning process. For this purpose, interfiber water-soluble substances, keratin-containing proteins, breakdown products of collagen, elastin, and reticulin, etc., are removed [3].

For tanning processes, multifunctional compounds are used to achieve interaction with the functional groups of collagen and ensure structure fixation: inorganic substances (basic salts of chromium, aluminum, iron, titanium, etc. [3, 4]), organic compounds of the fatty series

(formaldehyde, glutaraldehyde, higher unsaturated fats, etc. [5]) and organic aromatics (benzoquinone, polynuclear sulfoaromatic acids, vegetable tannins, etc. [6]. After tanning, leather acquires resistance to various external influences and resistance to storage.

Finishing is liquid and covering. Liquid decoration is carried out to provide the leather with the necessary physical, mechanical and hygienic properties, and covering, to a greater extent, is aimed at the formation of aesthetic properties and the appropriate appearance [6].

The main finishing stage of leather production is covering dyeing. It consists in applying a colored and sometimes colorless covering film to the leather to give the surface a good appearance and protect it from external influences [3, 6, 7].

The essence of covering decoration consists in the formation of films of covering paints on the surface of the leather, which are applied in the form of thin layers of solutions or dispersions. After the solvents evaporate from the paint during the drying process, a thin polymer film is formed attached to the leather, that is, a covering that gives the leather color, covers minor facial defects, makes the leather resistant to water and dirt, and gives it a shine or matte finish.

There are several types of leather finishing, which differ in nature, composition, sequence and method of covering formation. The main types of decoration are: aniline, semi-aniline, emulsion [8, 9].

Aniline decoration consists in creating a very thin colorless or colored covering film on the leather, through which the natural lace of the leather is clearly visible. In order to achieve high adhesion, film formers are used that penetrate well into the dermis.

Semi-vanillin decoration is more common, because it involves the processing of an unevenly colored semi-finished product with minor facial defects. Semi-vanillin finish leathers have a natural lace, uniform two-tone color and aniline finish effect.

Emulsion finishing is performed for leathers with a natural or polished front surface with successive application of non-pigmented and pigmented primers, middle and fixing layers of the covering. Non-pigmented soil, which firmly binds to the surface of the leather, ensures the adhesion of subsequent layers of the covering and eliminates defects – wrinkles and swelling. The pigmented soil ensures complete and uniform coloring of the entire leather area, evens out micro-unevennesses and sanding streaks. The middle layer of the covering is created by applying covering paint on the primed surface of the leather. Hard film formers are used for the middle layers of the covering, as they must ensure the resistance of the covering to various deformations and the use of leather products; to the action of elevated temperatures; give the leather a beautiful appearance. The fixing layer increases the resistance of the covering to wet and dry friction, the action of water, elevated temperatures and organic solvents. Fixation of coverings, especially emulsion ones, is caused mainly by their thermoplasticity.

The covering paint includes the following components: film formers; pigments; plasticizers (for inelastic film formers); solvents and thinners; emulsifiers; dispersants and other auxiliary substances [7].

The basis of the covering are film formers that form a polymer film. Polymer materials that are used for modern covering decoration of the leather are divided into:

- polymerization or emulsion – dispersions of copolymers of acrylic acid derivatives [10];
- nitrocellulose – solutions of nitroenamel in organic solvents and nitrowater emulsions;

– polyurethane – solutions of polyurethanes in organic solvents and their aqueous dispersions.

Polymerization film formers or polyacrylates are polymers based on esters of acrylic $CH_2=CH-COOR$ methacrylic $CH_2=C(CH_3)-COOR$ acids, where $R=CH_3$; C_2H_5 and C_4H_9 . The properties of polyacrylates change significantly depending on the ether radical R, the presence of free carboxyl groups and free acrylic acid in the polymer [7].

Polyacrylates have a number of advantages: they bond well with pigments, are compatible with other film-forming agents, can form colorless, transparent, very elastic, water- and light-resistant films with high adhesion to the leather and resistance to aging. However, polyacrylic films are thermoplastic and have low heat and frost resistance. As the temperature rises, they soften and become sticky. The films are also unstable to the action of organic solvents. In order to obtain high-quality covering films, it is necessary to add polymers to polyacrylates that expand the temperature range of elasticity.

Nitrocellulose film formers [7] are used very rarely today, mainly as nitro-water emulsions for fixing the covering.

Polyurethanes are modern polymers containing the group $-NH-COO-$. The advantages of polyurethane coverings are high wear resistance, resistance to water and organic solvents, good gloss, appearance, high adhesion, good compatibility with other film formers.

Polyacrylates and polyurethanes are the most widely used today [11]. Polyurethane film formers provide high resistance to physical and mechanical loads, have sufficiently flexible chains and are easily modified. Given that polyurethanes are polar compounds, they show resistance to non-polar organic solvents, fat-containing materials. Polyacrylates are able to provide hardness, flexibility, resistance to organic solvents, gloss, etc. in the covering. They provide good water resistance to the covering, but do not provide high chemical and physical resistance.

Pigments or pigment concentrates are an important component of covering finishing compositions [12]. Pigments provide a specific color. Pigments are white or colored highly dispersed substances of organic or mineral origin, insoluble in water and film formers. A characteristic property of pigments is covering ability – the ability to cover the color of the painted surface, that is, to make it invisible [13]. Depending on the pigment content, the covering of hides is divided into three types [11]: aniline – a transparent covering without the use of pigments; semi-aniline – characterized by a small content of pigments to provide, mainly, a shade; and pigmented – with a significant content of pigments for complete covering of the facial leather surface with a colored layer [7].

Pigments in leather finishing provide the color and covering of the covering. Organic or inorganic pigments are used in the covering of hides. Organic pigments are characterized by a sufficiently large surface area, but during decoration they can complicate mechanical operations [12]. For the formation of the covering composition, it is necessary to dose a larger amount of binders, and the covering is characterized by low light resistance and heat resistance. At the same time, covering compositions with organic pigments differ in gloss and brightness of colors. Inorganic pigments create a high-quality covering with good light and water resistance, but are characterized by a high tendency to sedimentation and are limited in color and brightness [12].

To provide decorative effects, mixtures of pigments are usually used, which allows creating a wide color range of coverings. For this, pigments must be insoluble in water, organic solvents, plasticizers and wax emulsions to avoid migration with the subsequent change in color and light-fastness. The ability of the covering to form a uniform film that is stable over time, to form the required layer thickness depends on the properties of the pigment, the nature of their surface and the size of the particles.

Based on the size of the particles, all pigments are divided into transparent and covering. Transparent pigments include pigments whose particle size is smaller than the wavelength of light ($\lambda \leq 0.5 \mu\text{m}$). In this case, most of the light that falls on the pigment layer is absorbed and only a small part is reflected. These pigments are used for aniline decoration. Covering pigments have optimal particle sizes of 0.8...1.5 microns [3].

To give the covering gloss or dullness, water resistance, leather-like texture and other properties, auxiliary substances are added: wax emulsions, casein, plasticizers, etc. Wax emulsions are designed to give the covering hydrophobic properties and prevent it from sticking to the hot plate when pressing the semi-finished product. Plasticizers are part of covering paints to lower their glass transition temperature. Dispersants wet the pigment during the preparation of pastes and ensure the stability of pigment particles in paints. Emulsifiers provide stability to the film-forming dispersion. Alkyl sulfates, alkyl aryl ethers, quaternary ammonium compounds are used as emulsifiers. Stabilizers are used for film-forming dispersions in order to prevent their premature coagulation.

This indicates the multicomponent nature of covering compositions and the complexity of their purposeful selection in order to form a high-quality finishing covering on the leather.

In general, the finishing of natural leathers provides the necessary resistance of leathers to mechanical loads, atmospheric phenomena and gives a good appearance. The correct choice of the film former, the selection of the pigment to give the color and stability of the covering paint, as well as the introduction of auxiliary plasticizing and stabilizing substances provides the optimal version of the covering composition, the main function of which is to achieve high adhesion of the covering to the surface of the leather, a uniform film, resistant to multiple folds and friction. Observance of all factors ensures effective finishing of leather and provision of the necessary quality indicators of natural leather.

Innovative approaches in the covering decoration of leather are mainly based on the creation of new film-forming agents and pigments, improvement of the composition of covering compositions, purposeful selection of film-forming agents, pigments and auxiliary substances, development of complex materials that would simplify the composition of the composition and ensure the formation of a covering with operational and aesthetic properties.

The creation of new film-forming materials is based on methods of chemical modification during the synthesis of polymers, in solutions, latexes, in the process of making mixtures, etc. When creating new or improving existing formulations for leather finishing, the fact that coverings based on polyacrylates and polyurethanes have good water resistance and resistance to wet friction, as well as vapor permeability is taken into account [14]. Aqueous dispersions of acrylurethane

compositions are used due to the possibility of adjusting their colloidal chemical properties by changing concentrations and introducing auxiliary impurities. The combined use of acrylic dispersions and polyurethanes is promising in the production of elastic leathers. Synthesized polyurethane-acrylate film-forming compositions, depending on the molecular weight of the oligourethane component, can contribute to directed structural and chemical modification, which opens perspectives and opportunities for regulating the properties of materials based on them.

To improve covering compositions, their composition is optimized, components or the number of covering layers are changed, the film thickness is reduced, etc. In order to increase the effectiveness of covering painting, the use of structurally colored film formers based on acrylate derivatives is proposed [15]. But at the same time, questions arise regarding the low resistance of the resulting color to wet and dry friction, the tendency of the covering to age, the processes of dye migration to the surface of the covering, which requires additional fixing of the covering film. One of the ways to solve the above problems is to create colored polyurethanes. Colored polyurethanes are obtained by the interaction of polyol and organic diisocyanate in the presence of 0.1–5.0 % coloring agent – liquids or solids with a melting point of 48–226 °C [16].

Modern trends in covering painting are also aimed at the use of a rational method – compact decoration, the technology of which involves the use of the same composition for all layers of the covering composition [7]. For a compact decoration, the mixture of polymer dispersions should have universal properties: high curvature at a minimum film thickness, the ability to ensure its high adhesion to the leather while maintaining the elasticity of the covering in a wide temperature range.

A number of innovative developments have established the possibility of creating pigments or nanocomposites for covering leathers on a mineral basis, namely, on the basis of montmorillonite [17, 18]. The ecological and economical use of the mineral opens up the possibility of obtaining pigments of different colors, saturated colors and polymer-mineral nanocomposites with improved technological properties (heat resistance, elasticity, good hiding power) [18, 19]. The high dispersity of montmorillonite, the ability to thixotropy contributes to the production of hybrid pigments and time-stable polymer covering compositions based on them.

It is known [18] that an organic-inorganic pigment based on the mineral hydrocalcite and azo dyes is recommended for creating polymer composites as a filler or for providing a deep, intense color. Such a pigment is characterized by high thermal stability, which causes an increase in the resistance to flammability of coverings. Also, the combination of pigment with film formers helps to increase the physical and mechanical characteristics of the covering.

An increase in the brightness and intensity of color, resistance to atmospheric phenomena, high aggregative stability is characteristic of painted pigments based on clay. The authors note the characteristic phenomenon of pigment intercalation in the polymer covering and uniform distribution of nanoclay particles in the polymer medium [18].

The use of nanocomposites based on montmorillonite changes the rheological behavior of polymer systems. The dominant elasticity and high physical stability of the "polymer-nanocomposite" system becomes characteristic. The obtained nanocomposite polymer emulsions show a good film-forming

ability and increase the elasticity of the covering during the decoration of the front surface of natural leathers for clothing. The authors note that using montmorillonite solves the problem of obtaining stable nanocomposite polymer dispersions of organically modified montmorillonite with latexes. The obtained nanocomposite latex is aggregatively stable and contributes to the formation of a thin covering due to the nano-sized characteristics of the mineral particles [19]. Nanocomposite latexes are electrostatically stable and provide increased temperature resistance to the covering.

It has been shown that pigments can be obtained by deposition on inorganic substrates (metal oxides or salts, clay) of acidic and direct fixatives [20]. The latter are cationic products obtained by condensation of primary amines (or mixtures of amines and phenols) with formaldehyde. The obtained pigments are resistant to the action of water, organic solvents and light, but are unstable to the action of alkali solutions. To increase the specified stability, substances obtained by alkylation of condensation products of primary, secondary or tertiary amines with formaldehyde are used as fixatives.

The synthesis of organobentonite pigments is known [21] by modifying natural bentonite minerals with cationic polyelectrolytes (salts of aminoformaldehyde resins, their N-methyl substituted) followed by deposition of water-soluble anionic (direct) dyes on the formed aminoorganominerals. The use of organobentonite pigments makes it possible to reduce the cost of the technology of obtaining pigments of saturated shades with high technological properties: high heat resistance and covering ability, lack of bronzing in acrylic coverings, etc. The high dispersion of organobentonite pigments and the ability to thixotropy make it possible to obtain aqueous pigment pastes that do not delaminate in the absence of a binding component.

Organobentonite pigment concentrate can also be obtained [21] by adsorption modification of aqueous silicate dispersion with aminated collagen hydrolyzate, followed by deposition of water-soluble organic dyes on the formed organobentonite. Montmorillonite modified with an aminated hydrolyzate has a higher affinity for dyes than its non-aminated counterpart. The dye itself is sorbed on the surface of the organomineral, while low molecular weight impurities remain in the filtrate. The high resistance of the coloring of the obtained pigments to the action of alkalis and alcohols is due to the penetration of the anion of the dye into the interlayer space of the organomineral. The resulting pigment concentrate does not contain a binding component, mixes well with the components of the covering composition, has high aggregative stability and covering ability. Physico-chemical properties of the covering film formed on the leather based on organobentonite concentrate meet regulatory requirements [22]. Finished leather has a pleasant neck, with the effect of additional filling of the face layer with a mineral that is part of the pigment concentrate.

In general, according to the analysis of scientific developments [7, 17–22] regarding the effectiveness of the use of montmorillonite in the covering of leather, it was found that by modifying montmorillonite with multifunctional substances, pigments can be obtained, which are characterized by nano-sized particles, brightness and color saturation, and a wide range of colors. As part of the polymer covering, montmorillonite will provide aggregative and electrostatic stability of the polymer system, it is able to improve the physical and mechanical properties of the resulting covering, and increase its heat resistance.

All of the above indicates the promising use of montmorillonite for the creation of nanopigments and improvement of the polymer-mineral decoration of leather.

2.2 NANO PIGMENTS-BASED ON MODIFIED MONTMORILLONITE

Montmorillonite (MMT) is the main mineral of bentonite clays. MMT belongs to the group of layered water silicates and is characterized by high dispersion and hydrophilicity, ability to sorption, ion exchange, etc. Given these properties, MMT is widely used in the light, chemical, pharmaceutical, textile, paper industries, oil and gas production, geological exploration, etc. [23].

According to the structure, MMT consists of two tetrahedral meshes and one octahedral mesh located between them (**Fig. 2.1**). All the vertices of the tetrahedra face the center of the structural layer and form a single layer with the hydroxyls of the octahedral mesh, in which oxygen atoms are located at the vertices shared by the tetrahedral and octahedral meshes, and hydroxyls are located at the vertices of the octahedra that are not connected to the tetrahedra – hydroxyls OH.

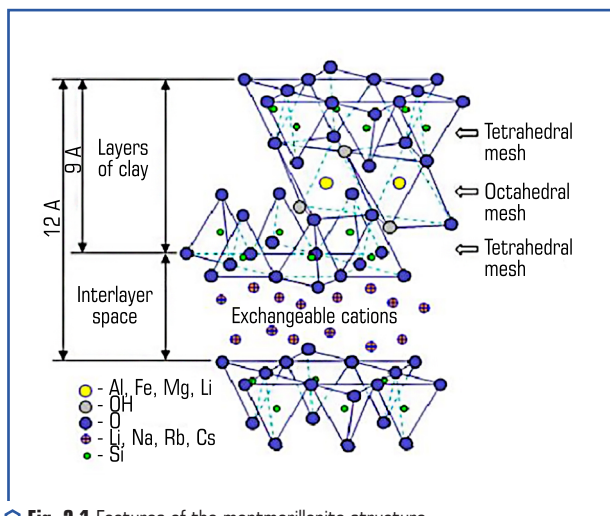


Fig. 2.1 Features of the montmorillonite structure

In the structure of montmorillonite packets, the oxygen surface of one layer contacts and interacts with the similar oxygen surface of the adjacent layer due to van der Waals forces, which indicates a weak connection between the layers. In this regard, molecules of water or other polar liquids can freely penetrate into the interstructural space and expand it. The basic basal distance

between the layers in the montmorillonite lattice is a variable value and, depending on the number of water molecules or exchangeable cations, can vary from 0.96 nm in the dry state to 14.0 nm and more in the state of strong water saturation [24]. Given that MMT particles are highly aggregated in aqueous dispersions, and their surface is bifunctional, for purposeful application of the mineral, it is necessary to eliminate the electrical inhomogeneity of the surface and maximally disperse aggregates of particles in the dispersions, which will allow further modification of the MMT surface and give it the necessary properties.

The specified features of the MMT structure explain the possible variety of physico-chemical, colloidal-chemical, rheological and other properties of the mineral, which is manifested in the cation exchange capacity, specific surface area and particle size (**Table 2.4**).

● **Table 2.4** Basic physical and chemical characteristics of the research objects

Mineral	Average particle size, (μm) [3, 6]	Exchange capacity, E, (mg-eq/100 g)	Specific surface area, S, (m^2/g) during adsorption		The value of the layer charge item/[Si_4O_{10}]
			water	methylen blue	
Cherkasy montmorillonite	0.05–0.3	72	311	520	0.35

Bentonite clay – $\text{Al}_2\text{O}_3 \cdot 4\text{SiO}_2 \cdot 2\text{H}_2\text{O} \cdot n\text{H}_2\text{O}$ (Dashukivske deposit, Cherkasy region, Ukraine) was used to obtain nanopigments. The main mineral of bentonite clay is montmorillonite, its content is 85 ± 3 %. The value of the exchange capacity is 72 mg-eq/100 g of clay. Humidity – 27 ± 3 %.

To obtain the most dispersed dispersions of montmorillonite, after cleaning and washing, the bentonite clay was transferred to the Na-form by introducing into the water dispersion of the mineral a concentration of 100 g/l of sodium carbonate with a consumption of 6 % or 10 % of sodium pyrophosphate based on the mass of the mineral.

To predict the change in the properties of montmorillonite as a result of modification, it is taken into account that there is a special van der Waals bond between neighboring structural elements, which is easily broken when polar molecules enter the interpacket space, causing a significant "swelling" of the lattice up to the complete rupture of individual packets. As a result, montmorillonite particles in water can disperse spontaneously, their number per volume unit increases significantly, and the number of direct contacts for further interactions also increases. In general, strong spatial coagulation structures are formed at a low concentration of the dispersed phase.

A manifestation of such transformations is a change in the number and size of the mineral particles in the volume, which is important for the creation of potential nanopigments for leather decoration. Under this condition, the size of the pigment particles should not be greater than the thickness of the covering formed on the front surface of the leather.

The analysis of studies on the distribution of montmorillonite dispersion particles by intensity, number, and volume after treatment with sodium carbonate and pyrophosphate is presented

in **Fig. 2.2**. Aqueous dispersion of montmorillonite with a solid phase concentration in water of 100 g/l (**Fig. 2.2, a**) is characterized by a monomodal distribution of mineral aggregates in size, intensity, and volume. In the dispersion of native montmorillonite, there are mainly aggregates with sizes of 1678 nm, 2265.8 nm, and 3059.5 nm. The volume of the dispersed medium is 40 % filled with aggregates with a size of 2265.8 nm, and the number of particles in this volume is 60 % of the total number in the dispersion. As a result of adding to aqueous dispersions of montmorillonite sodium carbonate in the amount of 6.0 % (**Fig. 2.2, b**) or 10.0 % (**Fig. 2.2, c**) of sodium pyrophosphate based on the mass of the dry mineral, significant changes in the distribution of montmorillonite particles were established.

After processing montmorillonite with sodium carbonate, the largest number of mineral particles with sizes of 34.6–93.2 nm was found, which indicates the dispersion of montmorillonite aggregates into individual smaller particles. It was also found that the number of mineral particles with sizes in the range of 153.0–1826.9 nm increases in the volume, which indicates the polymodal nature of the dispersion of montmorillonite after treatment with sodium carbonate.

After treatment of the aqueous dispersion of montmorillonite with sodium pyrophosphate (**Fig. 2.2, c**), a higher level of dispersion of montmorillonite into particles with a size of 16.8–28.3 nm was found, however, a significant part of the volume is filled by larger particles with a size of 2375.7–2082.6 nm.

The revealed effect is possible due to the nature of four-charge phosphate anions. It is likely that nanosized particles in aqueous dispersions are prone to coagulation and clumping. Considering the idea of creating nanopigments based on montmorillonite, it is reasonable to obtain dispersions without coagulation or peptization effects.

A comparative analysis of the effect of sodium salts on the level of dispersion indicates the expediency of carrying out the first stage of modification of montmorillonite with sodium carbonate and obtaining a sodium-modified dispersion (MMT- Na^+). At the same time, this dispersion contains nano-sized particles with a significant number of contacts for further purposeful modification with hydrochromic complexes and obtaining a cationic form of montmorillonite, as a basis for creating colored dispersions of montmorillonite and, subsequently, nanopigments.

The basis of obtaining nanopigments is the idea of adsorption of anionic dyes on the surface of particles of modified cationic montmorillonite. To ensure a high level of adsorption of dyes on the surface of the mineral, it is important to achieve the maximum value of the positive charge of the latter, that is, to carry out cationization of the surface of montmorillonite particles or "recharging". As stated in the paper [25], the maximum effect of recharging the surface of the mineral can be achieved by superequivalent adsorption of multi-charged metal hydrox complexes (Al^{3+} , Fe^{3+} , Cr^{3+} , Zr^{4+} , Ti^{4+}) [26].

Cr (III) compounds are traditionally used in leather practice as tanning agents. They have the maximum tendency to complex formation with the formation of reactive polynuclear positively charged hydroxocomplexes, therefore they are able to ensure the production of stable cationic forms of montmorillonite in a certain pH range of 3.9–6.9.

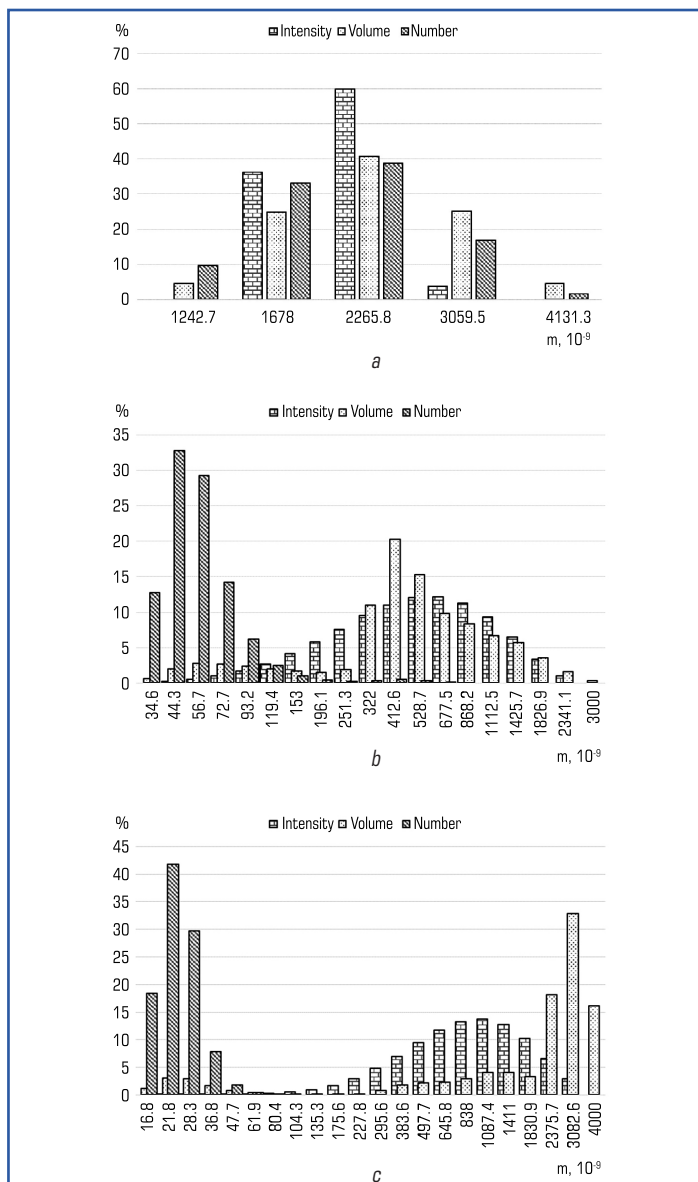


Fig. 2.2 Distribution of montmorillonite particles in an aqueous dispersion: *a* – native, *b* – modified with sodium carbonate, *c* – sodium pyrophosphate

To obtain the cationic form of montmorillonite, the expediency of using basic chromium (III) sulfate with a consumption of 10–12 % of the mineral mass has been proven [27]. Basic chromium sulfate was used for research – $\text{Cr}_2(\text{SO}_4)_n(\text{OH})_{6-2n}$ (Kazakhstan), chromium (III) oxide content 25.6 %, basicity 33 %. To modify montmorillonite, a solution of basic chromium sulfate in the amount of 10.0–12.0 % of the mass of the mineral in terms of Cr_2O_3 was added to the Na-form dispersion. Mixing continued for 120 minutes until a homogeneous mass of gray color was obtained. The pH of the modified cationic montmorillonite dispersion was 4.3–4.5. Chromium-modified montmorillonite dispersion ($\text{MMT}-\text{Cr}^{3+}$) was obtained as a result of successive treatment of aqueous dispersion of montmorillonite with sodium carbonate and basic chromium (III) sulfate.

Modification of montmorillonite with basic chromium (III) sulfate is accompanied by changes in the mineral's surface chemistry and structure. According to the obtained diffractograms (**Fig. 2.3**), changes in the structure of the mineral were established after the replacement of native Ca^{2+} and Mg^{2+} ions of native montmorillonite with Na^+ and Cr^{3+} cations after successive treatment with sodium carbonate and chromium (III) compounds.

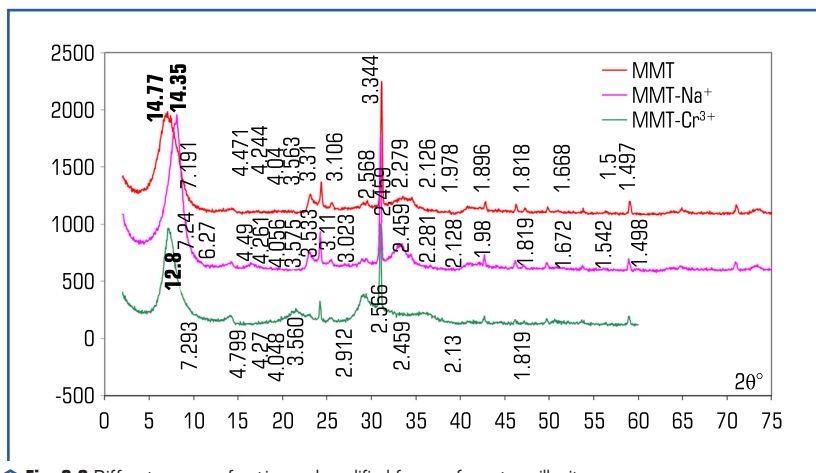


Fig. 2.3 Diffractograms of native and modified forms of montmorillonite

Taking into account that the value of the interplanar distance is determined as the difference between the value of d_{001} and the thickness of the elementary package of montmorillonite of 9.6 Å, it is established (**Table 2.5**) that the level of the indicator is 14.8 Å for native montmorillonite.

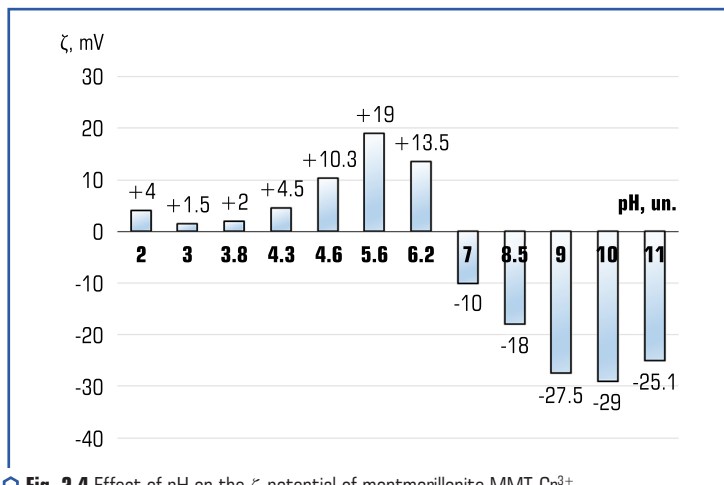
The replacement of exchangeable cations Ca^{2+} and Mg^{2+} of native montmorillonite with Na^+ cations in modified montmorillonite leads to a shift of the basal reflex to larger 2θ -angles (**Fig. 2.3**) and a decrease in d_{001} to 12.8 Å (**Table 2.5**). The transformation of $\text{MMT}-\text{Na}^+$ into the form of $\text{MMT}-\text{Cr}^{3+}$ is accompanied by a shift of the basal reflex toward smaller 2θ -angles and a

subsequent increase in the value of d_{001} to 14.4 Å. At the same time, the change in the diffraction pattern is caused by the different placement of chromium (III) complexes in the interlayer space of montmorillonite. This indicates structural changes in the mineral and is further confirmed by an increase in the specific surface area of montmorillonite (**Table 2.5**) from 60 to 280 m²/g. The growth of chemical affinity and expansion of the interpacket space is a prerequisite for effective modification of the montmorillonite surface with anionic dyes.

● **Table 2.5** Indicators of structural changes of montmorillonite

Indicator	A form of montmorillonite		
	native	MMT–Na ⁺	MMT–Cr ³⁺
Value of basal interplanar distance d_{001} for native MMT, Å	14,8	12,8	14,4
Adsorption (specific) surface area of montmorillonite, m ² /g	60	160	280

A study of the surface chemistry of the modified MMT–Cr³⁺ revealed that in the pH range of 4.3–6.2 the surface of the mineral particles acquires the maximum positive charge (**Fig. 2.4**). Increasing the pH level above 7.0 contributes to the return of the anionic surface charge of the mineral particles, which is associated with the destruction of the chromium (III) complex [28].



○ **Fig. 2.4** Effect of pH on the ζ-potential of montmorillonite MMT–Cr³⁺

Taking into account the fact that the composition of the nanopigment includes mineral and organic components, it is necessary to ensure the maximum fixation of the organic dye on the

MMT-Cr³⁺ surface. The presence of an unbound dye in the nanopigment will require the use of additional binding components in the preparation of the covering paint for finishing the leather, or will have a negative effect due to the migration of the dye to the surface of the covering film with its subsequent contamination. At the same time, an important condition is the achievement of high covering power of pigments without delamination as part of the covering composition for finishing the leather.

The key aspect of ensuring effective and complete adsorption of the anionic dye [29] on the surface of the MMT-Cr³⁺ dispersion is:

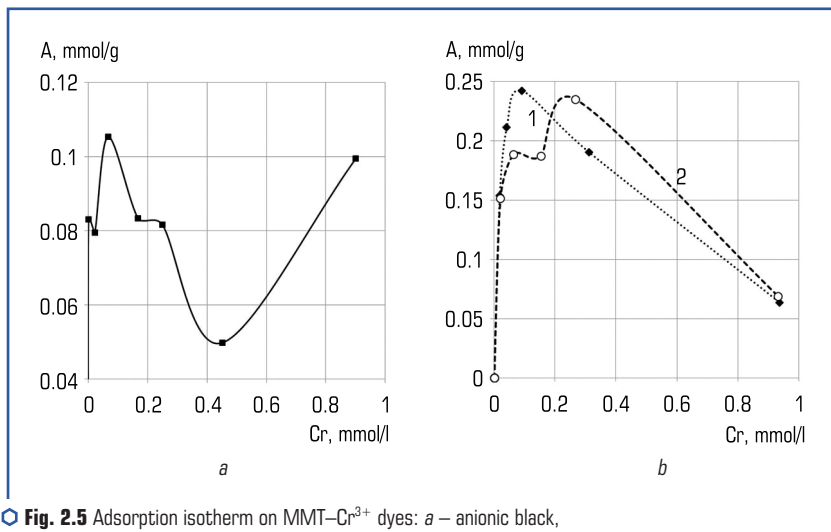
- the presence of a sufficiently long chain of conjugated bonds in the polarized dye molecule;
- linear and coplanar structure of the dye;
- the presence of substituents in the structure for a positive conjugation effect in dye molecules;
- the presence of active groups in dyes capable of forming a coordination bond with chromium compounds introduced into the montmorillonite dispersion for the purpose of cationization.

For adsorption on the cationic surface of montmorillonite, the most typical anionic dyes for leather production were used: anionic dark green; anionic black; anionic blue (**Table 2.6**). Anionic dyes or azo dyes are mono-, di-, or triazo compounds of a cyclic structure with active hydroxyl, amine, nitro, and sulfo groups. The dye molecule contains one or more azo groups -N=N- that bind two or more aromatic radicals.

● **Table 2.6** Physicochemical characteristics of dyes

Dye / molecular weight	Structural formula
Anionic dark green, Mr 863	
Anionic black, Mr 859	
Anionic blue Mr 637	

Quantitative assessment of the adsorption of anionic black, anionic blue, and anionic dark green dyes to MMT-Cr³⁺ [30, 31] is represented by isotherms of dye adsorption on the surface of modified montmorillonite (**Fig. 2.5**).



○ **Fig. 2.5** Adsorption isotherm on MMT- Cr^{3+} dyes: *a* – anionic black, *b* – anionic dark green (curve 1) and anionic blue (curve 2)

It should be noted that the nature of adsorption for all dyes corresponds to the Langmuir curve. At the beginning, the curves are characterized by rapid growth, the dye molecules are adsorbed on the surface of the montmorillonite particles due to the electrostatic interaction of the chromium cation with the dye anion. Next, the peak of the curve is reached, the surface of the mineral is saturated with dye molecules and the surface charge of montmorillonite is neutralized. The interaction with montmorillonite is completed by polymolecular dye adsorption due to Vander-Waals forces [30, 31].

Comparison of adsorption isotherms of different dyes (**Fig. 2.5**) indicates the maximum adsorption of anionic dark green (**Fig. 2.5, b, curve 1**). Despite the fact that the adsorption of all dyes increases, the smallest adsorption maximum is observed for an anionic black dye (**Fig. 2.5, a**). This is explained by earlier micelle formation in anionic black solutions. It is steric complications that explain the fact of a lower level of adsorption of dyes from micellar solutions than from molecular solutions. But increasing the concentration of anionic black above 0.4 mmol/g causes rapid polymolecular adsorption, which is positive when obtaining a pigment [30, 31].

An increase in the concentration of anionic blue and anionic dark green dyes (**Fig. 2.5, b**) causes a further decrease in the dye adsorption level, which may be due to the predominant micelle formation.

It should be noted that for all the selected anionic dyes, it was established to obtain colored modified montmorillonite dispersions (MMT-AD) of saturated, intense color, especially in the case of using the anionic black dye.

In order to identify the optimal conditions for obtaining colored modified montmorillonite dispersions as nanopigments, the influence of pH of the environment on the efficiency of sorption of anionic dyes by the surface of modified montmorillonite was investigated [30, 31]. The presented data (**Fig. 2.6**) show that the maximum adsorption occurs in the range of pH 5–6.5, which is consistent with the data in **Fig. 2.6**.

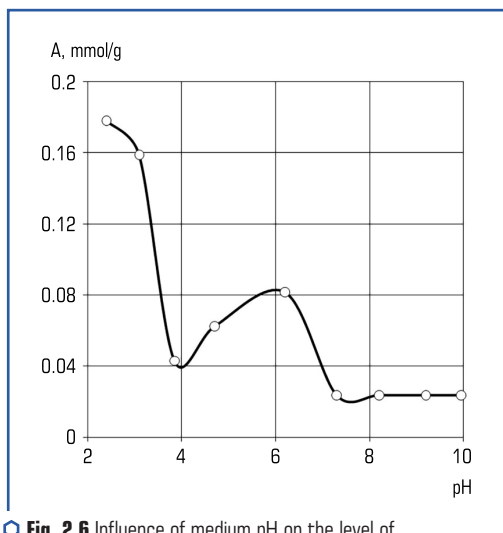


Fig. 2.6 Influence of medium pH on the level of adsorption of anionic black on MMT-Cr^{3+}

The high level of anionic black adsorption in the range of pH 2.0–4.0 is due to inhibition of the dissociation of acidic functional SO_3H groups on the surface of MMT-Cr^{3+} , a sharp decrease in solubility and precipitation of the dye. The decrease in adsorption and its plateau when $\text{pH} \geq 7$ shifts to a more alkaline zone is associated with the transformation of the composition of chromium (III) complexes and the recharging of the montmorillonite surface from cationic to anionic, which indicates a change in the sign of the surface charge from positive to negative. On the positive side, it should be noted that the adsorption of anionic black on the surface of the cationic form of montmorillonite is stable within pH 3–10, while no desorption of the dye was detected.

Spectroscopic studies of MMT-Cr^{3+} revealed the following characteristic absorption bands, taking into account the fact that the studied silicate molecules contain hydroxyl groups, silicon oxide groups, and a chromium complex (**Fig. 2.7, 2.8**) [32].

The interpretation of the bands characteristic of silicates was carried out by isolating the characteristic bands associated with the vibrations of the Si-O group, which lies in the region

of 1034 cm^{-1} and $798\text{--}779\text{ cm}^{-1}$. In the spectra of the azo dye and MMT-Cr^{3+} there are bands of functional groups capable of forming hydrogen and van der Waals bonds between the dye and exchangeable cations of montmorillonite.

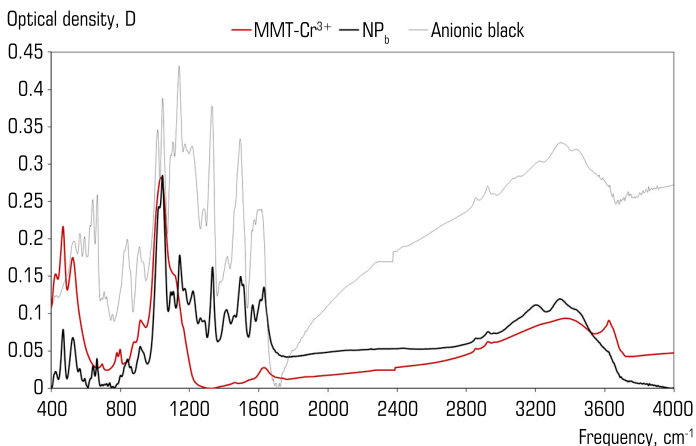


Fig. 2.7 Absorption spectra of MMT-Cr^{3+} montmorillonite, black nanopigment and anionic black dye

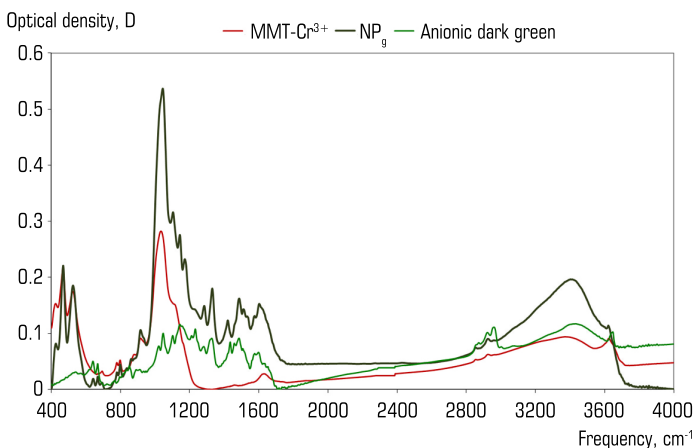


Fig. 2.8 Absorption spectra of MMT-Cr^{3+} montmorillonite, dark green nanopigment and anionic dark green dye

As can be seen from **Fig. 2.8**, a number of differences are observed in the spectra of the green nanopigment (NPg) compared to MMT-Cr³⁺. Bands identical to the azo dye appear at 3621 cm⁻¹, 3401 cm⁻¹ corresponding to bound hydroxyl groups, and a broad band at 3600–3100 cm⁻¹ characteristic of hydroxyl groups of water of crystallization. There is also a shift of the 1629 cm⁻¹ band to the lower frequency zone for the refinery, which characterizes the deformation oscillations of the H-O-H group, found in the spectrum of montmorillonite.

The appearance of a band in the region of 1510 cm⁻¹, and an increase and shift of the vibration bands at 1231 cm⁻¹ and 1021 cm⁻¹ to the low-frequency region by 60 and 100 cm⁻¹, respectively, as well as an increase in the intensity of the pigment concentrate bands at 1143 cm⁻¹ and 1104 cm⁻¹, which are characteristic for the oscillation of the -O-NO₂, -O-NH₂, SO₃H groups, probably indicate van der Waals bonds between the indicated functional groups of the dye and the oxygen atom of montmorillonite.

To evaluate the interaction of azo dye and MMT-Cr³⁺, a comparative analysis of the optical densities of the absorption bands of MMT-Cr³⁺ and NP (**Table 2.7**) was performed using the internal standard method. The band 2925 cm⁻¹ was chosen as standard bands for frequencies 4000–2500 cm⁻¹, and 916 cm⁻¹ for frequencies 1900–400 cm⁻¹, which are characteristic of valence and deformation vibrations of CH groups. Such changes in optical densities, as well as broadening and shifting of the corresponding bands on the NP spectra, indicate the formation of new bonds with the participation of functional groups of dyes and MMT-Cr³⁺.

As can be seen from the **Table 2.7**, on the spectra of the black nanopigment (NPb) with an anionic black dye, mainly in the region of 1629–600 cm⁻¹, changes in the optical densities of the characteristic bands of the -SO₃H, -ONO₂, -ONH₂ groups are observed.

The amino group, one of the most reactive, is manifested at frequencies of 3339 cm⁻¹ and 3202 cm⁻¹ by valence vibrations of NH groups. The hydroxyl group is manifested by valence vibrations at 3435 cm⁻¹ and 3339 cm⁻¹ and deformation vibrations at 1629 cm⁻¹.

The mechanism of obtaining colored dispersions of montmorillonite as the NP basis for leather decoration by successive modification of montmorillonite with sodium carbonate, basic chromium sulfate, and anin dyes is presented in the diagram (**Fig. 2.9**).

According to the proposed scheme, native montmorillonite is treated with sodium salts to disperse the aggregates and expand the distance between the aluminosilicate layers, which is confirmed by X-ray structural analysis and the values of the basal interplanar distance of MMT. Further treatment of MMT-Na⁺ with chromium hydroxocomplexes leads to the formation of MMT-Cr³⁺ with a turbostratic highly developed structure, which is accompanied by wedging of the marginal areas of the aluminosilicate layers of MMT and an increase in the adsorption surface of montmorillonite to the level of 280 m²/g.

At the same time, the montmorillonite layers have a cationic surface charge at the level of +4.5–13.5 mV in the range of pH 4.3–6.2. The maximum value of +19.0 mV the level of the cationic charge of the MMT-Cr³⁺ surface reaches at pH 5.4. Subsequently, effective adsorption grafting of anionic dyes occurs on the surface of highly developed MMT-AD as the basis of nanopigments.

● **Table 2.7** Change in optical densities in the spectra of modified montmorillonite

Band, cm ⁻¹	Group	Optical density, D/Ds		
		MMT–Cr ³⁺	NPg	NPb
3732–3621	NH, OH	1.43	1.18	0.65
3401–3339	NH ₂ , NH val., OH val., OH bound	1.5	1.58	1.45
3202	NH ₂ , NH val	–	1.45	–
2855	C–H val., OH crystal	–	0.88	0.88
1629	H–O–H def.	0.31	2.5	–
1608–1602	C=C arom., NO ₂ as., C–N=N–C	–	2.14	2.04
1575–1564	C=C arom., NH ₂ def.	–	2.14	1.69
1510	NH ₂ def.	–	–	2.5
1494–1486	C=C arom	–	2.68	2.5
1460	C=C arom, C=N	–	1.75	–
1420–1413	C=C arom, C=N	–	1.96	1.79
1330	NO ₂ val., sym.	–	2.86	2.86
1284–1261	OH, R–SO ₃ H, –SO ₂ [–] val.	–	1.61	1.61
1218	O–NH ₂	–	2.32	–
1171	–SO ₂ –N, C–NO ₂ , O–NH ₂	–	2.32	2.32
1143	–SO ₂ –N, C–NO ₂ , O–NH ₂	–	3.21	3.21
1104	O–SO ₂	–	2.32	2.32
1045–1034	OH, –SO ₃ –H val., Si–O	3.2	5	5
916	OH, C–N=N–C	1	1	1
840–862	O–NH ₂	–	0.71	0.5
797	CH arom., (Si–O) ₄	0.55	–	0.3
780	CH arom., (Si–O) ₄	0.53	–	0.11
737	CH arom., (Si–O) ₄	–	0.13	–
694	CH arom., (Si–O) ₄	0.36	0.09	0.09
663–668	(Si–O) ₄ , Cr ⁺³	–	1.24	0.4
642	O–NH ₂ , O–NO ₂ def, monosub. benzene ring	–	0.23	0.5
593–564	O–NH ₂ , O–NO ₂ def, m monosub. benzene ring	–	0.46	–
524	(Si–O) ₄ , Cr ⁺³	1.94	1.21	1.12
468	(Si–O) ₄ , Cr ⁺³	2.39	1.41	1.41
425	(Si–O) ₄ , Cr ⁺³	1.11	0.04	0.35

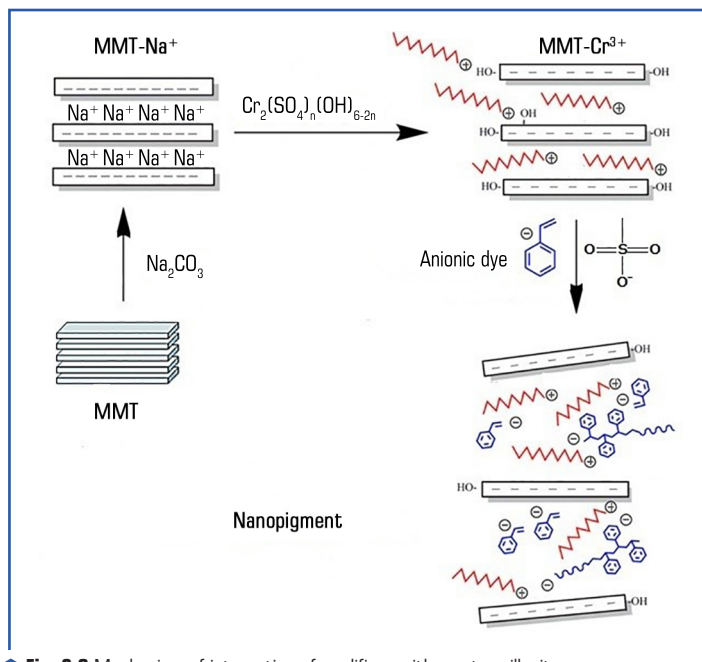


Fig. 2.9 Mechanism of interaction of modifiers with montmorillonite

The obtained results of structural and electro-surface changes of montmorillonite indicate the expediency of mineral modifications by sequential treatment with multifunctional substances to obtain nanopigments for leather decoration.

The diagram of the stages of obtaining a nanopigment is presented in **Fig. 2.10**. Nanopigments were prepared by gradually mixing the modified cationic form of montmorillonite with a dye. Mixing was carried out using a mechanical stirrer at a certain temperature to obtain time-stable dispersions in the form of nanopigments of a saturated deep color. The pH of the obtained nanopigments is 5.8–6.0.

According to the chemical composition, the nanopigment contains montmorillonite, sodium salt, basic chromium sulfate, anionic dye and water in the following ratio of components, by weight. %:

- montmorillonite – 10;
- sodium salt – 0.6;
- basic chromium sulfate in terms of Cr_2O_3 – 1.0–1.2;
- anionic dye – 10.

For comparison with typical pigment concentrates used in the practice of finishing natural leather, the chemical composition and variants of the obtained nanopigments are presented (**Table 2.8**).

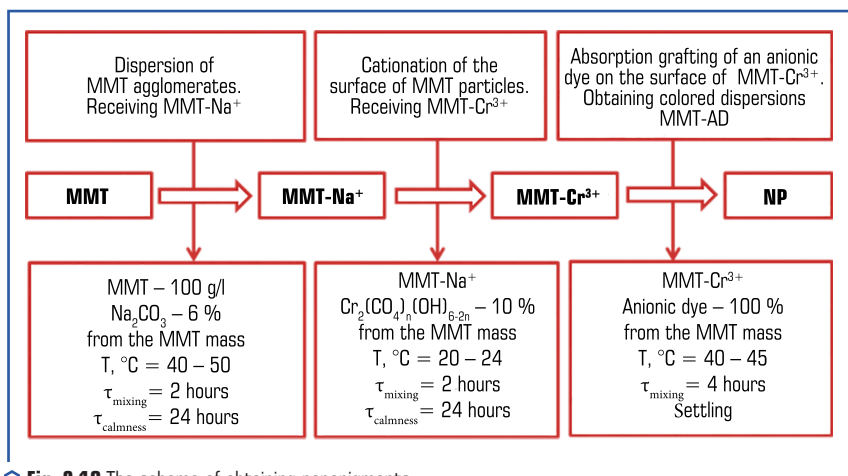


Fig. 2.10 The scheme of obtaining nanopigments

Table 2.8 Chemical composition of nanopigments for leather decoration

Components, mass %	NP	
	NPb	NPg
Montmorillonite	10	10
Sodium carbonate	0.6	0.6
Basic chromium sulfate *	1.0	1.0
Black anionic dye	10	–
Dark green anionic dye	–	10
Water	78.4	78.4

Note: *in terms of Cr₂O₃

Table 2.9 shows the properties of nanopigments. According to the results of the evaluation of the NP quality indicators, it was established that the nanopigments are characterized by high curvature and stability over time, their delamination is not observed for 24 hours or more.

In general, nanopigments are characterized by high covering, stability over time, which will allow to reduce the thickness of the covering film during leather finishing and obtain a covering with high quality indicators in terms of adhesion to dry and wet leather, resistance of the covering to multiple bends, dry and wet friction while reducing the cost of nanopigments and reducing the cost of covering paint for decoration. At the same time, an expansion of the range of NPs for leather finishing is ensured.

● **Table 2.9** Properties of nanopigments for leather decoration

Quality indicators	NP		
	NPb	NPg	Analogue
Color of pigment concentrate	Black	Dark green	Black
Dry residue of pigment concentrate, %	22.9	20.1	16.5
Curvature of pigment concentrate, g/m ²	9.1	9.5	11.0
Sedimentation of pigment concentrate, %	95.6	95.5	87.7
Color uniformity, points	5	5	5

Note: *studies were carried out on samples without fixation

2.3 APPLICATION OF NANO PIGMENTS FOR POLYMER-MINERAL LEATHER DECORATIONS

The polymer is used in covering compositions as a film former to create a uniform protective covering on the surface of the leather of a certain color or shade. However, in the process of using leathers, for example, as parts of the uppers of shoes, furniture, clothes, etc., significant physical and mechanical loads, repeated bending and bending, abrasion in dry and wet conditions, stretching, etc. occur. Because of this, the required level of operational properties of the covering on the leather depends on the physico-mechanical and physico-chemical parameters of the covering films [33]. In this regard, one of the ways to improve the quality of the covering on the leather is the use of nanopigments, which would allow correcting and purposefully forming a complex of physical and mechanical indicators of the polymer covering of the leather.

To study the effect of the developed nanopigments on the structure and properties of the polymer film former, nanopigments of black (NPb) and dark green (NPg) colors were used.

As a film former, an acrylic polymer was used – copolymer acrylic emulsion MBM–3 (aqueous dispersion of methacrylate copolymer), butyl acrylate and methacrylic acid in the amount of 3.0 % by weight of monomers [12]. The molecular structure of the copolymer determines sufficient elasticity and strength of the polymer in the temperature range necessary for covering on the leather. The emulsion is characterized by a high molecular weight, which determines the film-forming ability necessary for the covering. Dry residue MBM–3 – 38.5 %, pH – 4.35.

The introduction of nanopigments into the composition of the polymer matrix can purposefully adjust the quality of the finishing covering on the leather. It can be predicted that the mineral particles of nanopigments, having a high sorption surface and exchange capacity, will be able to adsorb on their surface and interact with the active groups not only of the dye used to modify the mineral dispersion, but also with polymer acrylic emulsions [34, 35].

The study of the effect of nanopigments on the physical and mechanical properties of polymer acrylic matrices (**Fig. 2.11**) indicates structural and elastic changes in the parameters of polymer films under conditions of varying degrees of loading and elongation. The introduction of

montmorillonite into the polymer matrix (concentration of montmorillonite C-MMTb and C-MMTg, respectively, according to the color of the pigment) in the form of NPs helps to increase the strength (σ) of polymer films. The maximum level of strength of the films is achieved at consumption of 1.5–2.0 % of montmorillonite from the dry polymer residue (**Fig. 2.11, a, c**). The introduction of NPb and NPg increases the modulus of elasticity of the films by 3.5 times, as evidenced by the strength indicators of the films at 100 % elongation (**Fig. 2.11, a, c, curve 1**).

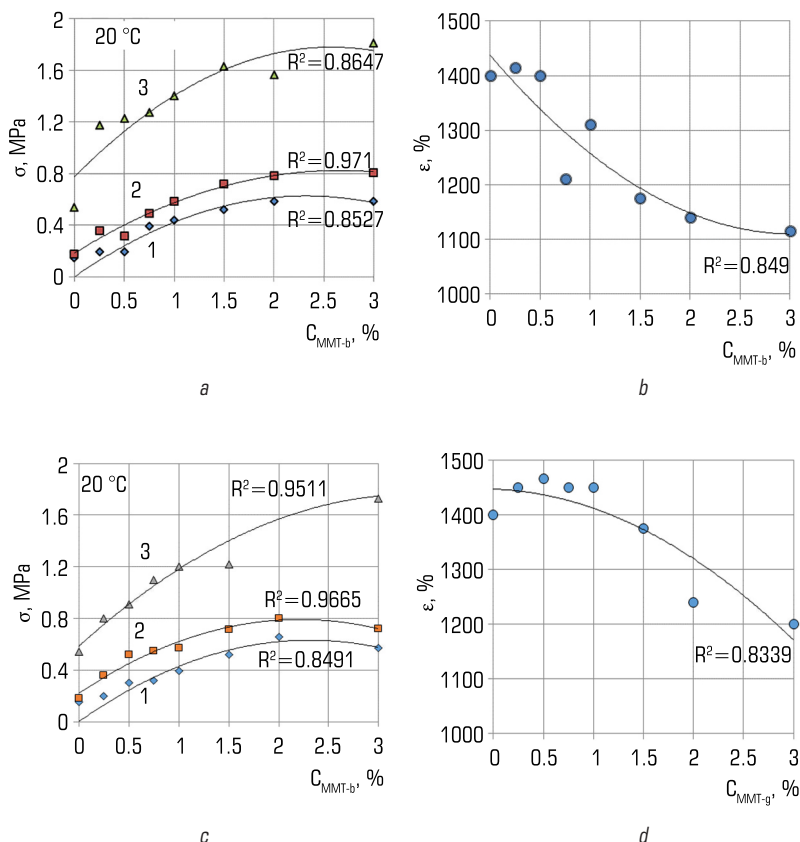


Fig. 2.11 Changes in the physical and mechanical properties of polymer films as a result of the addition of black (*a, b*) and green (*c, d*) nanopigments at elongation 100 % – 1, 300 % – 2, and break – 3

For the indicated consumption, the level of strength at the break (**Fig. 2.11, a, c, curve 3**) in the case of the use of NPb dispersion increases to the level of 1.6 MPa, and in the case of the use of NPb – to 1.7 MPa. Compared to the strength indicators of the native polymer film (0.54 MPa), as a result of the modification of the polymer with NPb and NPg dispersions, it is possible to achieve its strengthening by almost 3 times. A significant increase in the break strength indicators (**Fig. 2.11, a, c, curve 3**) of polymer films is associated with conformational strengthening of the polymer structure due to the formation of strong compact crosslinks with the participation of active functional groups of the polymer and azo dyes in the composition of colored montmorillonite dispersions. Also, the introduction of nanoparticles [31] of montmorillonite in the composition of NPb and NPg with a characteristic highly developed sorption surface of mineral particles contributes to the physical adsorption of the polymer and the corresponding stabilization of its structure.

A further increase in the consumption of montmorillonite in the polymer matrix above 2.5 % slightly reduces the level of strength of the polymer films. Due to the introduction of a significant number of adsorption centers of montmorillonite, more structuring of the polymer occurs, which leads to a decrease in its film-forming ability due to a significant content of mineral particles.

The introduction of a mineral in the polymer matrix as part of NPb and NPg contributes to the correction of the relative elongation of the films (ϵ) (**Fig. 2.11, b, d**). The structuring of the polymer matrix by montmorillonite with a consumption of 2.0–3.0 % manifests itself in a decrease in the relative elongation index to the level of 1100–1200 %. In the case of application of NPg dispersion in the range of 0.25–1.5 % of the polymer mass, a slight (by 3.0–3.5 %) increase in elasticity and corresponding elongation of polymer films is observed. A further increase in the consumption of NPg dispersion to the level of 2.0 % leads to a decrease in the relative elongation of polymer films by 11.5 % (**Fig. 2.11, d**). In the case of using NPb, a gradual decrease in relative elongation is characteristic already at consumption above 0.5 % of the polymer mass (**Fig. 2.11, b**). The maximum reduction of the relative elongation to the level of 1180–1200 % is typical for NPb consumption in the range of 1.5–3.0 % of the dry polymer residue.

Such changes in the physical and mechanical properties of polymer films are positive in the formation of a covering on the surface of the leather with high resistance to operational loads, abrasion and repeated bending. Because the difference in elongation and significant ductility of polymer films can have a negative effect on the quality of leather decoration due to the characteristic differences in the physical and mechanical loads of the polymer matrix and the collagen structure [31–33].

Due to the highly developed sorption surface, nanoparticles of modified montmorillonite adsorb the polymer, stabilize its structure and increase the colloidal stability of the polymer-mineral composition (**Fig. 2.12**). Such polymer compositions are effective for forming the finishing covering of elastic leathers for various purposes [34–36].

It was also established that montmorillonite as part of a nanopigment can improve the physical and mechanical properties of the polymer covering and increase its heat resistance [35].

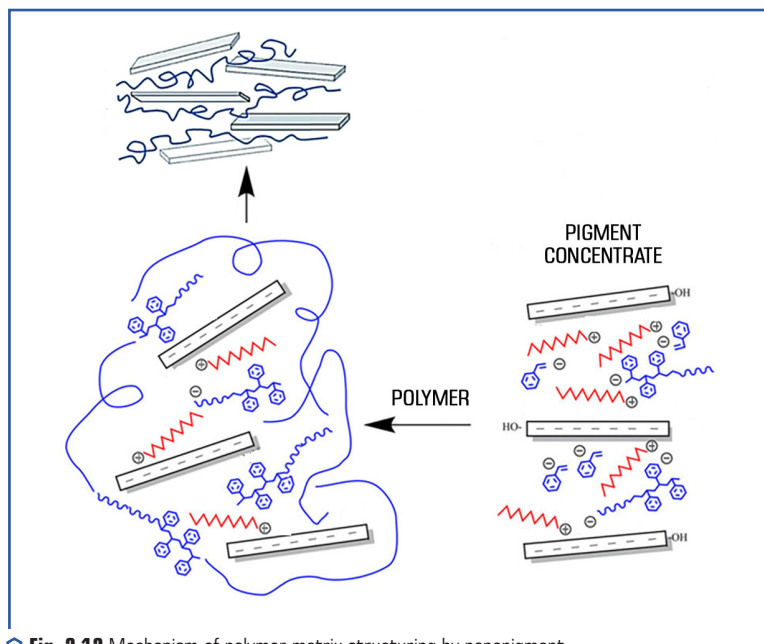


Fig. 2.12 Mechanism of polymer matrix structuring by nanopigment

In general, MMT consumption at the level of 1.5–2.0 % (based on the mass of montmorillonite from the mass of dry polymer residue) is appropriate for creating a high-quality polymer-mineral covering on the leather, resistant to operational loads.

Further research made it possible to optimize the composition of the covering composition based on film-formers and nanopigment to improve the quality indicators of the leather finishing covering [37]. To optimize the composition, the method of simplex-lattice planning was used [38].

Covering compositions were prepared for the research, including NPch and NPz nanopigments and film formers. A film former with a high modulus of elasticity (soft polymer) and a film former with a low modulus of elasticity (hard polymer) were used as film formers. Polyacrylate SMITCRYL 2100 (Smit & Zoon) was chosen as a soft polymer – highly elastic, flexible, with high covering capacity, the covering of which is characterized by resistance to water and cracks at low temperatures, as a hard polyurethane PUR 3365 FF (Codyeco, Smit & Zoon) – high strength, resistant to physical and mechanical loads, friction and wear.

When studying the properties of the mixture, which depend only on the ratio of components, the factor space is a correct simplex [38, 39]. For such systems, the ratio is performed when the sum of the relative concentrations of all components of the mixture is equal to 1. The relative concentration of each component varies from 0 to 1, that is, within 0–100 %.

It is known [3, 7, 37] that a significant content of pigment in the covering causes an increase in its hardness, but insufficient content negatively affects the covering ability of the covering. Therefore, the following intervals for changing the concentration of components in the studied composition [13, 38] were chosen: pigment (x_1) – 0–30 %, hard film former (PUR 3365 FF) (x_2) – 0–100 %, soft film former (SMITCRYL 2100) (x_3) – 0–100 %. The parameters of the covering films were selected as response functions: Y_1 – modulus of elasticity at 100 % elongation, MPa; Y_2 – tensile strength, MPa; Y_3 – relative elongation at break, %; Y_4 – covering adhesion to the leather, N/m; Y_5 – covering resistance to wet friction, rotation.

If there are restrictions on changes in the concentrations of some components (for example, pigment) in the mixture, the local area on the diagram represents an irregular simplex. In this case, renormalization is carried out and the compositions at the vertices of the local simplex are taken as pseudo-components (z_1, z_2, z_3) so that the condition (2.1) is fulfilled:

$$\sum_{i=1}^q x_i = 1, \quad (2.1)$$

where $x_i \geq 0$ – component concentration; q – the number of components.

Planning the experiment and obtaining its mathematical model were performed in the coordinate system of pseudo-components. To conduct the experiment, the transition from pseudo-components z_1 to initial components x_1 was performed. The plan of the experiment and the values of the response functions are given in the **Table 2.10**.

● **Table 2.10** Characteristics of the experimental plan

Experiment No.	Plan						Y_1	Y_2	Y_3	Y_4	Y_5
	z_1	z_2	z_3	x_1	x_2	x_3	MPa	MPa	%	N/m	Revolutions
1	1	0	0	30	0	70	9.6	9.7	110	160	40
2	0	1	0	0	100	0	2.1	12.6	990	320	120
3	0	0	1	0	0	100	0.43	4.8	1285	160	230
4	0.7236	0.2764	0	21.71	27.64	50.65	4.9	5.9	250	180	20
5	0.2764	0.7236	0	8.29	72.36	19.35	2.8	6.3	625	240	50
6	0.7236	0	0.2764	21.71	0	78.29	4.1	10	610	200	20
7	0.2764	0	0.7236	8.292	0	91.71	1.34	5.1	750	320	40
8	0	0.7236	0.2764	0	72.36	27.64	1.63	7.1	825	225	80
9	0	0.2764	0.7236	0	27.64	72.36	0.8	4.35	1070	230	130
10	0.3333	0.3333	0.3334	10.00	33.33	56.67	2.03	6.35	690	195	40
11	0.22	0.56	0.22	6.6	56	37.4	2.0	6.6	915	290	40
12	0.44	0.12	0.44	13.2	12	74.8	2.4	8.4	700	290	20

A polynomial of the third order (3.2) was used as a model for a three-component system:

$$y = \beta_1 x_1 + \beta_2 x_2 + \beta_3 x_3 + \beta_{12} x_1 x_2 + \beta_{13} x_1 x_3 + \beta_{23} x_2 x_3 + \gamma_{12} x_1 x_2 (x_1 - x_2) + \gamma_{13} x_1 x_3 (x_1 - x_3) + \gamma_{23} x_2 x_3 (x_2 - x_3) + \beta_{123} x_1 x_2 x_3, \quad (3.2)$$

where x_i is the concentration of components; β_i , β_{ij} , γ_{ij} , β_{ijk} – the corresponding polynomial coefficients, and $1 \leq (i, j, k) \leq 3$; $i \neq j \neq k$.

The resulting models of the output variables have the following form:

Model 1. $Y_1 = 9.6z_1 + 2.1z_2 + 0.43z_3 - 9.9998z_1z_2 - 11.475z_1z_3 - 0.25z_2z_3 - 7.0102z_1z_2(z_1 - z_2) - 7.4955z_1z_3(z_1 - z_3) + 0.46498z_2z_3(z_2 - z_3) + 10.814z_1z_2z_3$.

Model 2. $Y_2 = 9.7z_1 + 12.6z_2 + 4.8z_3 - 25.25z_1z_2 + 1.5z_1z_3 - 14.875z_2z_3 + 5.0138z_1z_2(z_1 - z_2) + 15.142z_1z_3(z_1 - z_3) - 4.1265z_2z_3(z_2 - z_3) + 43.425z_1z_2z_3$.

Model 3. $Y_3 = 100z_1 + 990z_2 + 1285z_3 - 537.49z_1z_2 - 62.499z_1z_3 - 949.99z_2z_3 + 128.62z_1z_2(z_1 - z_2) + 2179.8z_1z_3(z_1 - z_3) - 632.12z_2z_3(z_2 - z_3) + 1905.1z_1z_2z_3$.

Model 4. $Y_4 = 160z_1 + 320z_2 + 160z_3 - 150z_1z_2 + 499.99z_1z_3 - 62.499z_2z_3 + 64.579z_1z_2(z_1 - z_2) - 670.83z_1z_3(z_1 - z_3) - 427.95z_2z_3(z_2 - z_3) - 1357.5z_1z_2z_3$.

Model 5. $Y_5 = 40z_1 + 120z_2 + 230z_3 - 225z_1z_2 - 524.99z_1z_3 - 349.99z_2z_3 + 32.289z_1z_2(z_1 - z_2) + 363.19z_1z_3(z_1 - z_3) - 4.5169z_2z_3(z_2 - z_3) + 869.95z_1z_2z_3$.

The adequacy of the obtained equations was checked using the Student's t-test, using 2 control points (experiment number 11–12) of the experimental plan (Table 2.10). With the number of experiments $N = 12$, the number of parallel experiments $n = 5$ and the level of significance $p = 0.05$, the tabular value of the Student's criterion $tt = 2.17$. For all control points, the t-ratio is less than the tabular one, that is, models (1–5) are adequate [37–39].

For the practical use of the results of the analysis of regression models, the transition from pseudo-coordinates to natural variables was performed using formulas for transferring coordinates from one system to another [37]. Using the calculated formulas of the connection between the coordinates z_i and x_i :

$$x_1 = 0.3z_1; \quad x_2 = z_2; \quad x_3 = 1 - 0.3z_1 - z_2 = 1 - x_1 - x_2;$$

the optimal ratios of the components of the covering composition in the initial (natural) coordinates and the optimal values of each output variable are determined.

The problem of optimization of processes characterized by several feedbacks, as a rule, is reduced to optimization according to one criterion with constraints in the form of equations and inequalities. Depending on the response surface and the nature of the constraints, a number of methods are used for optimization. One of the most successful ways to solve the optimization problem with a large number of responses is to use the so-called Harington criterion or the generalized desirability function D as a generalized optimization criterion, as well as the fair trade-off method. To construct a generalized desirability function D , the measured feedback values were converted

into a dimensionless scale of desirability d using the method of quantitative assessments with an interval of desirability values from zero to one. The value $d=0$ (or $D=0$) corresponds to an absolutely unacceptable value of this response; $0.63-0.79$ = good; $0.80-0.99$ = very good value; and $d=1$ (or $D=1$) = the best response value, and its further improvement is either impossible or unreasonable [38].

As can be seen from **Fig. 2.13**, the generalized desirability function D has a maximum value of $D=0.60-0.65$ in the specified region of the simplex, which characterizes this region of the simplex as the region of optimal values of the initial variables, and allows optimization of the composition of the covering composition with high reliability.

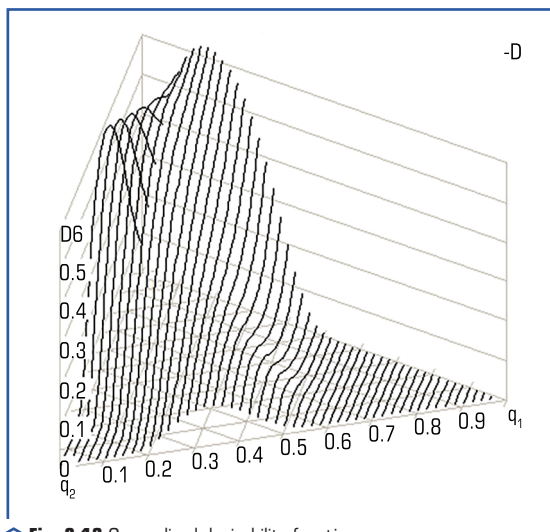


Fig. 2.13 Generalized desirability function

If a certain process is described by several regression equations and the results of several output variables are important, then in this case a compromise problem should be solved – to determine the extreme value of one output variable under the conditions of restrictions imposed on others and on the border of the research areas (fair compromise method). Optimum parameters, which are achieved when such conditions are met, are called conditional or relative, and the area of process parameters, within which the output variables that satisfy all the specified requirements are obtained, are called the rational or compromise area [38, 39]. The peculiarity of the optimization method is that by changing the limits of the initial variables, it is possible to adjust the ratio of the components of the covering composition in order to obtain the initial variables, taking into account the technological requirements for the formation of the covering on the leathers of a certain assortment.

Determination of the optimal (rational) composition of the covering composition was carried out by means of multi-criteria optimization using a graphical method based on the curves of equal values of the covering indicators Y_1 – Y_5 on the plane of the regular simplex (**Fig. 2.14**).

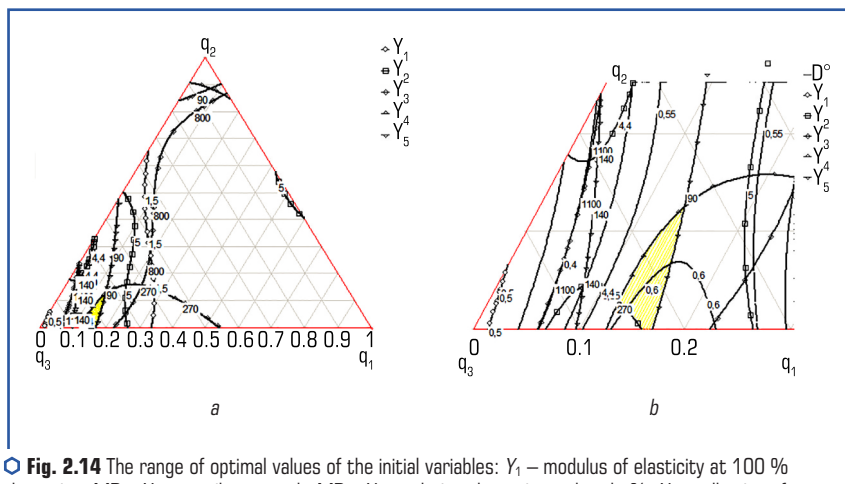


Fig. 2.14 The range of optimal values of the initial variables: Y_1 – modulus of elasticity at 100 % elongation, MPa; Y_2 – tensile strength, MPa; Y_3 – relative elongation at break, %; Y_4 – adhesion of the covering to the leather N/m; Y_5 – covering resistance to wet friction, rotation

Taking into account the special requirements for covering leathers for the upper of shoes, namely strength, adhesion to the leather and resistance to wet friction, the following restrictions of minimum and maximum values were imposed on the output variables: $Y_1=0.5$ – 1.5 MPa; $Y_2=4.4$ – 5.0 MPa; $Y_3=800$ – 1100 %; $Y_4=270$ – 300 N/m; $Y_5=90$ – 140 revolutions.

As a result of the optimization, optimal ratios of the components of the covering composition were obtained, which provide the covering film with the necessary quality indicators [37].

The optimal composition of the covering composition (%):

- nanopigment – 4.5–5.0;
- urethane film former PUR 3365 FF – 3.0–5.0;
- acrylic film former SMITCRYL 2100 – 90.0–92.5.

The use of this covering composition ensures the formation of a covering on the leather with the following quality indicators: $Y_1=0.96$ – 1.06 MPa; $Y_2=4.4$ – 4.5 MPa; $Y_3=900$ – 915 %; $Y_4=280$ – 290 N/m; $Y_5=100$ – 110 revolutions.

To confirm the results of the optimization of the composition of the covering paint, a covering paint of the optimal composition was prepared and the front surface of the leathers was decorated. The results of studies of the quality of the leather finishing covering are given in **Table 2.11**.

● **Table 2.11** Indicators of the quality of leather covering

№	Covering quality indicators	Value	
		calculated	experimental
1	Modulus of elasticity σ_{100} , MPa	0.98	1.1
2	Tensile strength limit σ_p , MPa	4.48	4.65
3	Relative elongation at break, ε %	915	905
4	Adhesion of the covering to the leather, N/m: – dry; – wet	285 –	300 185
5	Covering resistance to: – wet friction, spins; – multiple bends, thousands of bends	100 –	110 <100000
6	Air permeability, $\text{cm}^3/\text{cm}^2 \times \text{h}$	–	42.3
7	Evenness of color, points	–	5
8	Color fastness to wet rubbing, score	–	5

The obtained experimental data (**Table 2.11**) correlate with the calculated data of mathematical modeling, which confirms the reliability of the optimization results and indicates the high quality of the developed covering on the leather. A slight difference between the experimental and calculated indicators of the quality of the covering may be related to the conditions of the formation of the covering film.

Later, taking into account the results of the optimization of the covering paint composition [37], leathers were decorated with covering compositions of black and dark green colors based on nanopigments and the quality indicators of the obtained leathers were evaluated (**Table 2.12**).

A characteristic feature of the covering according to the developed formulations is high hiding power. With a minimum consumption of covering paint at the level of 33.7–33.8 g/m², it is possible to achieve a complete uniform coloring of the leather surface. At the same time, the minimum thickness of the covering film and high color uniformity at the level of maximum points are obtained. It should be pointed out a sufficiently high level of air permeability for leathers after polymer-mineral finishing, which indicates increased hygienic properties. Since the presence of a mineral component in the polymer composition and obtaining an exfoliative type of composite allows to avoid the creation of a monolithic polymer covering layer on the surface of the leather.

Dark green coverings are characterized by adhesion to dry leather at the level of 360 N/m, to wet leather at 190 N/m and high resistance to wet friction at the level of 385–390 revolutions, which depends on the nature of the interaction of montmorillonite particles with an anionic dye and on the level structuring and plasticizing covering paint based on film formers. The formation of a black covering on the leather is characterized by high values of adhesion to dry and wet leather at the level of 380 N/m and 205 N/m, the indicators for the dark green covering are slightly lower,

but not significantly – 360 N/m and 190 N/m for the corresponding type of adhesion that, in general, meets the requirements of the standards.

● **Table 2.12** Indicators of quality of covering and finished leathers

№	Covering quality indicators	Covering colour		
		Black	Dark green	DSTU 2726-94 [22]
1	Adhesion of the covering to the leather, N/m: – dry; – wet	380 205	360 190	100/200 50/100
2	Covering resistance to: – wet friction, rotation; – multiple bending, points	390 5	385 5	60 >3
3	Air permeability, $\text{cm}^3/\text{cm}^2 \times \text{h}$	42.3	41.5	–
4	Evenness of color, points	5	5	–
5	Color fastness to wet rubbing, score	5	5	–
6	Covering ability of the covering, g/m^2	33.7	33.8	–
7	Thickness of the covering film, g/m^2	13.5	15.1	–

The analysis of the obtained indicators indicates the formation of a thin-layer, uniformly colored covering with a high level of air permeability and operational stability, which indicates the feasibility of using the proposed nanopigments as part of a polymer-mineral covering for the formation of a finishing film on the front surface of leathers. This covering allows to enhance the effect of "naturalness" of the leather surface, volume, graininess and fullness of the network. At the same time, the high level of adhesion to the leather surface, the elasticity and strength of the film based on the polymer-mineral composition creates a high-quality covering and ensures its resistance to repeated bending and wet loads.

In general, it can be concluded that the use of nanopigments based on modified montmorillonite makes it possible to obtain a high-quality leather covering with good performance indicators at a reduced cost of covering paint for decoration, allows to purposefully regulate the technological processes of leather production related to providing the necessary color range, level and depth of color and its resistance to external influences.

CONCLUSIONS

1. The work is devoted to the development of nanopigments based on montmorillonite for polymer-mineral decoration of natural leather.

2. According to the analysis of the dynamics of Ukraine's foreign trade activity, key trends in the development of the leather industry in the production of leather with a natural face surface have been identified as the most competitive and in demand on the world market.

3. The role of leather decoration through the rational selection of film-forming materials and pigments of different nature in the formation of high performance indicators of leather is shown. It has been proven that modern approaches in covering leather are based on the principles of using compact finishing, which involves an improved composition of covering compositions, a reduction in covering thickness, a rational selection of film-formers and pigments with high covering ability and compatibility.

4. The influence of sequential modification of aqueous dispersions of montmorillonite with cationic and anionic compounds was established, and the change in structural and charge characteristics of mineral dispersions after dispersion and cationization of the surface of mineral particles for intensive attraction of molecules of the dispersion medium of anionic dyes was proved. The maximum level of adsorption of anionic black and dark green dyes on the cationic surface of montmorillonite occurs in the range of pH 5–6.5 and is characterized by stability in the range of pH 3–10, which is explained by the presence on the surface of modified montmorillonite of chromium cations with strong complexing ability and susceptibility to chemical and physico-chemical interactions between oxygen atoms of the mineral and nitro-, amino- and sulfo groups of dyes due to the formation of hydrogen and van der Waals bonds.

5. The mechanism of obtaining colored dispersions of montmorillonite was substantiated and the composition of nanopigments with high hiding power and stability over time was developed.

6. It is shown that the use of colored dispersions of montmorillonite and nanopigments based on them increases the physical and mechanical properties of polymer films, plasticizes and structures the polymer-mineral composition, contributes to the production of leathers with high organoleptic characteristics of the front surface, namely, the volume of the network, graininess, nice vulture.

7. The composition of the covering composition was optimized by the method of simplex-lattice planning, which includes (%): pigment – 4.5...5.0; film former with high and low modulus of elasticity (polyurethane) – 3.0...5.0; film former with a high modulus of elasticity (acrylic) – 90.0...92.5. It is shown that the combination of film-formers and nanopigments based on modified montmorillonite ensures the formation of a thin-layer covering with the required level of operational properties, characterized by high adhesion of the covering to the leather, resistance to repeated bending, dry and wet friction, elasticity and strength.

CONFLICT OF INTEREST

The authors declare that they have no conflict of interest in relation to this research, whether financial, personal, authorship or otherwise, that could affect the research and its results presented in this paper.

REFERENCES

1. Bondarieva, A., Zhaldak, M., Mokrousova, O. (2021). Ukraine on the world market of leather materials. The International Scientific-Practical Journal "Commodities and Markets", 38 (2), 16–32. doi: [https://doi.org/10.31617/tr.knute.2021\(38\)02](https://doi.org/10.31617/tr.knute.2021(38)02)
2. Mazaraki, A. A., Melnyk, T. M., Iksarova, N. O.; Mazaraki, A. A. (Ed.) (2016). Zovnishnia torhivlia Ukrainy: KhKhI stolittia. Kyiv: Kyiv. nats. torh.- ekon. un-t, 600.
3. Hryshchenko, I. M., Danykovich, A. H., Zvarych, I. T. (2018). Efektyvni ekoloohoorientovani tekhnolohii vyrobnytstva khutrovyykh i shkirianykh materialiv. Kyiv: Svit uspiyku, 352.
4. Jian-Xun, L., Yan-Juan, F. (2019). Cleaner Chrome Tanning – Technology of Chrome-reduced Tanning Without Salt, Pickling and Short Procedure. Journal of the Society of Leather Technologists and Chemists, 103 (6), 289–296.
5. Jian-Xun, L., Yan-Juan, F. (2022). A Novel Eco-Combination Tannage of Chrome-free Leather with Softness and High Shrinkage Temperature. Journal of the Society of Leather Technologists and Chemists, 106 (3), 99–106.
6. Danykovich, A. H., Mokrousova, O. R. (2017). Efektyvni tekhnolohii formuvannia elastychnykh shkirianykh materialiv. Kyiv: Feniks, 277.
7. Kasian, E. Ye. (2019). Fyzyko-khimiia polimernykh plivkoutvoriuvachiv dlia ozdoblennia shkiry. Kyiv: Osvita Ukrainy, 178.
8. Kothandam, R., Pandurangan, M., Jayavel, R., Gupta, S. (2016). A Novel Nano-finish Formulations for Enhancing Performance Properties in Leather Finishing Applications. Journal of Cluster Science, 27 (4), 1263–1272. doi: <https://doi.org/10.1007/s10876-016-0997-8>
9. Kondratiuk, O. V., Kasian, E. Ye. (2017). Properties of modified polymer compositions for leather finishing. Herald of Khmelnytskyi national university, 5 (253), 62–66.
10. Niculescu, O., Leca, M., Coara, G., Macovescu, G. (2012). Characterization of coating aqueous disperse systems used in natural leather finishing. Chemistry Magazine, 9, 900–905.
11. Chunhua, W., Changdao, M., Wei, L. (2018). Effect of Novel Synthetic Clay on the Property of Waterborne Polyurethane Leather Finishing Agent: Enhanced Thermal, Mechanical and UV-resistant Performance. Journal of the Society of Leather Technologists and Chemists, 3, 155–159.
12. Winter, C., Borges Agustini, C., Elizabeth, M., Schultz, R., Gutterres, M. (2017). Influence of pigment addition on the properties of Polymer films for leather finishing. Journal-Society of Leather Technologists and Chemists, 101 (2), 78–85.
13. Danykovich, A. H. (2016). Osnovni materialy i tekhnolohii vyrobnytstva shkiry. Kyiv, 175.
14. Liu, Q., Liao, B., Pang, H., Lu, M., Meng, Y. (2020). Preparation and characterization of a self-mating coating based on waterborne polyurethane-polyacrylate hybrid dispersions. Progress in Organic Coatings, 143, 105551–105597. doi: <https://doi.org/10.1016/j.porgcoat.2020.105551>
15. Calvino, C., Henriët, E., Muff, L. F., Schrettl, S., Weder, C. (2020). Mechanochromic Polymers Based on Microencapsulated Solvatochromic Dyes. Macromolecular Rapid Communications, 41 (7), 102–124. doi: <https://doi.org/10.1002/marc.201900654>

16. Danylkovych, A., Sanginova, O. (2023). Influence of finishing on the material performances. *Proceedings of the NTUU "Igor Sikorsky KPI". Series: Chemical Engineering, Ecology and Resource Saving*, 2, 69–75. doi: <https://doi.org/10.20535/2617-9741.2.2023.283526>
17. Kondratiuk, O. V., Kasian, E. Ye. (2017). Rozrobka skladiv pokryvnykh kompozytsii dlia ozdoblennia naturalnykh shkir. *Herald of Khmelnytskyi national university*, 6, 255–262.
18. Mahmoodi, A., Ebrahimi, M., Khosravi, A., Eivaz Mohammadloo, H. (2017). A hybrid dye-clay nano-pigment: Synthesis, characterization and application in organic coatings. *Dyes and Pigments*, 147, 234–240. doi: <https://doi.org/10.1016/j.dyepig.2017.08.009>
19. Cova, M., Yarza, F., Famá, L., Verdi, C., Fernández, M., Escobar, M. (2019). Functional clays as reinforcement of nitrile latex films. *Progress in Organic Coatings*, 129, 271–277. doi: <https://doi.org/10.1016/j.porgcoat.2019.01.004>
20. Mokrousova, O. R. (2012). *Naukovi osnovy formuvannia struktury shkiry modyfikovanyimi vysokodispersnyimi mineralami v pislia dublynykh protsesakh*. Kyiv, 391.
21. Mahmoodi, A., Ebrahimi, M., Khosravi, A., Eivaz Mohammadloo, H. (2017). A hybrid dye-clay nano-pigment: Synthesis, characterization and application in organic coatings. *Dyes and Pigments*, 147, 234–240. doi: <https://doi.org/10.1016/j.dyepig.2017.08.009>
22. DSTU 2726-94. *Shkira dlia verkhу vztutia. Tekhnichni umovy* (1995). Kyiv: Derzhspozhyvstandart Ukrainy, 14.
23. Fan, Q., Ma, J., Xu, Q. (2019). Insights into functional polymer-based organic-inorganic nanocomposites as leather finishes. *Journal of Leather Science and Engineering*, 1 (1). doi: <https://doi.org/10.1186/s42825-019-0005-9>
24. Pavlyshyn, V. I., Dovhyi, S. O. (2019). *Mineralohiia*. Kyiv: KNT, 528.
25. Yotsuji, K., Tachi, Y., Sakuma, H., Kawamura, K. (2021). Effect of interlayer cations on montmorillonite swelling: Comparison between molecular dynamic simulations and experiments. *Applied Clay Science*, 204. doi: <https://doi.org/10.1016/j.clay.2021.106034>
26. Hryshchenko, I. M., Danylkovych, A. H., Mokrousova, O. R. (2013). *Polifunktsionalni shkiriani materialy*. Kyiv: Feniks, 295.
27. Bondarieva, A. O., Mokrousova, O. R., Okhmat, O. A. (2020). Pat. No. 144635 UA. *Sposib otrymannia pihmentnoho kontsentratu dlia ozdoblennia shkir*. MPK S14S 3/06. No. u202003432; declared: 05.06.2020; published: 12.10.2020, Bul. No. 19.
28. He, X., Ding, W., Yu, Y., Zhou, J., Shi, B. (2020). Insight into the Correlations Between Fiber Dispersion and Physical Properties of Chrome Tanned Leather. *Journal of the American Leather Chemists Association*, 115 (1), 23–29. doi: <https://doi.org/10.34314/jalca.v115i1.1465>
29. Kuzhel, Ya. A., Mokrousova, O. R. (2019). *Perevahy zastosuvannia modyfikovanoho montmorylonitu u pokryvnomu ozdoblenni shkir*. *Naukovi rozrobky molodi na suchasnomu etapi*. Vol. II. Kyiv: KNUTD, 429–430.
30. Bondaryeva, A., Zhaldak, M., Mokrousova, O., Okhmat, O. (2022). Nanopigments for Leather Finishing Coatings. *Proceedings of the 9th International Conference on Advanced Materials and Systems*, 37–42. doi: <https://doi.org/10.24264/icams-2022.i.4>

31. Bondaryeva, A., Mokrousova, O., Okhmat, O. (2021). Hybrid Pigments Based on Montmorillonite and Anionic Dyes for Leather Finishing. *Solid State Phenomena*, 320, 198–203. doi: <https://doi.org/10.4028/www.scientific.net/ssp.320.198>
32. Bondarieva, O. A., Mokrousova, O. R., Okhmat, O. A. (2020). Preparation and application of hybrid pigments for finishing leather. *Herald of Khmelnytskyi national university*, 2 (283), 26–35.
33. Zhdak, M., Mokrousova, O. (2019). Studying chemical transformations of the modified derma collagen. *Eastern-European Journal of Enterprise Technologies*, 4 (6 (100)), 6–15. doi: <https://doi.org/10.15587/1729-4061.2019.176006>
34. Bondaryeva, A., Mokrousova, O. (2020). The acrylic/montmorillonite nanocomposites for leather finishing. *Proceedings of the 8th International Conference on Advanced Materials and Systems*, 43–48. doi: <https://doi.org/10.24264/icams-2020.i.3>
35. Bondareva, A., Mokrousova, O. (2020). Formation of physico-mechanical properties of polymer-mineral coating for leatherfinishing. *The International Scientific-Practical Journal "Commodities and Markets,"* 34 (2), 97–109. doi: [https://doi.org/10.31617/tr.knute.2020\(34\)08](https://doi.org/10.31617/tr.knute.2020(34)08)
36. Mokrousova, O. R. (Ed.) (2020). *Perspektyvni materialy ta innovatsiini tekhnologii: biotekhnologii, prykladna khimiia ta ekolohiia*. Kyiv: Svit Uspikhu, 492.
37. Bondaryeva, A., Kasyan, E., Mokrousova, O. (2021). Modeling of quality indicators of the leather coating. *Herald of Khmelnytskyi National univeRsity*, 299 (4), 115–122. doi: <https://doi.org/10.31891/2307-5732-2021-299-4-115-122>
38. Lapach, S. M. (2020). *Teoriia planuvannia eksperymentiv: Vykonnannia rozrakhunkovo-hrafichnoi roboty*. Kyiv: KPI im. Ihoria Sikorskoho, 86.
39. Danylkovich, A. H., Zlotenko, B. M. (2017). *Metodolohiia naukovykh doslidzhen z osnovamy intelektualnoi vlasnosti*. Kyiv: KNUTD, 433.

CHAPTER 3

MODERN TECHNOLOGIES OF REPAIR AND RESTORATION WORKS OF BUILDINGS IN USE

ABSTRACT

Rational use of resources requires a new approach to many management issues.

Renewal of residential and industrial production potential based on the reconstruction and technical conversion of buildings using new technologies is the shortest way to increase the quality level and competitiveness of domestic products, the integration of the economy of Ukraine into the European and World Community, to the successful functioning of production entities in market conditions. Carrying out repair and restoration works of buildings within the specified time depends to a large extent on providing them with a sufficient amount of technical resources in a timely manner, the need for which is determined not only by the volume of work, but also by the conditions of operation. Being a specific type of construction production, repair and restoration works are performed in more difficult conditions, which significantly affect the efficiency of construction machines and equipment and the quantitative composition of the used resources.

The production conditions of repair and restoration work do not always allow the use of typical machines, known technological schemes of work performance. For repair and restoration work in the conditions of an operating enterprise in hard-to-reach places, it is necessary to have fundamentally new schemes and appropriate equipment adapted for work in hard-to-reach places, and structures with a complex configuration at height. The use of a typical set of mechanisms reduces the efficiency of their use, reduces productivity, increasing the duration of the repair cycle and the consumption of materials.

The existing methods of determining construction needs in equipment do not allow to properly take into account the production conditions inherent in repair and restoration works, to assess their impact on the efficiency of use.

This leads to an underestimation of resource needs, which negatively affects the work of construction organizations and the quality of work.

During repair and restoration works, the issues of heterogeneity, dispersion and small volume of the performed works become more relevant. Execution of a complex of works uncharacteristic for new construction: replacement or restoration of individual structural elements, replacement of anti-corrosion coatings on individual areas, etc. All work is performed in difficult conditions, which

often significantly affects the general scheme of organization and technology of work. Increasing the efficiency of repair and restoration works depends on the level of automation.

The conditions of repair and restoration work in hard-to-reach places are reflected in the principles of the technology of automated processes, taking into account the factors of compactness, limited space, difficult access, various configurations, etc. The most time-consuming processes are: preparation of surfaces, cleaning and application of anti-corrosion coatings. Therefore, the question of choosing rational options for automating these works determines the level of exploitation. All this requires the development of more advanced mechanisms of automated systems.

The process of repair and restoration works is complicated due to the greater variety of volume-planning and constructive solutions. Therefore, a difficult and important problem is the industrialization and improvement of the quality of the coating in the conditions of the objects that are operated.

KEYWORDS

Rational use of resources, reconstruction and technical re-equipment, industrial production potential, repair and restoration works, automation, pneumatic spraying technology, equipment for coating application.

The consequence of the above-mentioned main features is that in construction organizations that perform mainly repair and restoration work, the costs associated with the organization and elimination of workplaces increase by 1.5 times, and the costs of operation increase by 1.5–3 times compared to with new construction, the specific cost increases by 1.2–1.4 times. Most of the aspects and ways of solving the issues of coating are reflected in the works of scientists of the Research, Design and Technological Institute of Concrete and Reinforced Concrete, Research Institute of Construction Economics, Central Research Institute of Industrial Buildings, Kharkiv Industrial Buildings Research Institute Project, Kharkiv Agricultural Research and Development Project, HEI of the State Research Institute of Building Constructions, State Research Institute of Building Constructions of the City of Kyiv, etc.

Analysis of the modern level of technology for performing processes on a vertical surface makes it possible to identify the main directions of their improvement and to formulate the goal and objectives of the research.

The aim of the research is to improve the technology and develop equipment for applying coatings on a vertical surface by the method of pneumatic spraying using automated systems.

To achieve the aim in the work, a number of tasks are set:

1. Systematize and classify the technological schemes of applying protective coatings of building structures, as well as to evaluate the possibility of using them for applying coatings in hard-to-reach places.
2. Establish rational technological parameters for applying coatings, taking into account operating conditions.

3. Develop a device for applying protective coatings with adjustable technological parameters and modes.

4. Investigate the work cycle of technological operations and the quality of coating applied using the developed device.

5. Prepare recommendations for the implementation of research and experimental works on applying coatings to a vertical surface; perform research and experimental work on applying a protective coating in the cramped conditions of an existing building.

6. Develop a methodology for selection and comprehensive assessment of the effectiveness of coatings when applied to a vertical surface.

The following research methods and apparatus were used to solve the problems: logical, morphological, classification, typification, mathematical statistics and probability theory, correlation-regression analysis, systematization and generalization of experience.

The scientific novelty of the obtained results is:

- in determining the dependence of effective application of anti-corrosion coatings on technological parameters;
- in determining the dependence of the physical and mechanical properties of anti-corrosion coatings on technological parameters;
- in the substantiation of the automated device for applying protective anti-corrosion coatings and removable nozzles to it for performing work in hard-to-reach places;
- in determining the impact of technological processes on the service life of the anti-corrosion coating.

The validity and reliability of the obtained scientific results, conclusions and recommendations is confirmed by: analysis and generalization of a significant number of works on the technology of construction production and the creation of mathematical models and methods of their management; adequacy of mathematical models used in scientific research due to their correct formulation; positive results of the comparison of theoretical and experimental research data; implementation of work results in production and educational developments.

The practical significance of the obtained results lies in the determination of specific technological parameters and modes of cleaning, facing and applying a film coating on a vertical surface; the means and methods of applying a film coating, technological schemes for performing works in cramped conditions have been developed; automated devices for applying film coatings with the necessary technological parameters were made; rational technological parameters of applying film coatings on various forms and configurations of structural elements are scientifically substantiated.

3.1 ANALYSIS OF THE TECHNICAL AND ECONOMIC NATURE OF THE PROBLEM

The types of surface contamination, methods of preparing the surface of the structure, applying a primer to the surface, and methods of applying film coatings (**Fig. 3.1–3.3**) [1, 2] were studied.

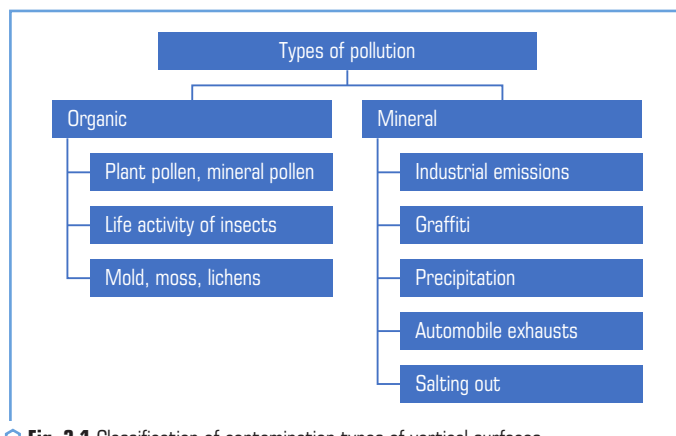


Fig. 3.1 Classification of contamination types of vertical surfaces

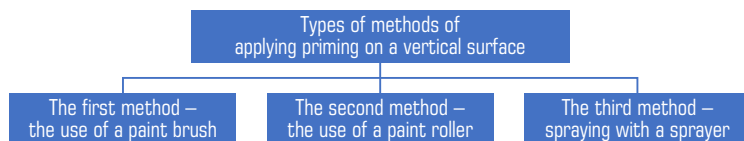


Fig. 3.2 Classification of priming application methods

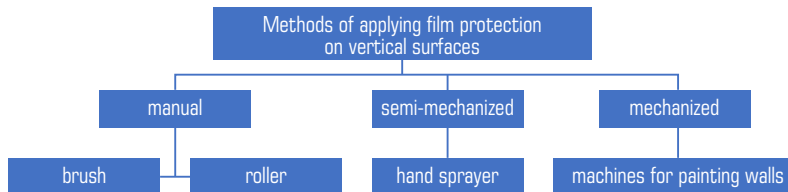


Fig. 3.3 Classification of methods of applying paint to a vertical surface

The development of issues of theory and practice of methods of applying film coatings is given in the works of a number of domestic and foreign scientists. In these works, the issue of applying coatings, their crack resistance, the technology of manufacturing paint and varnish materials, their main physico-chemical and mechanical properties, as well as the peculiarities of the properties of coatings, including reliability in aggressive environments, the use of various surface-active additives to improve the quality and durability of coatings, etc.

Paints and varnishes can be classified by appearance, composition and purpose (**Fig. 3.4**).

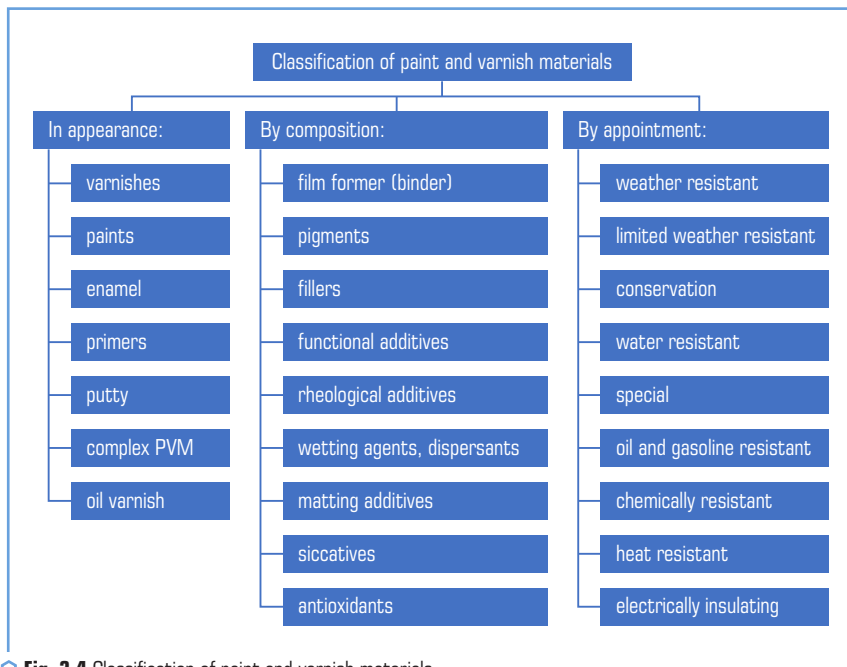


Fig. 3.4 Classification of paint and varnish materials

According to the composition, paint and varnish materials are divided into (**Fig. 3.5**):

- oil varnish – used for preparing oil-based and diluting thick-ground paints, oil-resin varnishes, primers, putties. They are also used for priming and oiling wood and other porous surfaces before painting. Drying in air, oils form soft elastic films with low protective and mechanical properties;
- primers – materials that are suspensions of pigments, as a rule, anti-corrosion pigments (or pigments with fillers) in film-forming substances and a homogeneous opaque film formed after drying, which must reliably protect the surface to be painted (metal – from corrosion, wood – from decay); reliable adhesion of this film both to the surface to be painted and to the materials that are applied on top of the soil layer (filling the pores of the wood) of the plaster, ensuring the water and air tightness of the coating. Primers are applied directly to the surface of products prepared for painting, and after hardening, putty or enamel is applied to the soil layer;
- putty – materials that are a viscous pasty mass consisting of a mixture of pigments with fillers in a film-forming substance. Intended for filling irregularities and depressions, grooves, pot-holes, seams, joints, i.e., smoothing the surface of products to be painted. Putties consist of film formers, fillers, cheap, often natural pigments, and a small amount of solvents. Putty is usually

applied to a previously primed surface with a layer up to 300 microns thick. Before applying the next layers of paint, the putty layer is subjected to dry or wet sanding. Alkyd, nitrocellulose, epoxy and other putties are used in everyday life;

- paints – suspensions of pigments or their mixtures with fillers in a film-forming substance (for example, oils, oils, emulsions, casein, latex), which, after drying, form an opaque painted homogeneous film. Oil paints are produced ready-to-use and thickly rubbed, which are diluted with oil before use. In addition, oil paints include zinc, titanium and lithopone whites;

- enamels – suspensions of pigments or their mixtures with fillers in synthetic resins or other high-molecular compounds dissolved in an organic solvent, which form a solid opaque film with a different texture after drying. Depending on the type of film former, alkyd (glyphthalic and pentaphthalic) enamels, nitrocellulose, organosilicon, urea- and melamino-formaldehyde and other enamels are produced. Enamels obtained by mixing and rubbing pigments with oil, and then diluted with varnish, are called oil enamels. In terms of physico-mechanical and protective properties, enamels are superior to oil paints;

- varnish – a solution of film-forming substances in organic solvents or in water, which forms a solid, transparent homogeneous film after drying;

- complex PVM – coating consisting of several PVM layers, arranged in the following order: primer, putty, enamel, varnish – if necessary.

Paint and varnish materials are divided into two large groups: water-based compositions and compositions containing volatile organic solvents. The solid opaque film formed during the PVM hardening applied to the surface of the product performs protective and decorative functions. Simply put, it should hide the surface under it and protect it from possible mechanical influences, as well as provide the necessary level of visual comfort. These PVM characteristics are provided by its formulation, i.e., the properties of the components that make up the PVM and their ratio in the formulation:

- film-forming agent (binder) – the main component of any PVM, a substance that, after hardening in one way or another, is able to form a fairly hard film on the surface to be painted and adheres well to it. The convenience of LFM, the speed of hardening (drying), the strength and durability of the coating largely depends on the properties of the binders;

- pigments – highly dispersed inorganic or organic substances, insoluble in film-formers and capable of forming protective, decorative or decorative-protective coatings with them. Pigments give PVM color, coverage (opacity), increase hardness, weather resistance of the coating, improve protective, decorative and other properties;

- fillers – white or slightly colored highly dispersed inorganic or organic substances, which have a lower light distortion index than pigments. They do not have protective and decorative properties, but they can partially replace expensive pigments and improve the properties of PVM and coatings based on them. Fillers often perform specific functions (for example, increase the viscosity of paints, reinforce the coating, preventing the formation of flows on vertical and inclined surfaces, reduce the gloss of the coating);

- functional additives – components of the PVM formulation, which are usually introduced in small quantities (usually no more than 1–2 %) and give the PVM and the coating based on it special properties.

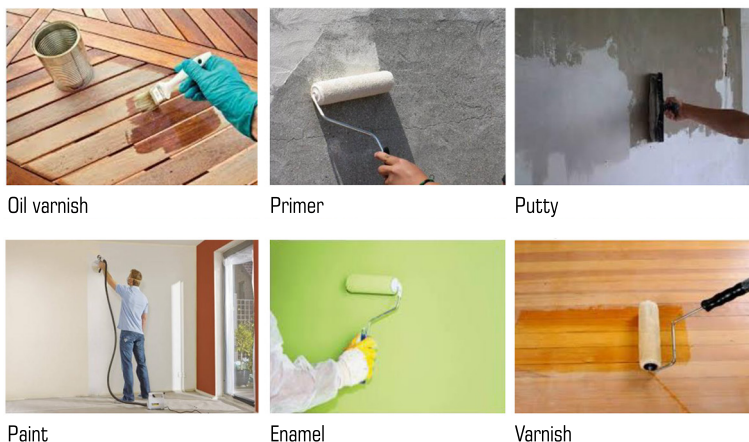


Fig. 3.5 Examples of types of materials

Example:

- rheological additives – prevent the settling of the pigment part and the PVM delamination under the influence of gravity during PVM storage, and also give PVM the property of thixotropy – the ability not to form flows;

- wetting agents, dispersants – substances that provide effective dispersion of pigments and fillers in the film-forming solution;

- matting additives – substances that reduce the degree of PVM gloss;

- desiccants – substances that ensure the PVM drying, a film-former, which hardens due to the reaction of oxidation by air oxygen;

- antioxidants – substances that prevent the formation of oxide films on the PVM surface during their manufacture and storage.

For water-dispersion (WD) PVMs, it is possible to say:

- emulsifiers – substances that ensure the stability of the WD-paint emulsion;

- antifreezes – substances that prevent the freezing of water-dispersed PVMs at low temperatures and ensure the recovery of PVM properties after several freeze-thaw cycles;

- fungicidal additives – substances that are part of PVM and provide protection of painted wood from mold fungi and insects;

- antiseptics – substances that are part of water-dispersible PVMs and prevent their destruction during production and storage in containers under the influence of bacteria and microorganisms;

- solvents – liquid components of the PVM formulation that provide the necessary viscosity and fluidity.

As the theoretical and practical research shows, it covers a large number of technological parameters of the process. In a number of works, trends towards the analysis of characteristics, properties and dependencies, such as strength, viscosity of the material, distance to the applied surface, angle of inclination of the nozzle, speed of the supplied jet, etc., can be clearly traced. However, these works did not allow to combine the properties of the materials and the technology of the works.

In the works, too little attention is paid to increasing the effectiveness of anti-corrosion coatings, to the development of advanced technology for performing work in the compressed conditions of buildings in use.

An analysis of various types of anti-corrosion materials was performed, one of which is protective paint coatings. Their field of application is application to the vertical surface of structural elements of buildings during repair and restoration works and new construction. The conditions for the formation of protective coatings are considered.

Based on literature data and field data, an analysis of the influence of technological factors on the service life of film coatings was performed.

To increase the service life and reduce the loss of material, it is necessary to develop the design of the device with special nozzles for applying film coatings, the concept of the methodology of comprehensive evaluation of the effectiveness of film coatings taking into account technological factors.

Practice suggested the use of a wide range of materials in the process of performing works. In particular, to increase the strength and thickness of the film coating, it is necessary to take into account such factors as the viscosity of the material and the fineness of grinding with or without pigment. Changing these factors or replacing them caused an increase in material loss and, in some cases, a decrease in strength. The influence of these factors has not yet been fully studied for the conditions of applying film coatings during repair work on a vertical surface.

During repair and restoration works, existing stationary devices are used for applying a coating of paint and varnish materials. However, due to high productivity, their use is inefficient.

The experience of operating the existing equipment has shown that high-quality coatings are obtained only if a whole series of restrictions related to the use of special equipment, nozzles of a special design, the composition of raw materials, the mode of application, the qualifications of workers, etc., are met.

According to most authors, the strength properties of film coatings are mainly influenced by such technological factors as the distance from the nozzle to the protected surface, the angle of inclination of the material supply, the speed of the jet exiting the nozzle.

However, the numerical values of the above factors have significant limits and are set with a number of restrictions. This is explained by the fact that the research was carried out on different equipment and different materials were used.

The condition of the surface is considered one of the main factors that affect the strength of the film coating.

All methods of surface treatment are aimed at obtaining a clean surface for coating. Based on the study of the influence of technological factors, the authors came to the conclusion that

in the process of operation, these factors affect the life of the protective (film) coating. The **Table 3.1** presents the types of preparation of vertical surfaces of film coatings that affect the service life.

● **Table 3.1** Effect of preparation of the vertical surface on the service life of the film coating

No.	Type of preparation	Service life of paint coatings		
		Environment		
		Weak	Medium	Strong
1	Without preparation (application on old paint, scale)	3	2	up to 1 year
2	Manual rust removal	4	3	2
3	Mechanical rust removal	5–6	4	3
4	Fire rust removal	4–5	3–4	2–3
5	Digestion	6–8	5–6	4
6	Sandblasting	7–8	6–7	3–4

Analysis of the table shows that any type of surface preparation extends the service life of the coating by 2 or more times in a highly aggressive environment under other different conditions (the same coating, thickness, application methods, etc.).

The influence of the thickness and methods of application on the service life, the influence of the method of preparation of the surface of structures and the degree of aggressiveness of the environment on the service life of the coating have been established.

The analysis of literature data and data from the state survey of structures operated in an aggressive environment showed that the conditions for the formation of film coatings are influenced by technological factors (surface cleaning, priming and application methods), the theory and practice of which need to be improved and special equipment for applying coatings in building conditions needs to be developed, which is used during repair and restoration works [1–3].

3.2 THEORETICAL ASPECTS OF THE INFLUENCE OF TECHNOLOGICAL PARAMETERS OF FILM COATING PROCESSES ON IMPROVING THEIR QUALITY

Greater losses of material occur when protective coatings are applied to the surface of structures. This is due to a number of technological factors, such as the speed of material supply, the distance from the nozzle to the surface of the supplied mixture, the diameter of the outlet hole, pressure, viscosity of the material, fineness of grinding, spray angle and other factors.

Currently, there are the following methods of performing work on the restoration of vertical surfaces.

Table 3.2 provides types of methods for applying an anti-protective coating to a vertical surface.

For each individual case, a method that has sufficient technical and economic justification is used.

● **Table 3.2** Types of methods when applying an anti-protective coating to a vertical surface

The name of the method of work performance	Use of an economically justified method in case of damage to the facade			
	Local damage	Vertical damage	Horizontal damage	Damage over the entire area of the facade
From the car tower	+			
From the scaffolding		+	+	+
From a cradle		+		+
Industrial climbers	+	+	+	+
Robotic devices		+		+

Below let's consider the works that are performed during the preparatory period. Currently, the following methods of cleaning the vertical surface are used.

There are four main methods of cleaning a vertical surface in the world. Each of them has a field of application, a type of equipment, and a type of surface:

1. Wall washing using high-pressure equipment. This method is the simplest and widely used in practice. At the same time, the facade can be treated both with special cleaning agents and with ordinary water. The type of cleaning liquid is selected depending on the material of the walls and the type of contamination.

2. Cleaning with a steam generator. It is used to remove old, deeply ingrained dirt. The steam generator is often used after unsuccessful cleaning of walls with a high-pressure unit.

3. Processing of the facade with a sandblasting device. With it, dirt is removed with the help of abrasive particles fed under high pressure.

With a competent selection of the size and structure of the abrasive, sandblasting solves a wide range of tasks. For example, in this way, it is possible to remove thin layers of paint and remove deep pockets of metal corrosion.

4. Mechanical cleaning. Most often, it is a preliminary stage of facade repairs. Old plaster, paint, putty, etc. are removed mechanically. A hammer with a chisel, spatulas, an angle grinder, a perforator and a steel brush help to remove them [2, 4, 6].

Next, let's consider the methods of priming the surface vertically. In modern conditions, three methods of surface priming are known. Each of them has disadvantages and advantages, scope of application.

The first method is the use of a paint brush (Fig. 3.6).

Let's pour the necessary amount of primer into a clean plastic bucket, dip a squeegee into it and evenly treat the wall.

The advantage of this method is the low price of the tool, the possibility of applying a high-quality coating, since the bristles bring the product into all recesses. The disadvantage is that during processing, the liquid flows down the handle onto the hand, which is unpleasant. In addition,

due to the small contact area of the brush with the surface, applying the primer takes a long time compared to other methods.



Fig. 3.6 Photo fragment of the method of applying the primer with a brush

The second method is the use of a paint roller (Fig. 3.7).

The roller is used in approximately the same way as a paint brush, i.e. it is dipped in a special paint trough, pressed a little against the edge, and then rolled along the wall.



Fig. 3.7 Photo fragment of the method of applying the primer with a roller

The use of the roller is characterized by simplicity and high productivity. Among the disadvantages, the primer applied with a roller does not fill the relief of the surface as intensively as a paint brush. But if you put the roller on the bar, then applying the mixture becomes much faster and better than if you had to work with a paint brush.

The third method is spraying with a sprayer.

If there is to be work on a large surface, it is better to use a spray gun.

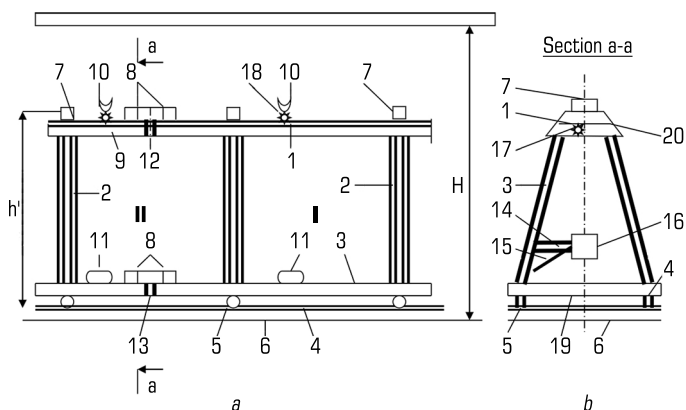
Applying a primer with a pneumatic gun has a number of advantages over manual application:

- automated priming is carried out quickly and evenly;
- the appearance of dry spots on the surface is minimized;
- mixture costs are reduced due to saturation of the solution with air;
- long service life.

The disadvantages include the difficulty of adjusting the distance from the surface to the nozzle. It is possible to overspend the material during windy weather.

When performing work on a vertical ceiling, it is necessary to develop a device with the help of which the work will be performed qualitatively and without human casualties.

For work at height, the authors developed the device "Portal" [7]. It includes two blocks. At the same time, the first block is the main one, which ensures autonomous operation; the second block is a semi-block that can be extended to the first block and cannot work autonomously. There can be several similar semi-blocks depending on the length of the object (Fig. 3.8).



- | | |
|--|--|
| 1 – portal; | 11 – grips for holding an auger or a pile during their build-up; |
| 2 – rack; | 12 – hinged connection of a portal; |
| 3 – connecting shelf; | 13 – hinged connection of a connecting bar; |
| 4 – rail; | 14 – console; |
| 5 – wheel; | 15 – brace; |
| 6 – sleepers; | 16 – screw clamp; |
| 7 – jacks; | 17 – winch; |
| 8 – connecting bar; | 18 – trolleys; |
| 9 – semi-portal; | 19 – lower reinforcing shelf of the anchor element; |
| 10 – adjustable graduated element of verticality of drilling a well or sinking a pile; | 20 – upper reinforcing shelf of the anchor element |

Fig. 3.8 The device for performing works on strengthening the foundations of soils and foundations and performing pile foundations for strengthening slopes

"Portal" is an autonomous frame and a half-frame, including a longitudinal span (portal) – 1; racks – 2, which are installed with an inclination relative to the vertical to ensure a more stable condition, forming an anchor element; connecting shelf – 3, which ensures a rigid connection of two oppositely located end anchor elements, and the anchor elements themselves have reinforcing shelves, respectively, the lower one – 4; upper – 5; semi-portal – 6.

For free movement around the work site, "Portal" has wheels – 7 in the form of hinged connections and rails – 8, which are laid along the road near the building or on the parapet (depending on the height). To reduce the load, rails can be laid on sleepers – 9.

In the upper part of the "Portal" at specially defined points, plates are rigidly welded, on which portable screw jacks are installed – 10. Joint operation of the main block and half-block is ensured by a hinged connection – 11, 12 with the help of connecting bars – 13.

The "Portal" is equipped with a movable guide graduated element in the form of a toothed hemisphere – 14, on trolleys – 15, on which both the first block and the second block can be equipped with devices for intensifying the injection of the liquid mixture.

In connection with the works that can be performed at different heights, the portal is made in the form of various structural elements that are built up.

Holding on the weight of the device for intensifying the injection of the liquid mixture is carried out with the help of grippers – 16 with a clamp – 17, which are attached to the console – 18 with a brace – 19.

Rigging works are carried out with the help of a winch – 20, with stops, which include a ratchet wheel – 21, a shaft – 22, a dog – 23, an axis – 24, a spring – 25, different types of grips, etc. These devices do not prevent the lifting of the load, but exclude the possibility of its involuntary descent under the influence of its own weight.

For the manufacture of structures, steel alloys are used in accordance with the current standards for specific elements, depending on the operating conditions.

The "Portal" works as follows. For work in cramped, space-constrained conditions, the intensifier is used to inject a flowable mixture.

When applying the mixture to a vertical surface, the device is attached to the portal. The upper part of the portal frame is equipped with fasteners that allow the nozzle to move from top to bottom without changing its path.

This "Portal" has an advantage over the known ones in that:

- it increases labour productivity and complex mechanisation of production processes, reduces capital expenditures, which makes it possible to increase the operational suitability of buildings and structures;
- the structural elements of the main load-bearing device "Portal" are made of a mass that ensures the installation of elements manually, without mechanisms;
- during the transition to another car park, the entire complex of the mechanisation device does not require dismantling and installation during operation, due to the possibility of moving the entire assembly along rails, or by additional extension of semi-blocks;

- the hinged joint of the block and the half-block allows to perform work at the break;
- the connection of the block and the half-block ensures that work can be performed simultaneously on several clamps;
- due to the possibility of hitching equipment, simultaneous surface cleaning, priming and application of the mixture is ensured;
- the ability to apply the mixture with an inclination;
- further development of the theory and practice of modern methods of carrying out work in cramped, space-limited conditions of buildings and structures in operation and their reconstruction is achieved.

The following is a device that can be used to perform work at height (**Fig. 3.9, 3.10**). It is used for surface cleaning, underpinning and application of the mixture.

The dry mixture of the appropriate composition is supplied by the nozzle – 1, which has a hinged-layer – 3 or rigid connection with the hollow shaft – 7 and then to the body – 2, on which the forward auger – 4 and the reverse auger – 5 are freely mounted, which begin to rotate in different directions, and special spacers – 6 ensure their design position at the same time the hollow shaft – 7 rests on the plugs – 9, which are the boundary of the body – 2.

The dry mixture gradually moves to the wetting zone, where water is supplied through the holes – 8, which are located on a certain section of the shaft – 7. Then, under the influence of acceleration, the moistened mixture moves to the reverse auger – 5 and is fed to the corresponding part of the structure. In order to regulate the amount of the mixture supplied, the nozzle – 10 has a set of valves – 11 that can be replaced and, accordingly, increase or decrease the opening and the amount of the mixture supplied.

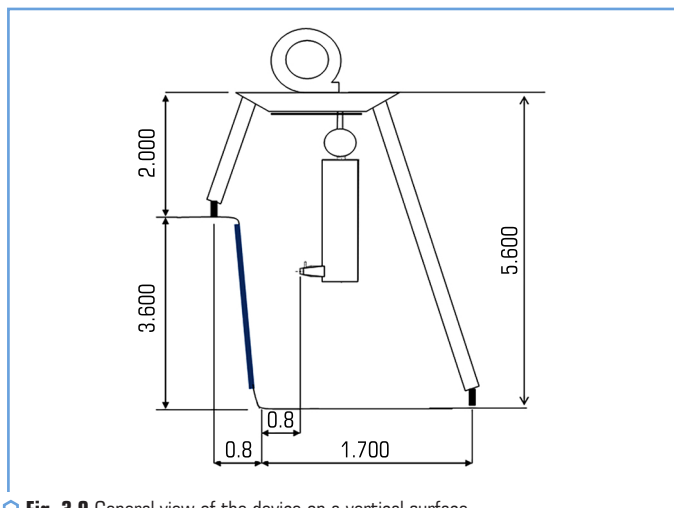


Fig. 3.9 General view of the device on a vertical surface

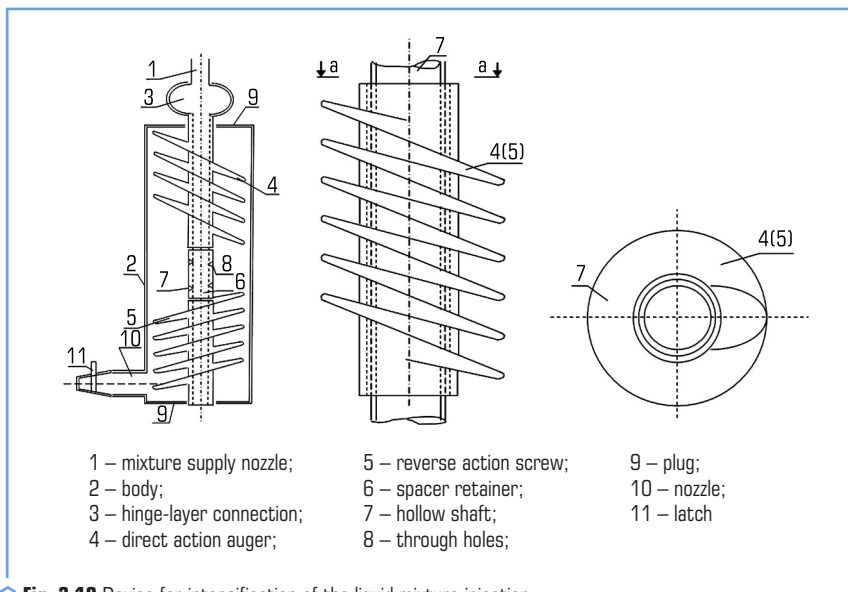


Fig. 3.10 Device for intensification of the liquid mixture injection

At the same time, to increase the feeding rate of the respective mixture, the nozzle – 10 is installed perpendicular to the axis of the hollow shaft – 7.

The specified technical characteristics ensure the use of the proposed technical solution in construction based on the following advantages:

- the quality of intensification of the spraying mixture increases;
- it becomes possible to regulate the quantity and, therefore, the speed of the supplied mixture by using one of the valves;
- operational suitability is increased, which ensures that such "Device..." meets the "Industrial suitability" criterion.

The set goal is achieved by the fact that the basis of the useful model "Device for the intensification of the injection of a fluid mixture" is a task in which, at the expense of the known technical solution "Device for the injection of a fluid mixture", replacing the purpose of some by means of structural changes and adding new elements and ensuring their interconnection connections during joint work, it became possible to create a corresponding "Device...", namely, a cylindrical body is limited by plugs in the centers of which a hinged or rigid hollow shaft is installed, on which the mixing elements are fixed, which rotate freely in different directions, and are equipped with spacer fasteners, so so-called direct and reverse action, creating conditionally active zones of activation and moistening, in a certain area in the moistening zone, the hollow shaft has through holes and is ball-hinged or rigidly connected to the mixture supply nozzle, and the nozzle in the form of

a conical cross-section is installed perpendicular to axis of the hollow shaft and is provided by a complex of certain latches.

New in the development of the invention is the use of mixing elements that rotate freely in different directions at the same time, and the placement of the nozzle perpendicular to the axis of the hollow shaft.

Several types of nozzles (nozzles) were developed and manufactured for future research protected by patents and copyrights. The advantages of these nozzles are that the quality of the coating application increases due to the adjustment of the paint supply angle, the crushing of the mass of the mixture in the air flow, which leads to an increase in the durability of the coating, therefore, the period between repairs of buildings and structures increases.

Next view of device for spraying a liquid mixture [8]. Unlike known devices of the same purpose, in the proposed device additional mixing of the dry mixture by a turbulent mixer and additional mechanical activation of the mixture components takes place. (**Fig. 3.11, 3.12**).

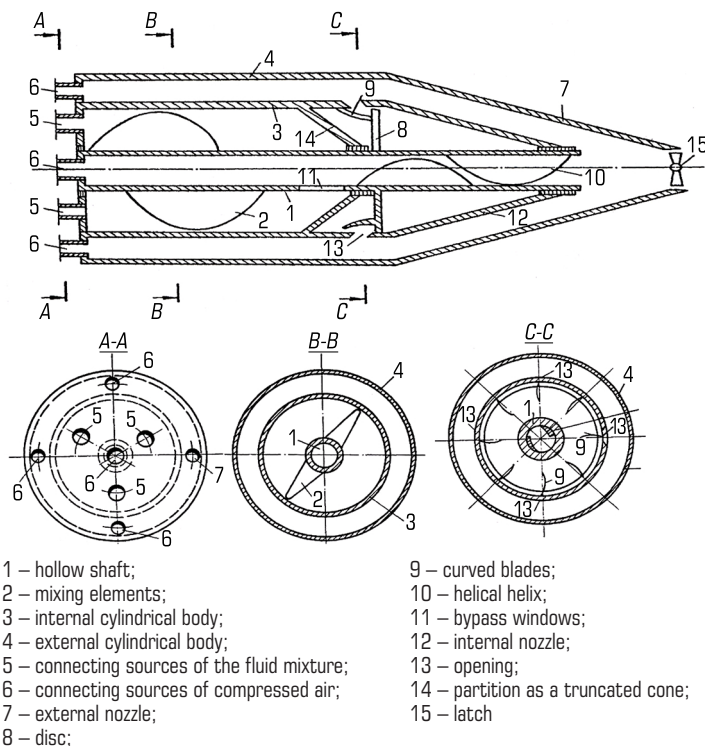


Fig. 3.11 Device (nozzle) for spraying the fluid mixture

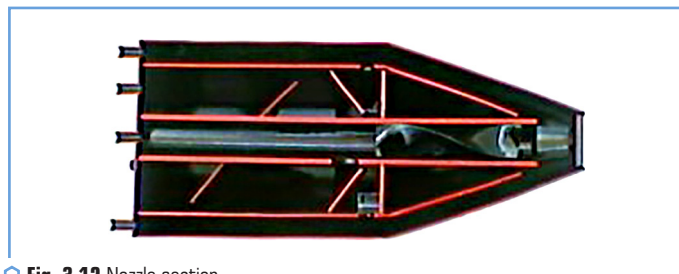


Fig. 3.12 Nozzle section

The device contains a hollow shaft with turbulent-type stirring elements on the outer surface and coaxially placed inner and outer cylindrical bodies on it. The latter are connected to the sources according to the fluid mixture and compressed air. On the outer surface of the hollow shaft is fixed a disk with curved blades in a circle. A helical spiral is made on the inner surface of the shaft.

In front of the disk in the direction of movement of the mixture on the opposite sides of the hollow shaft, bypass windows are made. The inner cylindrical body has a partition like a truncated cone. The smaller base of the latter faces the disk and is movably connected to the surface of the hollow shaft between the bypass windows and the disk. The surface of the inner cylindrical body above the curved disk blades has holes.

This design allows to adjust the amount of the mixture supplied, ensures high-quality mixing of the components, and additional mechanical activation of the components of the mixture reduces the energy consumption of the process and increases the quality of the coating.

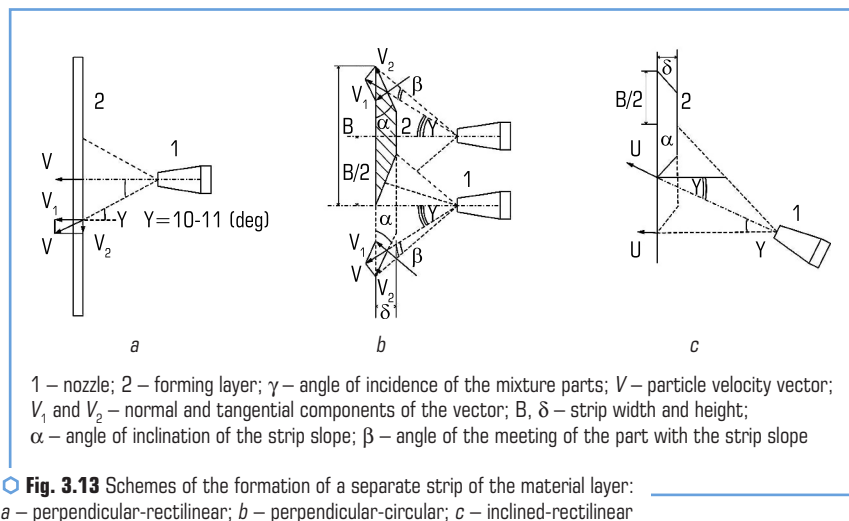
The operation of the device is ensured in the following way. The components of the mixture enter the cavity of the inner cylindrical body and with the help of mixing elements made in the form of curved disks, the mixture is mixed. When compressed air is injected into the curved discs, the latter begin to rotate and involve the hollow shaft in rotation, where additional mixing of the mixture components and activation of the binder occurs with the help of a spiral. The mixture is accelerated and, moving, hits a vertical surface through the output device.

The proposed nozzle meets the technical conditions that ensure the reliability of adhesion, uniformity of thickness, the required thickness and minimal removal of the applied material beyond the surface.

A number of laboratory experiments were conducted to select the optimal parameters. Schemes of moving the nozzle along the vertical surface were chosen, the values of the factors were changed and their influence on the strength of the coating was determined.

The formation of the film coating due to the variation of the angle of inclination of the nozzle and the linearity of the movement of the jet torch was investigated. The performance of theoretical and experimental studies is valid for the formation of a film coating in height when considering several schemes of torch movement: perpendicular-straight-line, circular-perpendicular, inclined-straight-line (**Fig. 3.13**). The greater the opening angle of the jet torch, the greater the tangential

velocity vector V_2 , which contributes to the increase in the loss of peripheral particles in the rebound, the smaller the shock pulse and their penetration depth, the more uneven the formation of the film layer structure.



By changing the nozzle design, it is possible to reduce the opening of the jet torch and improve the structure of the formed layer.

Research on the influence of the speed of application of the mixture depending on the distance to the vertical surface, the viscosity of the mixture, as well as the methods of preparation and application on the vertical surface are presented.

When the film mixture is applied to the surface, the speed of the jet exit changes. At the same time, the assessment of material losses in rebound was carried out. The data are presented in **Table 3.3** and **Fig. 3.14**.

• **Table 3.3** Dependence of the strength of the film coating and the amount of mixture loss on the speed of the jet exit

Indexes	Jet exit speed, m/s								
	70	80	90	100	110	120	130	140	160
R_{bend}	38	28	18.4	11.4	7	5.7	7.8	14.3	–
R_{gr} , MPa	10.2	16	21.2	25.7	28.4	27.5	23.4	16.7	–
The amount of the film mixture losses, %	21.56	17.8	15	12.3	11.2	12.2	16.9	25.6	–

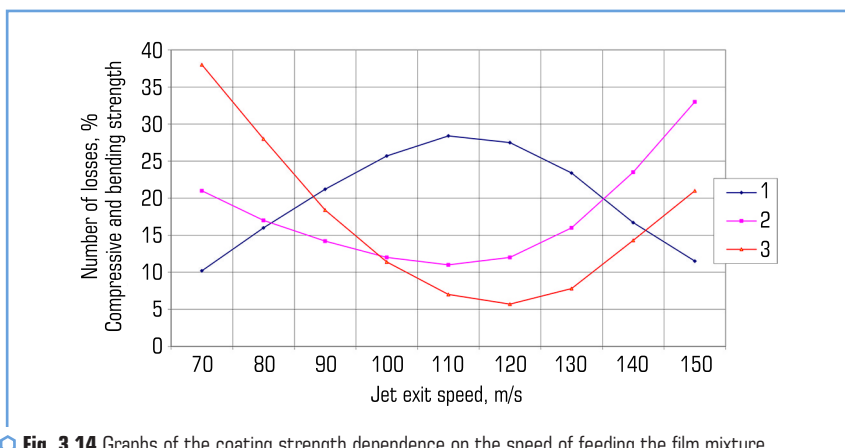


Fig. 3.14 Graphs of the coating strength dependence on the speed of feeding the film mixture and the amount of rebound

Summary graphs of the dependence of coating strength on the speed of feeding the film mixture and the amount of rebound were obtained. The graphs show the zones of change in the strength of the film coating depending on the speed of the mixture. In zone 1, with an increase in the feed rate of the mixture (from 70–100 m/s), the amount of rebound decreases, and the strength of the coating increases. At low values of the feed rate, the mixture on the surface is not compacted and almost all peripheral particles of the jet torch fall into the rebound. Zone 2 is the most favorable, because it increases the strength of the film coating to a maximum and the amount of rebound decreases to a minimum at a mixing speed of 110–140 m/s. In zone 3, at higher velocities (140–160 m/s) of the mixture supply, the force of the air jet does not compact, but rather loosens the previously compacted layer, pulling particles out of the layer, while the amount of rebound increases compared to the data obtained at lower jet velocities, therefore the strength of the coating decreases. In order to obtain optimal technological parameters when applying coatings in compressed conditions, equipment with devices for regulating the modes of supply and application of coating materials is required.

When determining the optimal values of the distance from the nozzle to the vertical surface being repaired, this parameter varied from 0.5 to 1.3 cm at fixed values of $v/c=0.4$ and the exit speed of the mixture from the nozzle of 110 m/sec. The data are presented in **Table 3.4**.

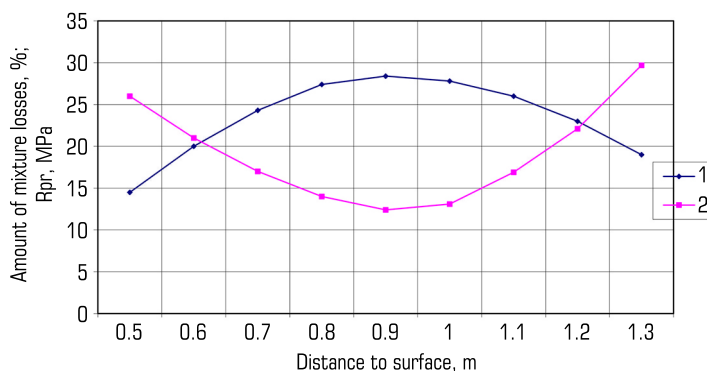
On the basis of **Table 3.4**, a graph of the dependence of the strength of the film coating and the amount of mass loss on the distance from the nozzle to the vertical surface is constructed (**Fig. 3.15**).

As can be seen from the data in **Table 3.2** and **Fig. 3.15**, the optimal distance from the nozzle to the vertical surface should be considered to be 0.8–1.1 cm. The limits of compressive strength may differ at different distances compared to the obtained strength characteristics

at the optimal distance by 15–30 %. The minimum loss of the film mixture is obtained at the optimal distance from the nozzle to the vertical surface.

● **Table 3.4** Dependence of the film coating strength and the amount of mixture loss from the distance of the nozzle to the vertical surface

Parameters	The distance of the nozzle to the vertical surface, cm								
	0.5	0.6	0.7	0.8	0.9	1	1.1	1.2	1.3
R_{pr} , MPa	14.5	20.1	24.3	27.4	28.4	27.8	26.3	23.4	19.1
Amount of mixture losses, %	25.4	21.2	17.1	14.3	12.4	13.1	16.9	22.1	29.7



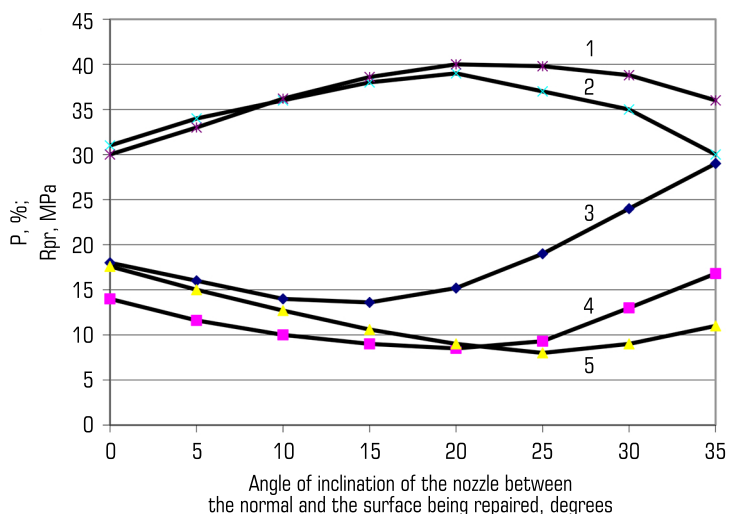
1 – compressive strength of the film coating; 2 – amount of losses of concrete mixture

○ **Fig. 3.15** Graph of the dependence of the number of losses on the distance to the vertical surface

During laboratory tests, the following results were obtained: the distance from the nozzle to the vertical surface was from 0.8 to 1.2 cm, while the amount of rebound varies from 17.2 to 16.4 %.

According to the obtained results, a graph of the dependences of the strength of the mixture and the amount of losses on the angle of inclination of the nozzle to the surface was drawn (**Fig. 3.16**).

Analysis of **Fig. 3.16** shows that the strength of the mixture and the amount of losses depend on the angle of inclination of the nozzle and the thickness of the laid layer. With a mixture layer thickness of 50 μm and a slope angle of 150 to 250, the amount of losses reaches a minimum level of 8.5–9.5 %, and the strength limit is 37 to 39 MPa. In the engineering sense, this angle of inclination is optimal according to the criteria for assessing the strength of the mixture with the surface and the amount of mixture losses.



1, 2 – compressive strength limit, R_{pr} , MPa;

3, 4, 5 – number of losses, P , % (3 – thickness of the layer strip 30 μm , 1, 4 – thickness of the mixture layer strip 50 μm , 2, 5 – thickness of the layer strip 80 μm)

Fig. 3.16 Graph of the dependence of the mixture strength and the amount of losses on the angle of inclination of the nozzle to the vertical surface

Theoretical data are in good agreement with experimental data. Based on these data, mathematical models of strength dependence on the complex influence of factors were developed:

$$y = ax^3 + bx^2 + cx + d,$$

where x_i is the angle of inclination; $y_{i,j}$ are the functions of quantities (i – amount of rebound, varies from 1... n ; j – film strength, varies from 1... m); a, b, c are the coefficients for the variable; d is free term that shows the position of the curves in the coordinate system.

The resulting mathematical models make it possible to determine and evaluate both the complex influence of all factors on the optimization parameters, as well as individual factors or their groups.

The coefficients of the obtained polynomials are partial derivative functions of the response on the corresponding variables. Their geometric meaning is the tangents of the angles of inclination to the x axis. A coefficient larger in absolute value corresponds to a larger angle of inclination, therefore, to a more significant change in the optimization parameter when this factor changes. In other words, the value of the regression coefficient is a quantitative measure of this phenomenon. The larger

the coefficient, the stronger the effect of the factor. The "+" and "-" signs show the position of the curves in the ordinate system. At the same time, in each individual case, one separate factor was taken into account, and all others were taken with the most favorable (min) influence.

On the basis of the conducted research, the author proposed a number of nozzles protected by a patent and author's certificates, two samples were made of them according to two applications, and later these nozzle samples were used to solve a number of problems and researches.

3.3 DESIGNS OF THE DEVICE ON THE TECHNOLOGY OF APPLYING FILM COATINGS IN THE CONDITIONS OF BUILDINGS THAT ARE IN USE

The device is automated, which moves with the help of guides. To improve the device operation, a nozzle was designed and manufactured. Device tests were carried out with specially selected mixtures of materials that are often used to protect building structures from corrosion.

The device was carried out in several stages in order to determine the desired scheme.

The device works as follows. Before the start of work, the work sites, their volume, and the complexity of the surface relief are determined. Depending on the volume of work, in one parking lot, components of the supporting frame – 1 of the appropriate sizes are performed, corresponding vertical tray-type guides of the supporting frame – 4, horizontal tray-type guides – 5 of the supporting frame – 1. Next, rollers – 6 are installed, in vertical tray-type guides – 4 supporting frame – 1 with attachment of horizontal tray-type guides – 5, supporting frame – 1 between a pair of working frame – 2 respectively with vertical tray-type guides – 14 working frame – 2 and horizontal tray-type guides – 15 of working frame – 2, on which has a bed made in a special cut-out – 3 for installing a nozzle – 11. For the safety of work and to prevent falling out of movable elements, which are made with rollers – 6, the corresponding guides are made depending on the type of rolled metal tray (channel) or square profile – 17, 16.

In the first case, tapes – 17 are welded to the floor on both sides of the walls of the tray, and the distance between them should not be greater than the size of stable fasteners of the roller axis – 7, 8. In the other case – create a slot under the same conditions, that is, the width of the slot – 16 should not be larger than the size of the stable roller mounts – 7, 8.

At the final stage, a nozzle – 11 is installed, which is connected to the corresponding 15 containers (not shown), as well as speed controllers for the movement of the supporting frame – 1, that is, its vertical tray-type guides – 4 of the supporting frame – 1, and vertical and horizontal tray-type guides – 14, 15 of the working frame – 2.

The rollers 6 are fixed on the axis 8 using a rack 7, the axis 8 is limited on both sides by washers 9 and fixed by pins 12. Otherwise, a nut 10 is screwed onto the axis 8 on both sides.

Next, general preliminary fastening – 13 is provided.

A traverse and a cable (not shown) are hung to the supporting frame 1. On a certain section of the roof, a block with a hoist is installed, through which a cable is pulled, and a winch is placed on

the ground. The assembled structure is lifted manually – 1, 2, 4, 5, 14, 15. On certain sections of the supporting frame 1 there are devices 13, which are used for final fastening with braces 21 to certain protrusions or other 25 details on the wall. The structure assembled in this way – 1, 2, 4, 5, 14, 15 is fixed on the traverse on one side, the cable is thrown through a block with a hoist, a winch (a block on the roof, a winch on the ground – we do not show it) and with braces 21 at the work site to wall 20 both from the top of the assembled structure and in the lower part – 1, 2, 4, 5, 14, 15.

Assembled together supporting frames 1 and working 2, which include vertical tray-type guides 4 of the supporting frame 1; horizontal tray-type guides 5 of the supporting frame 1; vertical tray-type guides 14 of the working frame 2, horizontal tray-type guides 15 of the working frame 2 are ready for device at the workplace.

Next, two workers – an operator and a climber, having previously installed a block with a hoist on the roof and a winch on the ground (not shown), after fixing the proposed device on the traverse with the help of a winch, lift it and with the help of braces 21 fasten it to the wall 20 by the protrusions on the wall. The device is ready for operation. Next, the climber in the cradle rises and begins to control the nozzle 11. After finishing on a certain part of the object, they move to another, removing the fasteners, lowering the device. On the new site, they ensure the device of the device in the same sequence as before. As usual, work on thermal insulation is performed from top to bottom.

If necessary, new chains 19 are added to the vertical tray-type guides 4 of the supporting frame 1 of a certain section and the work continues from top to bottom. In the process of work, special portable wedge-shaped stops 18 are additionally installed, which provide adjustment of the movement of the horizontal tray-type guides 5 of the supporting frame 1. **Fig. 3.17, 3.18** presents the general diagram and view of the device.

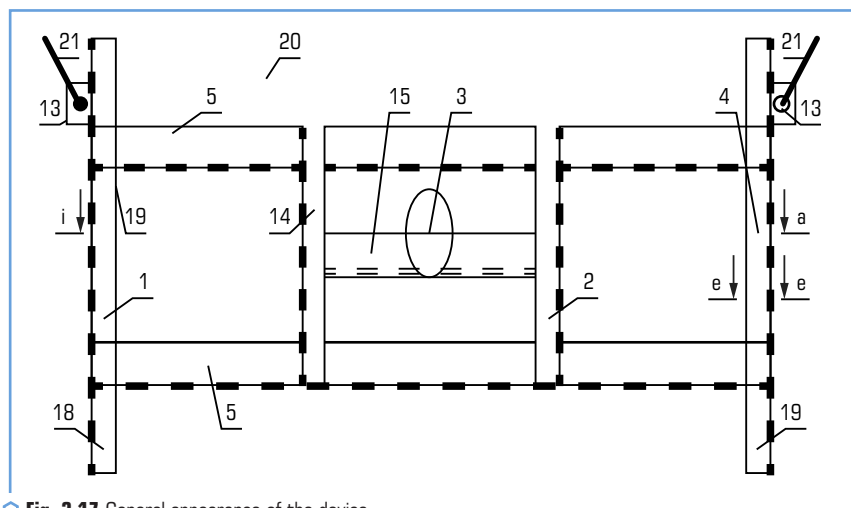


Fig. 3.17 General appearance of the device

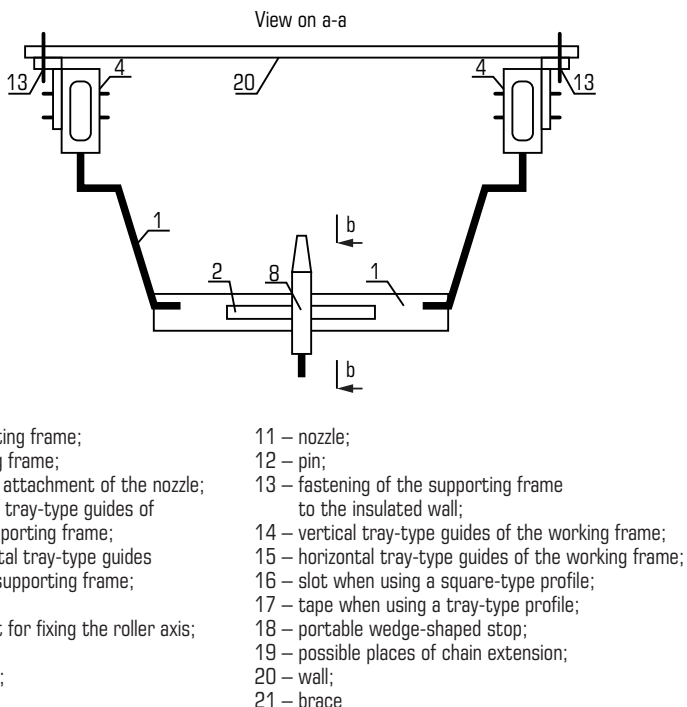


Fig. 3.18 Supporting frame, view from a-a

The device for performing film coating in front of the known has the following advantages:

- mobility, can be used in cramped conditions;
- provides mechanization of film coating application;
- transportable and easy to assemble;
- serves one climber and an assistant operator on the ground near the mortar mixers;
- it becomes possible to perform film coating more qualitatively;
- on one gripper, work can be performed from top to bottom by increasing the chains of vertical tray-type guides of the supporting frame;
- it becomes possible to perform film coating using remote control.

Setting up an experiment to study application of solutions

Experiment No. 1. The purpose of the experiments is to find the relationship between the working nozzle and the large-scale model of the nozzle for further calculation of the work

performance of the large-scale model. And comparison of real results with analytical calculation (Fig. 3.19, 3.20).

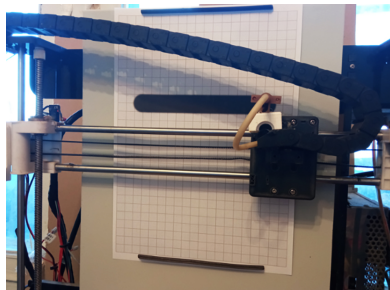


Fig. 3.19 General view of the proposed device

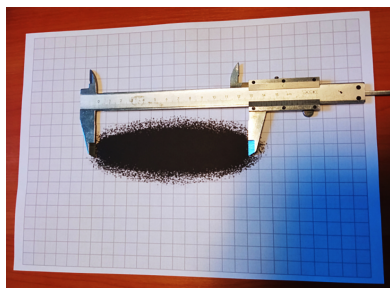


Fig. 3.20 Spot size

The purpose of the experiment: finding the dependence of paint consumption on the diameter of the torch of the working nozzle.

The technology of conducting the survey:

- device of the working nozzle on the fastening and connection of the compressor, supply of paint;
- fixing the paper on the screen;
- device at the maximum distance from the screen of a tripod with a nozzle;
- set working pressure 2 Bar;
- purging at minimum paint supply;
- regulation of paint supply;
- adjustment of the shape of the torch;

- search for optimal form and quality with replacement of paper;
- weighting of the target;
- after finding the optimal settings – setting the target on the screen;
- applying paint with a nozzle 1 s;
- weighting of the target;
- entering the results into the table;
- changing the distance between the nozzle and the screen, repeating the experiment.

The purpose of the experiment: finding the dependence of paint consumption on the diameter of the working nozzle torch.

Results of experiment No. 1. The results of experiment No. 1 are presented in **Table 3.5**.

● **Table 3.5** Results of experiment No. 1

No. of experiment	Torch diameter, cm	Paint consumption, g/min	Distance to the screen, cm
1	10	67	8
2	11	72	9
3	12	78	10
4	13	83	11
5	14	89	12
6	15	95	13
7	16	101	14
8	17	109	15
9	18	124	16
10	19	146	17
11	20	172	18
12	21	205	19
13	22	239	20
14	23	276	21

Let's build a graph of the dependence of paint consumption on the torch diameter (**Fig. 3.21**).

Let's build a graph of the dependence of the diameter of the torch on the distance from the nozzle to the screen (**Fig. 3.22**) and select the parameters for applying a film coating on a vertical surface (**Fig. 3.23**).

Based on the selected scheme, technical documentation and a prototype were developed, which were used for further research. Technological parameters of the device were determined, namely material consumption, spraying angle and productivity (**Table 3.6**).

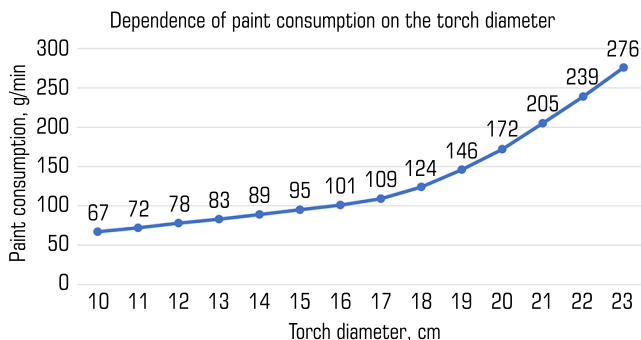


Fig. 3.21 Graph of dependence of costs of film coating on a vertical surface

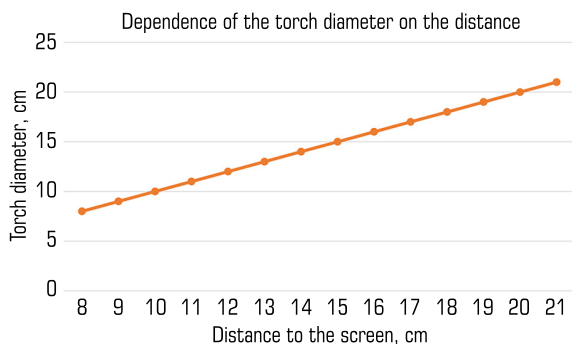


Fig. 3.22 Graph of the dependence of the torch diameter on the distance from the surface to the nozzle

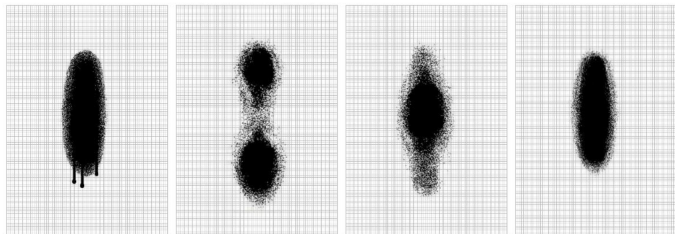


Fig. 3.23 Schemes for selecting parameters for applying a film coating on a vertical surface

● **Table 3.6** Technical characteristics of spray nozzles for paint and varnish materials

Spraying angle, degree, α	The length of the torch imprint, mm				Material consumption l/min depending on the outlet diameter, mm			
	For distance, cm							
	50	75	100	125	0.35	0.4	0.45	0.5
20	120	124	130	150	0.38	0.57	0.72	1.14
40	145	149	156	180	–	0.59	0.84	1.16
60	170	175	183	210	–	0.72	1.11	1.54
80	195	200	210	240	–	0.74	1.12	1.56

It was established that the consumption of material depends on such technical parameters as the diameter of the outlet hole, the viscosity of the given mixture, the degree of dispersion, temperature, pressure, and the spraying angle. The main technical characteristics of the material were determined by the raw material. Different variants of the film coating were considered depending on the viscosity of the raw material and the spraying angle. At the same time, the spraying angle varied from 20 to 80°.

Analysis of research results showed that:

- with the increase of the outlet opening, the consumption of the material increases by 2–3 times at the same viscosity;
- with changing the spray angle from 20 to 80°, the material consumption changes by 1.5 times at the same diameter of the outlet opening;
- with a change in viscosity (50–120 s), the consumption of the material changes by 1.2–1.5 times with adjustment of the diameter of the outlet hole.

Graphs of the dependence of material consumption on the diameter of the outlet hole (for medium-viscous materials) at different angles of inclination of the nozzle were obtained.

When applying a film coating, important technological factors are the spray angle and the length of the torch footprint.

By changing each of these values, the size of the spot was determined.

On the basis of the obtained data, graphs of the dependence of the length of the torch imprint on the height and angle of the torch spray were constructed.

Experiment No. 2. The purpose of the experiment: Finding the dependence of paint consumption on the diameter of the flame of a large-scale nozzle (**Fig. 3.24**).

The technology of conducting the survey:

- device of a large-scale nozzle on the fastening and connection of the compressor, supply of paint;
- fixing the paper on the screen;
- device at the maximum distance from the screen of a tripod with a nozzle;
- setting the working pressure 1 Bar;
- search for optimal pressure;
- search for optimal form and quality with replacement of paper;

- weighting of the target;
- after finding the optimal settings – setting the target on the screen;
- applying paint with a nozzle 1 s;
- weighting of the target;
- entering the results into the table;
- changing the distance between the nozzle and the screen, repeating the experiment.

The purpose of the experiment: finding the dependence of paint consumption on the diameter of the flame of a large-scale nozzle.

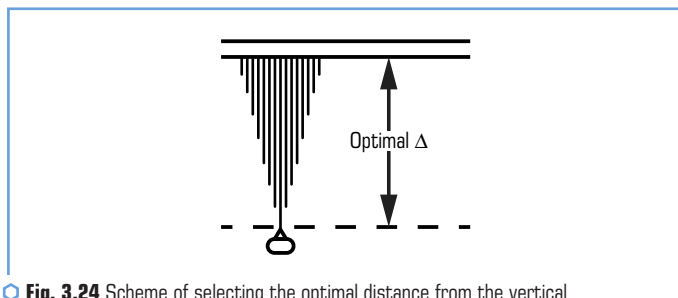


Fig. 3.24 Scheme of selecting the optimal distance from the vertical surface to the nozzle

Results of experiment No. 2. The results of experiment No. 2 are presented in **Table 3.7**.

Table 3.7 Results of the experiment No. 2

Experiment No.	Torch diameter, cm	Paint consumption, g/min	Distance to the screen, cm
1	1	6	1.2
2	1.2	7.5	1.4
3	1.4	9	1.6
4	1.6	11	1.8
5	1.8	12.5	2
6	2	14.5	2.2
7	2.2	16.5	2.4
8	2.4	19	2.6
9	2.6	21	2.8
10	2.8	23.5	3
11	3	26	3.2
12	3.2	28.5	3.4
13	3.4	32	3.6
14	3.6	36	3.8

Let's build a graph of the dependence of paint consumption on the torch diameter (**Fig. 3.25**).

Let's build a graph of the dependence of the torch diameter on the distance from the nozzle to the screen (**Fig. 3.26**). A fragment of film coating application is presented in **Fig. 3.27**.

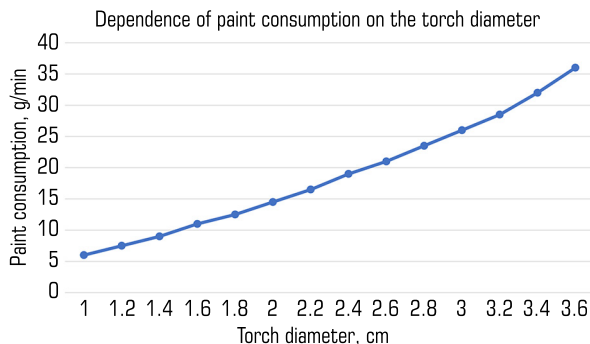


Fig. 3.25 Graph of dependence of the film coating on the torch diameter

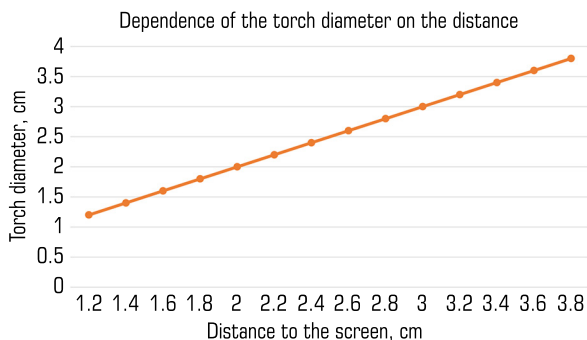


Fig. 3.26 Graph of the dependence of the torch on the distance

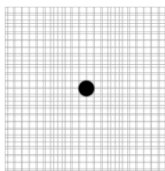


Fig. 3.27 Fragment of film coating application

3.4 METHODOLOGY OF COMPREHENSIVE ASSESSMENT OF THE ECONOMIC EFFICIENCY OF FILM COATING

On the basis of the analysis of technological factors that affect the protective coatings of construction structures in operation, a method of comprehensive evaluation of the economic efficiency of the film coating has been developed.

The methodology consists of two interrelated economic and mathematical problems:

- assessment of the comparative effectiveness of paint coatings;
- determining the optimal terms of operation of protective coatings.

The evaluation of comparative efficiency takes into account: production of paint coatings; selection of protective coatings at the design stage for use on specific objects.

The degree of economic significance of decisions made based on the results of technical and economic studies in the first and second cases is different. This also determines the difference in the requirements for the depth of the issue development, which in turn implies a different methodological approach in each case. Depending on the purpose of the technical and economic study, the following formulas are proposed by the authors for determining the total costs of production:

– when choosing directions for the development of the material and technical base for the production of paint and varnish coatings:

$$P_1 = P_k + P_m + P_{add} + P_e; \quad (3.1)$$

– when choosing a type of anti-corrosion coating for use in a specific object (on a construction site):

$$P_2 = P_k + P_m + P_{c.s.} + P_e + P_p, \quad (3.2)$$

where $P_k, P_m, P_{add}, P_o, P_{c.s.}$ – the corresponding part of the total costs of production, which depend on the costs of production of structures with paint coating at the factory (P_k); capital investments in the base (P_m); additional costs for applying a film coating after the device of structures and welding (P_{add}); operating costs (P_o); costs for equipment and coating on the construction site ($P_{c.s.}$); part of the costs that take into account the economic effect of early commissioning of the facility (P_p).

Capital and current repairs are carried out to maintain the operational qualities of industrial buildings. Expenses incurred during operation consist of expenses:

- a) for replacement (restoration) of the protective coating;
- b) for current and capital repairs.

The amount of costs for the restoration of coatings is determined by the formula:

$$P_e = \sum_{i=1}^{\gamma_{sk}-1} S_{es} / (1 + E_n) T_{z_i} = mC_{zk}, \quad (3.3)$$

where S_{ec} is the cost of replacing the old anti-corrosion coating, the service life of which has expired, with a new one, UAH.; T_z is the time from the start of operation to the i -th replacement of the old anti-corrosion coating with a new one, year; $(\gamma_{zk}-1)$ is the number of restorations of anti-corrosion coatings during the period of operation of the building; E_n is the standard for the reduction of various time costs, which is taken in the calculations as equal to 0.08, respectively.

The number of restorations of anti-corrosion coatings during the service life of the building is determined by the formula:

$$(\gamma_{zk} - 1) = (T_c / T_{zk} - 1), \quad (3.4)$$

where T_c is the period of building operation, the structures of which are protected against corrosion, year; T_{zk} is the period of operation of the anti-corrosion coating, year.

To determine the period of operation of the anti-corrosion coating (t_{cr} , t_{pr}) during the operation of the building, an analysis of the factors affecting it was performed.

The performed analysis of the factors allows to make a hypothetical schedule of the service life of anti-corrosion coatings depending on the degree of aggressiveness of the environment and the thickness of the coating.

As an example, graphs of capital investment, operating costs, and total production costs are given for a zinc-coated steel column operating in a mildly aggressive environment.

In order to ensure a minimized cost function for operating costs (overhaul and complete restoration), which are discrete in nature, are taken into account in the form of annual depreciation deductions.

Bringing the costs distributed according to the accepted scheme to a single point in time gives a quantitatively different result than with the real scheme.

The author proposes to base the calculations on a real scheme for the distribution of discrete and current costs.

For each type of structure (columns, trusses, beams, slabs, floors) the following graphs were compiled depending on the degree of aggressiveness of the environment (weak, medium, strong); from the type of coating (paint, metallization, combined). The dependence of the total costs of production on the terms of operation for three environments (medium, weak and strong) was obtained.

The analysis of the influence of technological factors on the service life of coatings made it possible to establish a single criterion – the economically optimal service life of anti-corrosion coatings, which is determined by minimizing the function of total production costs according to the formula:

$$y = ax^2 + bx + c - \min. \quad (3.5)$$

The search for the moment of time when the total costs of production will have a minimum value – by the method of least squares, which consists in the fact that at the given points x

and y obtained experimentally, let's find such values of a , b and c that approximate the given experimental curve.

Let's obtain a system of equations, after solving this system, let's obtain an expression:

$$x = \pm b/2a, \quad (3.6)$$

where x is the economically optimal service life of the anti-corrosion coating; a , c are the coefficients showing the position of the curve in the flat ordinate system; c is the distance from the y axis to the minimum x value.

Operating costs (P_e) associated with current (P_{pr}) and capital (P_{cr}) repairs are determined by the formulas:

$$P_e = P_{pr} + P_{cr}, \quad (3.7)$$

$$P_{pr} = \sum_{n=1}^{\gamma_{pr}-1} S_{pr} / (1 + E_{np})^{t_{pr}}, \quad (3.8)$$

$$P_{cr} = \sum_{\gamma=1}^{\gamma_{cr}-1} S_{cr} / (1 + E_{pr})^{t_{cr}}, \quad (3.9)$$

where S_{pr} is the cost of one current repair, hryvnias/m² of the structure surface; S_{cr} is the same as capital repair, hryvnias/m² of the surface of the structure; t_{pr} , t_{cr} are the term of operation of the i -th anti-corrosion coating according to current and major repairs, year; $(\gamma_{cr}-1)$ is the number of capital and current repairs for the entire period; $(\gamma_{pr}-1)$ is the period of operation of the building (not including the last repair).

The number of capital and current repairs is determined by the formulas:

$$(\gamma_{cr} - 1) = (T_c / T_{cr} - 1), \quad (3.10)$$

$$(\gamma_{pr} - 1) = (T_c / T_{pr} - 1), \quad (3.11)$$

where T_{cr} is the periodicity of capital repairs for the entire period of operation of the building; T_{pr} is periodicity of current repairs during the life of the building; T_c is the term of house operation.

The developed economic-mathematical model for choosing the optimal variant of constructive solutions with protective coatings for the house as a whole, taking into account the initial cost and operating costs, is determined by the sum of the maximum total production costs.

The problem is solved with the help of electronic computing equipment.

CONCLUSIONS

The following scientific conclusions and results were obtained on the basis of the research carried out in the work:

1. It has been shown that the repair and restoration work of industrial enterprises is characterized by a high degree of difficulties, difficult conditions of performance of work, which significantly affect the composition of the equipment and the efficiency of its use. For successful work, contracting construction organizations must have in their arsenal an effective tool for assessing the technological features of work in hard-to-reach places of the existing enterprise.

2. Small-sized, transportable devices based on the technology of applying film coatings in confined conditions have been substantiated and developed.

3. The technological parameters of the device for applying the mixture to the vertical surface of the material flow, the diameter of the outlet opening, the angle of inclination, the length of the torch footprint, the productivity of the knapsack device – 0.25 m³/h, the mobile device – 0.5 m³/h have been determined.

4. Dependencies have been obtained that establish the relationship between the considered factors and parameters, which allows to reasonably determine the degree of efficiency in the use of resources when solving practical problems.

5. The regularities of the interaction of the considered technological factors have been established:

- with the increase of the outlet opening, the consumption of the material at the same viscosity increases by 2–3 times;

- with a change in the spraying angle from 20 to 800, the consumption of the material changes with the same hole diameter and the same viscosity;

- with a change in viscosity (50–120 s), the consumption of material changes by 1.2–1.5 times with adjustment of the diameter of the outlet hole;

- the length of the torch footprint is affected by the spray angle and the distance from the nozzle to the surface to be covered.

6. Based on the analysis of resource and time constraints, multifactorial models of technological processes of application of anti-corrosion coatings have been determined. The dependence of the film strength on the angle of inclination and the thickness of the coating layer was obtained, theoretical and experimental data were determined through direct measurement of the amount of rebound in the process of applying the coating on a vertical surface.

7. The theoretical foundations of the formation of the film coating have been developed. To increase the strength and thickness of the coating, a number of factors must be taken into account (such as the opening angle of the jet torch, the speed of the jet, etc.), changing one of them or replacing it causes increased losses, and in some cases, a decrease in strength, which affects the quality of film coatings, and ultimately, their service life.

8. Methods of comprehensive assessment of the economic efficiency of protective coatings have been proposed, taking into account technological factors and conditions of anti-corrosion works.

9. Approbation of film coating methods using the proposed device with a nozzle protected by a utility model patent in laboratory conditions has been carried out.

CONFLICT OF INTEREST

The authors declare that they have no conflict of interest in relation to this research, whether financial, personal, authorship or otherwise, that could affect the research and its results presented in this paper.

REFERENCES

1. Svitalskiy, M. (2020). Zabrudnennia biosfery – dzherela, vydy, naslidky, pryklady, okhorrone biosfery. Available at: <https://nrv.org.ua/zaabrudnenya-biosfery/#nav2> Last accessed: 12.04.2023
2. Ochistka fasadov – 4 sposoba i luchshie moiushchie preparaty. Available at: <https://obustroeno.club/instrum-i-material/sten-material/material-fasad/170050-ochistka-fasadov> Last accessed: 12.04.2023
3. Stenovye materialy. Available at: <https://obustroeno.club/tags/sten-material> Last accessed: 12.04.2023
4. Halushko, V. O. (1999). Osobennosti proizvodstva remontno-vosstanovitelnykh rabot pri zashchite konstruktsii. Problemy rekonstruktsii ta ekspluatatsii promyslovyykh ta tsyvilnykh obiektiv. Dnipropetrovsk, 25–28.
5. Halushko, V. O. (2000). Metod opredeleniia ekonomicheskii optimalnykh srokov sluzhby anti-korroziionnykh pokrytii. Ekonomika: problemy teorii ta praktyky, 19, 239–243.
6. Halushko, V. O. (2002). Sovershenstvovaniya metodyky naneseniya zashchytnykh pokrytyi na ohrzhdaiushchye konstruktsyy. Zastosuvannia plastmas u budivnytstvi ta miskomu hospodarstvi. Kharkiv, 81.
7. Halushko, V. O. (2009). Pat. No. 45279 UA. Gantry for repair-renewal works. MPK E04G 23/00, E04G 21/00, B66C 17/00. declared: 21.05.2007; published: 10.11.2009, Bul. No. 21, 10.
8. Halushko, A. M., Donchenko, M. N., Halushko, V. O. et al. (1990). AS No. 1756502 A1 SRSR. Ustroistvo dlia nabryzga tekuchei smesi. Kl. E04F21/02.
9. Halushko, V. O., Halushko, A. M., Donchenko, M. N. (2002). Analiz tekhniko-ekonomychnykh faktorov, vliyaiushchykh na sroky sluzhby antykorroziionnykh pokrytyi. Humanitarnyi visnyk Zaporizkoi derzhavnoi inzhenernoi akademii, 8, 138–147.

10. Halushko, V. O., Halushko, A. M., Donchenko, M. N. (2003). Osobennosti proizvodstva remontno-stroitelnykh rabot pri zashchite konstruktsii. Problemy i perspektivy sovremenno-stroitelstva. Zaporozhe: ZGIA, 78–81.
11. Halushko, V. O. (2005). Sovershenstvovanie tekhnologii naneseniia plenochnykh materialov v stesnennykh usloviakh. Organizatsiia nerazrushaiushchego kontrolya kachestva produktcii v promyshlennosti. Alania: Antaliia, 103–105.
12. Halushko, V. O., Babii, I. N., Kolodiaznaia, I. V., Melnik, N. V., Pidrushniak, Iu. M. (2009). Tekhnologicheskii sposob uvelicheniia sroka sluzhby zhilykh i obshchestvennykh zdani. Stroitelstvo materialovedenie mashinostroenie, 50, 130–135.
13. Toropynin, S. I., Medvedev, M. S. (2009). Tekhnologii i tekhnicheskie sredstva vosstanovleniia lakokrasochnykh pokrytii selskokhoziaistvennoi tekhniki bez udaleniia produktov korrozii. Vestnik Krasnoarskogo gosudarstvennogo agrarnogo universiteta, 6, 116–121.
14. Kolesnichenko, S. V. (2020). Tekhnolohichna bezpeka budivelnykh stalevykh konstruksii. Kyiv: Vydavnytstvo «Stal», 344.
15. Kolesnichenko, S., Seliutin, I., Grytsuk, Y. (2021). Methodological approaches to creating the electronic databases of building operation safety. IOP Conference Series: Materials Science and Engineering. Iasi, 1141 (1), 012024. doi: <https://doi.org/10.1088/1757-899x/1141/1/012024>
16. Kolesnichenko, S. (2019). The Principles of Risk Assessment for Building Steel Structures with Imperfections. International Journal of Innovative Technology and Exploring Engineering, 8 (8), 2735–2739.
17. Kolesnichenko, S. (2019). Steel structures residual life's determination with the safety index. IOSR Journal of Mechanical and Civil Engineering, 16 (2), 12–18.
18. Kos, Z., Klymenko, Y., Polianskyi, K., Crnoja, A. (2020). Research of the Residual Bearing Capacity and the Work of Damaged Reinforced Concrete Beams' Inclined Sections. Tehnički Glasnik, 14 (4), 466–472. doi: <https://doi.org/10.31803/tg-20191125075359>
19. Yevhenii, K., Zeljko, K., Iryna, G., Kostiantyn, P. (2020). Investigation of Residual Bearing Capacity of Inclined Sections of Damaged Reinforced Concrete Beams. Croatian Regional Development Journal, 1 (1), 14–26. doi: <https://doi.org/10.2478/crdj-2021-0002>
20. Klymenko, Ye. V., Boiadzhi, A. O., Polianskyi, K. V. (2019). About the experimental investigation of residual bearing capacity of damaged reinforced concrete beams inclined sections. Bulletin of Odessa State Academy of Civil Engennering and Architecture, 75, 37–43. doi: <https://doi.org/10.31650/2415-377x-2019-75-37-43>
21. Slipych, O. O., Khokhlin, D. V. (2008). Modeliuvannia ta doslidzhennia zhorstkosti stin iz kam'ianoi kladky, pidsylenykh zalizobetonnymy elementamy pry dii horyzontalnoho navantazhennia. Budivnytstvo Ukrainy, 9, 41–44.
22. Yefimenko, V. I., Slipych, O. O. (2012). Osoblyvosti provedennia obstezhen i pasportyzatsii budivel i sporud. Visnyk Kryvorizkoho Natsionalnoho universytetu, 32, 177–180.

23. Slipych, O. O., Khokhlin, D. V. (2008). Modeliuvannia ta doslidzhennia zhorstkosti stin iz kam'ianoi kladky, pidsylenykh zalizobetonnyy elementamy pry dii horyzontalnoho navantazhennia. *Budivnytstvo Ukrainy*, 9, 41–44.
24. Slipych, O. O., Khokhlin, D. V. (2008). Modeliuvannia ta doslidzhennia zhorstkosti stin iz kam'ianoi kladky, pidsylenykh zalizobetonnyy elementamy pry dii horyzontalnoho navantazhennia. *Budivnytstvo Ukrainy*, 9, 41–44.
25. Ivanyk, I. H., Vikhot, S. I., Pozhar, R. S., Ivanyk, Ya. I., Vybranets, Yu. Yu., Ivanyk, Yu. I. (2018). *Osnovy rekonstruktsii budivel i sporud*. Lviv: Vydavnytstvo Lvivskoi politekhniki, 268.
26. Saviovskyi, V. V. (2018). *Rekonstruktsiia budivel i sporud*. Kyiv: Lira, 320.
27. Saviovskyi, V. V. (2018). *Rekonstruktsiia budivel i sporud*. Kyiv: Lira, 320.
28. Yakymenko, O. (2020). Repair and restoration of waterproofing of buildings and structures. *Urban Development and Spatial Planning*, 75, 403–410. doi: <https://doi.org/10.32347/2076-815x.2020.75.403-410>
29. Lisnychenko, S. (2022). Determination of the cost of recovery of buildings and structures which have received damage and destruction (enlarged approach). *Urban Development and Spatial Planning*, 80, 275–282. doi: <https://doi.org/10.32347/2076-815x.2022.80.275-282>
30. Shatrova, I. A., Demudova, E. A., Hryban, D. O. (2022). Problems of reconstruction of residential buildings of different periods of construction. *Ways to Improve Construction Efficiency*, 1 (49), 92–97. doi: [https://doi.org/10.32347/2707-501x.2022.49\(1\).92-97](https://doi.org/10.32347/2707-501x.2022.49(1).92-97)

CHAPTER 4

THERMODYNAMIC ASSESSMENT OF THE POSSIBILITY OF USING
POLYMERIC MATERIALS IN PROMISING LAUNCH VEHICLES

ABSTRACT

One of the ways to reduce the cost of space launches for the operational launch of constellations of satellites into the Earth's orbit is the creation of targeted launch vehicles based on light and ultralight class rockets. The solution to this problem lies, among other things, in the area of development and application of new structural materials. The presented work considers the possibility of using polymers on the one hand as a structural material for creating the hulls of launch vehicles, and on the other hand as solid fuel for rocket engines. Research is related to the development of a new type of ultralight launch vehicles: combustible or autophagic launch vehicles. A short historical excursion into the problem of creating polymer launch vehicles is given. The authors summarized the experience of their own research on the use of polymer materials for the creation of combustible rockets. The thermophysical and mechanical characteristics of various types of polymers were analyzed from the point of view of the possibility of their use as structural materials for the hulls of ultralight missile carriers.

The results of theoretical and experimental studies of thermal destruction of polymer materials under aerodynamic heating conditions are presented. It is shown that polymer materials, in particular polyethylene, under certain conditions, can be used to make fuel tanks for solid-fuel rockets that use a new principle of burning the structure during flight.

The development of such launch vehicles and the commercialization of scientific research in this area will allow domestic companies in the aerospace industry to occupy a niche in the market for launching small satellites.

KEYWORDS

Combustible rockets, polymer bodies, polymer fuel, aerodynamic heating, thermodynamic analysis.

Today, there is a situation where the needs and possibilities of manufacturing small satellites several times exceed the possibilities of their launch [1]. The issue of reducing the cost of putting

small satellites into orbit is urgent. The specific cost (USD/kg of payload) of launching such satellites by special small LVs is several times higher than that of large LVs and can reach tens, and sometimes even hundreds of thousands of dollars. for 1 kg of payload due to the scale factor. The absolute cost of launching modern small LV exceeds 10 million USD, which is not always acceptable for the main potential users of small satellites. The main means of delivering small satellites to LEO are still heavy rocket carriers designed to transport payloads weighing thousands of kilograms. Such an approach does not always meet modern requirements, in particular from the point of view of prompt delivery of cargo, and launch vehicles have a high price. The analysis of existing and prospective launch vehicles shows that there is now a tendency to enter the market of new light and ultra-light launch vehicles [2].

However, these small launch vehicles have the same complexity as large launch vehicles and require significant development costs, resulting in a high unit price. Thus, to meet the start-up needs, it is necessary to significantly reduce the specific output cost (in the case of using small LVs – the start-up cost, which is also determined by the specific cost of outputting the maximum payload).

Therefore, a new paradigm for the development of space launch systems is emerging, which requires a clear economic justification. Transportation costs should be lower than existing systems, and development costs should be minimized using modern design principles [3, 4].

In general, from a technical point of view, the problem of developing new means that could reduce the specific cost comprehensively in all 4 directions indicated above is relevant. Such TSSs should have low sensitivity to the scale factor, i.e. should be efficient for launching small payloads. A review of the current state of development, which was conducted by NASA experts [5], shows that the demand for small and cheap TSS has a constant tendency to increase in the coming years. At the same time, it is not excluded that the increase in the number of launches may contribute to the interest in the use of heavy LVs.

But today, launching a satellite using a specially designed launch vehicle is very expensive. Most often, satellites are transported as joint cargo by large LVs, which do not always allow saving money. In addition, finding a joint launch opportunity is difficult, and coordinating it with the micro-satellite operator's schedule is even more difficult. The costs associated with a co-launch increase as it waits. It should also be noted that a small satellite often needs its own special orbit, different from the orbit of the main payload of the common LV.

Therefore, the growing needs on the one hand, and fierce competition on the other, force the developers of aerospace equipment to look for new technical solutions.

One of the ways to reduce the cost of launches is the use of new construction materials, which makes it possible to advance in all the mentioned directions at the same time. As such materials, it is suggested to consider polymers, in particular polyethylene, polypropylene, etc. Polymers are used in rocket technology as part of composite materials of individual structural elements or thermal protection [6]. The properties of polymers: low cost, low weight, low thermal conductivity, as well as high energy characteristics, create the basis for their use as the main structural material for creating the missile body. At the same time, the polymer shell itself can be used as a solid fuel [7].

Although there are currently no known realized projects of rockets with combustion or discrete ejection of the tank shell, there are numerous proposals from the time of the pioneers of rocket technology to the present day.

The idea of using structural elements as fuel has been known for a long time. In 1929, Yuri Kondratiuk proposed to reduce the influence of the mass of the structure on the energy characteristics of the rocket. According to the idea, after the multi-stage rocket reaches the state of the Earth's satellite in outer space, it is necessary to disassemble the spent stages. These stages were proposed to be remelted with the help of "some additional devices" and used as fuel for interplanetary flights [8]. He also proposed the use of solid fuel (hydrogen), which is first gasified before being fed into the engine, and then fed using injectors.

The theoretical and practical development in this field was made by Friedrich Zander, who was a supporter of burning not only purely rocket structures (for example, suspended tanks), but also aviation elements intended for the atmospheric part of the flight – wings, motors, propellers, etc. [9]. He formulated the basic requirements for metals from which it is possible to make combustible elements. The use of plastics with a metal filler as materials for such elements was also proposed. In addition, Friedrich Zander was the first to propose the idea of a rocket plane that should burn itself. He outlined the main units necessary for melting and supplying solid fuel – this is a "melting boiler" with a "furnace"; an injector that feeds the melt into the combustion chamber with the help of a gaseous oxidizer; heated pipelines for transporting molten fuel, etc. Friedrich Zander conducted numerous experiments on the manufacture and testing of light alloys for flammability [10].

It should be noted that Friedrich Zander and Yuri Kondratiuk considered the structural elements considered only as an auxiliary component to the main liquid fuel. The opinion about the expediency of burning spent rocket parts is also present in the well-known work of Ary Sternfeld [11], although the author did not provide specific proposals for its implementation.

Walter Hohmann proposed a spaceship project that resembled a high-rise architectural structure and was to be built entirely of solid fuel [12]. Therefore, such a ship had to constantly shrink during the flight. The generator of its body is an exponential curve, and combustion could only occur from the end. Thanks to this, the flight should take place with constant acceleration. The disadvantage of this scheme is the lack of a combustion chamber, which would not allow to achieve the required specific impulse.

The above-mentioned works were rather theoretical reflections of the pioneers of cosmonautics. Real proposals for this kind of rocket technology appeared in the second half of the 20th century in the form of patents.

It is clear that the creation of a rocket with a burnt shell of a fuel tank requires the development of a new type of engine and other original units. The task of discarding the tank shells as they are emptied of fuel seems easier, since it can be solved based on the use of rocket engines that already exist. The logical development of the concept of a transport space system with disposable fuel tanks and reusable engine installations and other expensive elements seems to be the idea of discarding fuel tanks in parts, as they are emptied of fuel. This approach theoretically makes it

possible to reduce the energy costs for accelerating those parts of the tanks, the fuel from which has already been spent. There are known patents for proposals for such rockets that continuously eject fuel tanks [13, 14].

The idea of burning spent LV elements also attracted the attention of designers. In one of the projects, it is proposed to use the engine torch to burn the emptied parts of the tank shell and to use elastic elements to supply fuel to the engine. Pyrotechnic means were used to discretely throw off the stabilizers [15].

The patent [16] claims a rocket with the combustion of a fuel tank shell consisting of solid fuel. The authors of another patent [17] proposed to burn the composite shell of the fuel tank with flares of rocket engines and using injectors for air supply. The authors called their rocket autophagic.

The authors of [17] proposed to use autophase launch vehicles to clean up near-Earth space. At the same time, the use of autophase launch vehicles has a number of advantages, including the absence of a dry tank, which occupies approximately half of the total dry weight of a modern launch vehicle. According to the authors of [17], such a rocket can be developed as extremely cost-effective for picosatellites or as a transport for launching space debris removal devices into orbit.

Paper [18] presents the design and results of experimental studies of a solid-fuel autophase rocket engine with forced fuel supply to the combustion chamber similar to a liquid engine. The engine of this design (**Fig. 4.1**) can be considered as a suitable solution for use on small spacecraft, when conventional fuel storage and supply systems become unacceptably heavy and/or expensive for the following reasons.

Firstly, the polymer propellant charge forms a tubular structure that serves as a reservoir for the oxidant. Consequently, there are no special structures and massive fuel storage losses.

Secondly, the fuel delivery devices in autophase engines can be lighter than modern pressure or pump delivery systems. This is achieved by pulsed combustion. The propellant is fed into the engine by means of a small pressure between pulses, when the chamber pressure is minimal. It is similar to the well-known air pulse motors. The feed can be carried out, for example, by means of feed wheels driven by small electric motors, while the expected chamber pressure between pulses is several hundred kPa.

The third reason is the safe handling of the virtually separate components of the solid fuel: the solid polymer fuel (such as polypropylene or ethylene) and the solid oxidant (such as ammonium perchlorate) are not mixed before entering the combustion chamber.

When the engine is running, the fuel rod is fed into the evaporator via the injector to be converted into gases. Separate streams of oxidiser and fuel gas pass through collecting openings, channels, injectors and dampers into the combustion chamber. Combustion heats the evaporator and gasifies the next portion of fuel. Valves interrupt combustion to facilitate feeding when the pressure in the combustion chamber drops.

Compared to modern pressure or turbopump propulsion systems, the masses of forced-propulsion systems for autophase pulse engines are acceptable for small spacecraft [19–21], but they are undoubtedly too heavy for launch vehicles. At the same time, the concept of combustible fuel

tanks is promising for launch vehicles, which has been waiting for the development of new technologies for several decades. Therefore, the study of an alternative way to power the autophase engine is a subject of considerable interest.

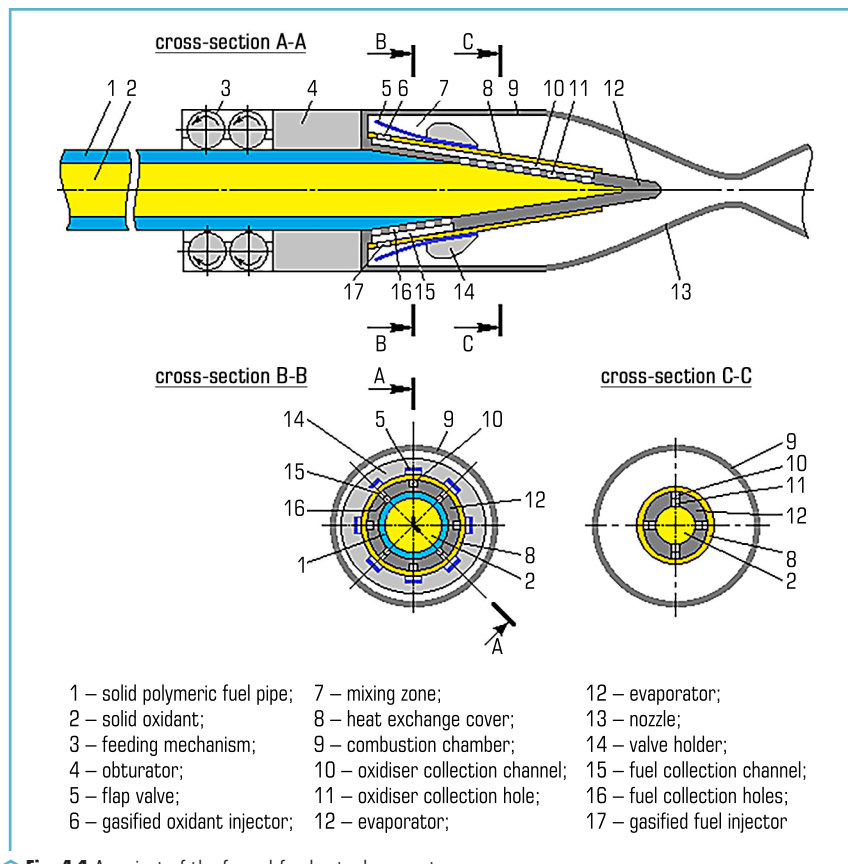


Fig. 4.1 A variant of the forced-feed autophase motor

It is impossible to manufacture structural elements from modern fuels, both liquid and solid, so one of the tasks of implementing the idea of a combustible rocket is to select materials that would combine sufficient strength, manufacturability and processing with high calorific value, low temperature and heat of melting or sublimation, etc. According to the authors of [22], the materials proposed for hybrid engines, namely metals, metal hydrides and solid hydrocarbons, can be used for the tank shells of combustible rockets.

Metals have long been widely used as rocket propellants [23, 24]. For example, by adding powdered metals to liquid propellants, their calorific value is increased, since metal combustion products have lower enthalpies of formation than hydrocarbon combustion products (**Table 4.1**) [22].

● **Table 4.1** Enthalpy of the formation of some combustion products

Fuel	Product of combustion, phase	Enthalpy of formation (ΔH_{298}^0), kJ/kg
C	CO ₂ , gas	–8 941
H	H ₂ O, gas	–13 423
Mg	MgO, condensate	–14 924
Al	Al ₂ O ₃ , condensate	–16 435
B	B ₂ O ₃ , condensate	–18 293
Li	Li ₂ O, condensate	–20 008
Be	BeO, condensate	–24 365

This increases the heat-forming capacity of the fuel, i.e. the difference between the enthalpies of 1 kg of fuel (ΔH_{298}^0) and 1 kg of combustion products at the nozzle outlet (ΔH_{Σ}^{SE}), and, accordingly, increases the rate of combustion products flowing out of the nozzle (w) according to the following ratio:

$$w = \sqrt{2(H_{298}^0 - H_{\Sigma}^{SE})}.$$

However, the combustion of metals alone is not advisable, as the high calorific value leads to high temperatures in the combustion chamber and, as a result, to an unacceptably high energy consumption of combustion products for their dissociation.

The highest values of the most important characteristic of rocket fuel – specific thrust impulse (I_{spec}) are achieved when the fuel contains hydrogen in addition to metal and oxidant.

In this case, the oxidant is consumed for stoichiometric combustion of the metal, and hydrogen is added to achieve the maximum specific impulse [22]. It is the decrease in molecular weight and, accordingly, the increase in the mass heat capacity of combustion products due to the increase in the amount of light hydrogen in them that explains the interest in compounds such as beryllium hydride, alumohydrides, borohydrides, etc. It is likely that some hydrides can be used to make a tank shell and fed into the combustion chamber after melting or turning into gas through thermal degradation. But, in the authors' opinion, it is necessary to study the mechanical and physical characteristics of potential materials first.

The most accessible and appropriate materials today may be solid hydrocarbon polymers, such as polyethylene, polypropylene, polystyrene, etc. Their chemical composition is close to that

of typical hydrocarbon fuels, they are strong enough to be used to make structural elements, and they melt and gasify easily, which simplifies the construction of supply systems.

Oxidising agents can include liquids such as nitrogen tetroxide and hydrogen peroxide, which are common in rocketry. By far the best non-toxic oxidant is liquid oxygen. However, almost all hydrocarbon polymers have a glass transition temperature significantly higher than the freezing point of liquid oxygen ($-222.65\text{ }^{\circ}\text{C}$), which means that their application is limited to oxidants with high boiling points. It is known that high-strength ultra-high molecular weight low-pressure polyethylene (e.g., grade 21506-000 with a molecular weight above 10^6) can be used in a wide range of operating temperatures: from -200 to $130\text{ }^{\circ}\text{C}$ [22]. In addition, ultra-high molecular weight polyethylene has fairly high strength characteristics, low friction coefficient, high resistance to aggressive media, and high impact strength [25–28].

An additional argument in favour of choosing hydrocarbon polymers is the possibility of using them together with powdered metal-containing fillers, which will both avoid the problems associated with the use of metal or hydride tanks and improve the energy characteristics of the fuel. It is known that in some solid fuels, the content of aluminium powder is 15–20 % (by weight), which can increase I_{pit} by 10–15 % [22]. But in liquid fuels, the use of metals is complicated by the problems of its storage and supply to the combustion chamber.

The introduction of nanodispersed fillers leads to a change in the structure of the polymer matrix, and thus to a significant improvement in performance properties. The nanosized particles of the modifier are evenly distributed in the polymer mass and provide its structuring due to the active surface of the nanoparticles. It was found that the introduction of 2 % (w/w) of aluminium-containing filler into ultra-high molecular weight polyethylene leads to an increase in tensile strength by up to 30 %, wear resistance by an order of magnitude, while maintaining the relative elongation during tensile stress and reducing the friction coefficient and temperature in the contact zone. At the same time, the filler particles behave as artificial structuring germs, which contributes to the formation of a more organised and ordered supramolecular structure [22, 29–32].

Incendiary rockets, in which metal-containing powdered filler is added to the polymer base during the production of the tank shell, will solve the problem of storing metal-containing fuels. In addition, the polymer base will, firstly, protect hygroscopic and highly reactive hydrides from environmental influences; secondly, the high viscosity of the molten polymer will prevent fuel stratification in the melting chamber and supply lines (if part of the polymer is not gasified, but only melted to supply fuel in the form of a suspension or colloidal solution) [22].

Thus, solid hydrocarbon polymers are a promising material for the manufacture of combustible rocket shells. Particular attention should be paid to ultra-high molecular weight polyethylene due to its high energy efficiency, environmental safety, and sufficient strength for tank shell structures.

It is known from the theory of solid rocket propellants that to increase I_{spec} , it is advisable to add metals such as Li, Be, Mg, Al to solid hydrocarbon propellants in the form of simple substances or as part of compounds. It can be assumed that in the engine chamber they are immediately completely oxidised to form the oxides Li_2O , BeO , MgO , Al_2O_3 . For these oxides, sublimation

or evaporation reactions with the formation of a gas of the same chemical composition as the starting substance or with decomposition into single-atomic gases in the temperature range of rocket engines are characterised by very low values of equilibrium constants, i.e. very low saturated vapour pressures. Therefore, it is assumed that the above oxides, after formation, almost immediately completely change to the condensed state and remain in it throughout the entire process in the combustion chamber and nozzle. For this reason, any reactions involving Li, Be, Mg, Al or their compounds were not taken into account, except for complete oxidation and condensation, since it was believed that the transition of these substances to the gaseous state was necessary for the reaction to take place.

It can be assumed that the oxides Li_2O , BeO , MgO , Al_2O_3 are in the condensed state in the form of simple substances without the formation of solutions, i.e., if the combustion products contain oxides of several metals, each of them forms a separate phase.

The authors of [22] calculated I_{spec} for two types of fuels – cryogenic and high-boiling – in which polyethylene was chosen as a fuel and oxygen and hydrogen peroxide as oxidants. The ratio of components was assumed to be stoichiometric. The pressures in the combustion chamber and at the nozzle section were 25.3 and 0.02 MPa, respectively. In addition to the above metals, their hydrides were considered as fillers: LiH , MgH_2 , LiAlH_4 , $\text{Mg}(\text{AlH}_4)_2$. Under the conditions of velocity and temperature equilibrium of heterogeneous combustion products, the values of I_{spec} were calculated and shown in the figure as a function I_{spec} of the mass fraction of the filler in the fuel (η). For the convenience of determining the increase in the specific impulse I_{spec} , a percentage scale is given.

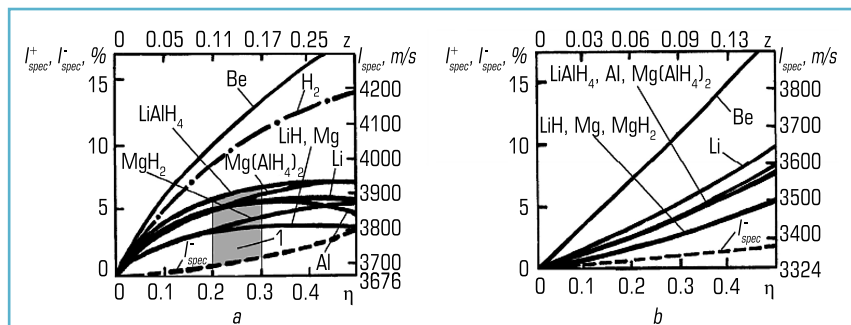


Fig. 4.2 The theoretical specific thrust impulse I_{spec} , its increase I_{spec}^+ and decrease I_{spec}^- vs. the filler (η) and condensate mass content (z) in combustion products: *a* – for polyethylene – oxygen propellant; *b* – for polyethylene – hydrogen peroxide (98 %) propellant; 1 – max ($I_{\text{spec}}^+ - I_{\text{spec}}^-$) area

From the above dependence, it is evident that fillers have a significant effect on I_{spec} . The authors of [22] suggest that a combustible rocket can be implemented with a filler content of

$\eta \approx 0.2\text{--}0.3$ (at such and lower values, the feeding system will still have satisfactory characteristics, and at a higher filler content η it will become unacceptably complicated), then the given increase in I_{spec} by 5–7 % in the first case and by 3–5 % in the second case deserves attention, since each additional percentage of I_{spec} will correspond to approximately 4–6 % of the payload gain in low Earth orbit.

At the same time, it should be noted that the use of thermoplastic polymers as structural materials requires an assessment of thermal and heat resistance in conditions of thermal loads due to aerodynamic heating. It is known that the problem of thermal destruction of traditional structural materials (metals) during launch and passing through the atmosphere is not critical today. At the same time, the strength characteristics of polymers depend significantly on temperature, which requires careful study of the processes of thermal degradation of the material in the atmospheric area.

4.1 EXPERIMENTAL STUDIES OF THERMODYNAMIC PROCESSES DURING THE THERMAL DESTRUCTION OF POLYMERIC MATERIALS

4.1.1 ANALYSIS OF THE PHYSICOCHEMICAL PROPERTIES OF POLYMERIC MATERIALS AS STRUCTURAL MATERIALS OF ULTRALIGHT LV

It is known that the use of polymers of petrochemical origin as fuel is possible due to the high calorific value of such substances [33]. Currently, many technologies have been developed to convert polymers, in particular polyethylene, both low and high density, into liquid fuel [34]. The liquid fuel obtained in this way is quite suitable, for example, for use as diesel fuel [35].

The use of high-density polyethylene as one of the fuel components for hybrid rocket engines is considered in works [36, 37]. The paper [38] analyzed the environmental aspects of polymer fuels when used in rocket engines. The possibility of using polyethylene as rocket fuel or a component of rocket fuel is shown in particular in works [39, 40]. The peculiarity of using polyethylene as a solid rocket fuel is the need for gasification before burning in the combustion chamber. For this, a special gasification chamber is provided in the design of the corresponding engine, the temperature of which reaches 450–550 °C [40]. Gasification of both fuel and oxidizer occurs under the influence of high temperatures. The efficiency of the engine depends on the course of thermodynamic processes in the working chambers of the engine, which requires appropriate research. The study of the physical picture of the processes that occur during the gasification of solid polyethylene under the influence of high temperatures, and the quantitative determination of the thermal effects that occur during the thermal destruction of polyethylene are important for building a mathematical model and determining the optimal parameters of the engine on polymer fuel.

On the other hand, the results of such research are of interest for assessing the possibility of using polyethylene as a structural material for launch vehicle bodies. It should be noted that

during the LV launch in the atmosphere there is aerodynamic heating of the surface, which is not a significant problem in the ascending section when using traditional structural materials for the manufacture of bodies (aluminum alloys). In the case of using polymers as structural materials, the stability of the LV polymer body will be determined by the heat resistance of the corresponding material. Therefore, it is necessary to evaluate the effect of thermal loads on the LV lateral surface.

Among plastics produced in the world, polyethylene (PE) and materials based on it account for approximately 35 % [41]. PE is one of the largest polymers by volume of production (84 million tons/year). The great demand for polyethylene is explained by the combination of a fairly low cost, a large volume of production enterprises, a diverse field of its use, and the variability of possible physical properties. The physical properties of polyethylene can be influenced by changing its density, structure, molecular weight, molecular weight distribution, etc. Accordingly, the field of use of polyethylene is very wide – from low-molecular adhesives, films with a thickness of 3–5 microns to high-strength pipes with a diameter of up to 1500 mm. Fibers with a modulus of elasticity up to 250 GPa are also obtained on the PE basis [41].

Traditional for industry are high pressure polyethylene (LDPE), low pressure polyethylene (HDPE) and medium pressure polyethylene (MDPE). Depending on the properties and purpose, different brands of polyethylene are produced, which differ in the degree of branching of the chain, degree of crystallinity, density and other indicators.

A feature of high-pressure polyethylene (LDPE) is the branching of the polymer chain, which is the reason for the formation of a loose, partially crystalline structure, and therefore a decrease in the density of the polymer and its physical and mechanical characteristics.

Low-pressure polyethylene (HDPE) is characterized by a linear structure and belongs to polymers capable of crystallization. The content of the crystalline phase of HDPE reaches 80 %. Density and other characteristics for HDPE are significantly higher than for LDPE. In terms of deformation-strength properties, HDPE is close to structural plastics. The introduction of reinforcing fibrous fillers into HDPE allows the use of this material for the manufacture of products of responsible purpose [41].

In addition to the main polyethylenes, ultra-high molecular weight polyethylene (UHMWPE), linear low-density polyethylene, high molecular weight high density polyethylene and a number of other brands are also produced [41]. Ultra-high molecular weight polyethylene (UHMWPE) is a linear polyethylene with a molecular weight in the range of 3,000,000 to 6,000,000, widely used in body armor, automotive, and aerospace industries [42, 43].

One of the most widespread and versatile polymers is polypropylene (PP), which due to its properties belongs to construction materials and is used for the production of structural products, pressure pipes, rigid films, household products, etc. PP, like HDPE, belongs to polymers capable of crystallization. The content of the crystalline phase is 73–75 %. PE, PP belong to non-polar polymers, they dissolve only at elevated temperatures in strong solvents (chlorinated, aromatic hydrocarbons), resistant to the action of acids and alkalis [41].

The main physical and mechanical properties of thermoplastic polymers that are important from the point of view of the problem are considered in [44].

To assess the practical suitability of polymeric materials, their mechanical properties are of primary importance. The physical and mechanical properties of PE and PP depend on the molecular weight of polymers, the structure of polymer chains, and their flexibility. At the same time, the properties of polyethylenes can differ significantly depending on the parameters of their production process and the selected catalytic system [41]. If the polymerization of ethylene takes place in the presence of radical initiators under conditions of high pressure and temperature, LDPE with a large number of side chains is obtained. HDPE, which is obtained by coordination-ion polymerization in the presence of Ziegler-Natta catalysts, has fewer side chains, its macromolecules are linear. This difference accounts for the higher density, strength and rigidity of HDPE, but at the same time it somewhat limits its use in cases where increased flexibility and impact toughness are required. An increase in impact strength and flexibility is achieved by introducing short side chains to macromolecules, which is possible due to the copolymerization of ethylene with other olefins.

The highest mechanical characteristics are typical for polymers of a linear structure. The strength of branched polymers depends on the degree and type of branching, and the physical and mechanical properties of network polymers depend on the number of intermolecular chemical bonds (crosslinks). With an increase in intermolecular bonds, the hardness and modulus of elasticity increase, and the relative deformation decreases [45].

The most important mechanical parameters from the point of view of the practical application of polymer materials are the modulus of elasticity, relative elongation and tensile strength. The main physical and mechanical properties of polyethylene and polypropylene are listed in **Table 4.2** [46].

The authors [47] investigated the physical and mechanical properties of pure PP (with a degree of crystallinity of 51 %) and HDPE (with a degree of crystallinity of 68 %), which demonstrated that the strength and modulus of elasticity of PP are higher than HDPE. The authors explain this by the fact that PP has a CH_3 group bound to the carbon atom, which prevents chain rotation and makes the material stronger, but inflexible. Compression, bending tests have shown that PP exhibits higher resistance to compressive forces than HDPE. The disadvantage of PP compared to HDPE is its lower resistance to dynamic loading. The presence of a crystalline phase allows polyethylene to maintain its mechanical strength in a wide range of temperatures.

The authors of [41, 46] note that at elevated temperatures there is a significant difference in the behavior of LDPE and HDPE. At a temperature of -60°C , the tensile stress for HDPE is 1.25 times higher, and at 100°C , it is approximately 4 times higher. Up to 20°C , the relative elongation for LDPE is higher than for HDPE, but when the temperature rises above 40°C , a decrease in relative elongation with increasing temperature is observed, unlike HDPE. The yield strength, modulus of elasticity, density of PE are determined by its composition. The difference in the value of the modulus of elasticity during bending for LDPE, HDPE increases with increasing temperature. Heat resistance increases with increasing degree of crystallinity in the series $\text{LDPE} < \text{MDPE} < \text{HDPE}$.

● **Table 4.2** Physical and mechanical properties of polyethylene and polypropylene

Physico-mechanical properties	LDPE	HDPE	UHMWPE	PE-X	PP	PP (iso)	PP (syndio)
Crystallinity, %	28.8–60	60–90	41.2–91.1	22–41	3.2–67	29–75	25–63
Density at 20 °C, kg/m ³	915–929	940–965	930–940	900–1010	840–1330	900–910	880–930
Tensile strength, MPa	10–31.8	13–51	21–50.2	9–26	26–32	30	15.2–25.2
Tensile modulus, MPa	130–348	500–1100	680–860	–	1700	825	483
Tensile stress at yield, MPa	10.8–14.1	21.4–31	17–41	–	31–35.2	33–36	–
Elongation, %	130–780	250–1200	250–600	350–600	10–140	90–500	250–300
Tensile yield strain, %	–	8.7–15	11–20	–	7–12	10–12	10–11
Flexural strength, MPa	7.5	–	20–26.5	–	41	38.9	–
Flexural modulus, MPa	230–495	750–1600	440–1340	–	1240–1600	1150–1570	345
Elastic modulus, MPa	–	700–1000	700–800	–	–	2357–3450	–
Young's modulus, MPa	–	800–1005	1800–3300	–	1200–2000	–	–
Compressive strength, MPa	–	20	23	–	40	–	–

The mechanical properties of polypropylene are determined by its structure. The atactic fraction has the properties of amorphous liquid polymers, the isotactic fraction has the properties of highly crystalline polymers. Industrial polypropylene consists mainly of isotactic macromolecules, which is why its high mechanical characteristics are determined.

Thermophysical and thermal properties

Similar to mechanical properties, the ability of polymer materials to undergo temperature deformation is determined by the chemical structure, physical organization of polymers, morphology of their supramolecular structure, type of intermolecular bonds, etc. Research has established that the lower the physical and mechanical properties of thermoplastic, the more sensitive it is to temperature changes. For example, PP loses approximately 25 % of its standard bending strength when heated to 80 °C, and HDPE at 60 °C loses half of its initial strength [41, 46].

The chemical structure of the molecules determines the values of the softening and melting temperatures, the rate of transition from the crystalline state to the amorphous state. HDPE softens

under load at 70–75 °C and melts at 128 °C. LDPE, which has a lower degree of crystallinity, softens at 65 °C and melts at 105–110 °C. Changing the chemical structure of polyolefin by replacing one hydrogen atom with a CH₃ group (PP) leads to an increase in softening and melting temperatures.

In order to determine the practical value of polymeric materials, it is necessary to know their thermophysical characteristics. The physical structure of the polymer significantly affects the coefficient of thermal expansion. When amorphous polymers are heated, the volume of the material increases in proportion to the temperature, but the speed of this process is determined by the physical state of the object. When a certain temperature is reached, thermal expansion increases. For crystalline polymers, at the temperature of crystallization, there is a jump-like increase in the rate of thermal expansion at a higher temperature. During the heating of partially crystallized polymers, the features of the amorphous and crystalline components are successively revealed [41, 46]. Temperature characteristics are given in **Table 4.3** [46].

The transfer of thermal energy by the polymer occurs due to the thermal fluctuations of the kinetic fragments of macromolecules. Therefore, the thermal conductivity of amorphous and partially crystalline thermoplastics changes differently depending on the temperature. For amorphous thermoplastics, when approaching the glass transition temperature, the value of the thermal conductivity coefficient increases slightly due to the increase in the vibrational activity of fragments of macromolecules. With a further increase in temperature, their thermal conductivity decreases due to a sharp increase in kinetic volume, activation of low-frequency oscillations of large fragments. For partially crystalline polymers, an increase in temperature is accompanied by a weakening of the intermolecular interaction due to an increase in the distance between neighboring macromolecules. A significant part of the thermal energy is spent on structural changes, which is the reason for the decrease in the coefficient of thermal conductivity. For example, after melting and transition of PE into an amorphous state, its thermal conductivity increases [41, 46].

The distribution of heat by the mass of the heated polymer depends on the activity of the kinetic fragments of the macrochains. Therefore, for example, the transition from a glassy physical state to a highly elastic one is accompanied by an increase in the amplitude and frequency of oscillatory and rotational movements and an increase in heat capacity. For partially crystalline polymers, the increase in heat capacity is associated with melting temperatures. For LDPE, the amplitude of the heat capacity peak, depending on the temperature, is at 105–110 °C. In general, when transitioning from a highly elastic to a viscous state, the heat capacity of polymers increases [41, 46].

The authors [47] note that PP exhibits higher thermal properties than HDPE. PP also exhibits higher thermal dimensional stability than HDPE because PP has stronger interatomic forces than HDPE. The coefficient of thermal expansion of HDPE is higher than that of PP due to stronger interatomic forces.

UHMWPE has high mechanical properties, for example, the yield strength of UHMWPE (Dyneema) is 2.4 GPa, but the specific gravity is very low at 0.97, which is the reason for the high strength-to-weight ratio of this grade of UHMWPE compared to carbon steel. One of the important

disadvantages of UHMWPE is poor temperature stability due to the weak bonding between UHMWPE molecules. When a certain temperature is reached, a local thermal excitation occurs at the bonds between molecules, which causes the bonds to break and the long chain to break into short parts [48]. According to the authors of this work, the melting point of UHMWPE (Dyneema) is in the range of 130–136 °C, and the working temperature is about 80–100 °C. However, the authors of [42] stated that the physical and mechanical properties of UHMWPE-based products depend on the parameters of pressing during their manufacture, namely the temperature and compression pressure, cooling rate, etc.

● **Table 4.3** Thermophysical and thermal properties of polyethylene and polypropylene

Thermophysical properties	LDPE	HDPE	UHMWPE	PE-X	PP	PP (iso)	PP (syndio)
Melting temperature, °C	105–115	125–135	133–140	110	120–176	157–171	117–156
Glass transition temperature, °C	–103 to –133	–118 to –133	–110	–	–8 to –51	–10	–15 to +3
Brittleness temperature, °C	–34 to –60	–20 to –76	–70 to –84	–76	–	–	–
Long term service temperature, °C	70	–50 to +82	82	130	–	–	–
Decomposition temperature, °C	–	>250	–	255–285	328	240	260
Thermal conductivity (melt), W/(m·K)	0.55	0.52–0.55	0.39–0.42	–	0.17–0.22	0.12–0.22	–
Specific heat capacity, J/(K kg)	–	2100–2900	1840–2010	–	–	2500–3400	–
Vicat temperature VST/A/50, °C	76–109	122–129	126	–	138–155	150–155	111
Ignition temperature, °C	340–343	340–343	340–343	–	>200	>200	>200
Autoignition temperature, °C	350	350	350	260–320	570	570	570
Heat of combustion, J/g	47740	47740	47740	–	45800	45800	45800
Volatile products of combustion	CO, CO ₂ , aldehydes, benzene	CO, CO ₂ , aldehydes, benzene	CO, CO ₂ , aldehydes, benzene	CO, CO ₂ , aldehydes, NOx	CO, CO ₂ , soot	CO, CO ₂ , soot	CO, CO ₂ , soot

In work [42], the thermal decomposition of UHMWPE samples produced by pressing from UHMWPE powder with a density of 940 kg/m³ from the Sigma company was investigated using

thermogravimetric analysis in the temperature range of 50–600 °C at a heating rate of 5 °C/min in a nitrogen environment Sigma-Aldrich Co (USA). It was established that the UHMWPE sample produced at a compression temperature of 100 °C and a pressure of 10 MPa remains stable in the temperature range of 50–216 °C, no loss of sample mass is observed. The maximum thermal decomposition is observed in the range of 216–526 °C.

The authors [49, 50] investigated the effect of temperature on mechanical parameters for Marlex 5003 polyethylene with a density of 965 kg/m³ and polypropylene with a density of 909 kg/m³. The study was carried out at an increase in temperature from 21 to 117 °C for polyethylene and from 22 to 143 °C for polypropylene under conditions of uniaxial tension up to the yield point. Using the methods of differential scanning calorimetry (DSC), it was determined that the melting point of HDPE is 140 °C, and the melting point of PP is 164 °C. For both polymers, it was found that the dependence of the yield strength on temperature is almost linear (**Fig. 4.3**) [49, 50].

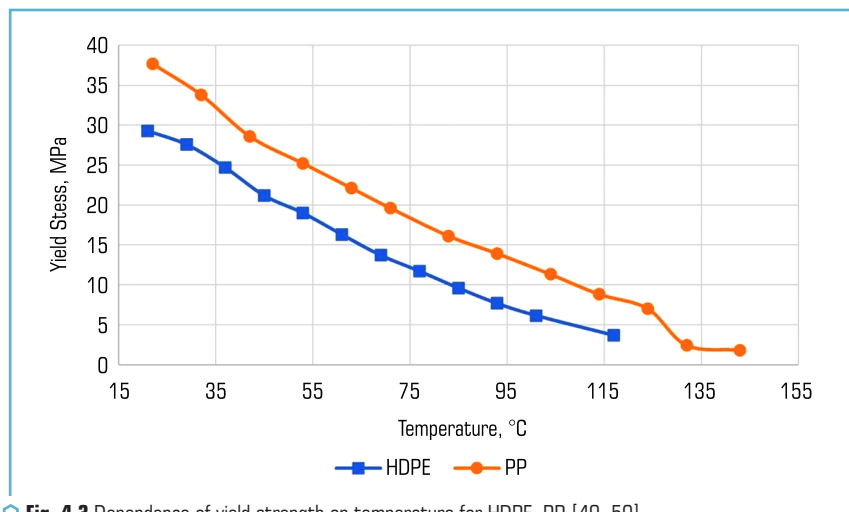


Fig. 4.3 Dependence of yield strength on temperature for HDPE, PP [49, 50]

When the temperature increases from 20 °C to 143 °C, a gradual decrease in the yield point for HDPE is observed by 88 %, for PP – by 95 %. The results of the study by the authors [49, 50] on the change of the Young's modulus under the same conditions demonstrate a decrease in the value of the Young's modulus by 95–97 % for both HDPE and PP (**Fig. 4.4**).

In addition to the polymer materials discussed above, structured (cross-linked) polyethylene PE-X can also be a rather interesting object of future research. According to the standard [51], pipes made of structured (cross-linked) polyethylene PE-X with a degree of cross-linking of at least 60 % are able to withstand a maximum operating temperature of 90 °C from one to ten years

(depending on the thickness of the pipes and stress in the pipe walls), and the maximum temperature of short-term exposure is 100 °C for 100 hours. The peculiarity of PE-X is that the structure of polyethylene changes in such a way that the polymer chains are connected to each other by chemical bonds in a three-dimensional network. At the same time, the new structure prevents the melting of the polymer before the destruction of the cross-linked structure. The density of PE-X used to make the pipes is 900–970 kg/m³, the relative elongation of the pipes at break at 23 °C is not less than 250 %, the tensile strength after heating at 100 °C is not less than 9 MPa, and the strength when stretched at 23 °C – not less than 19 MPa. The change in the length of the pipes after heating is no more than 3 %.

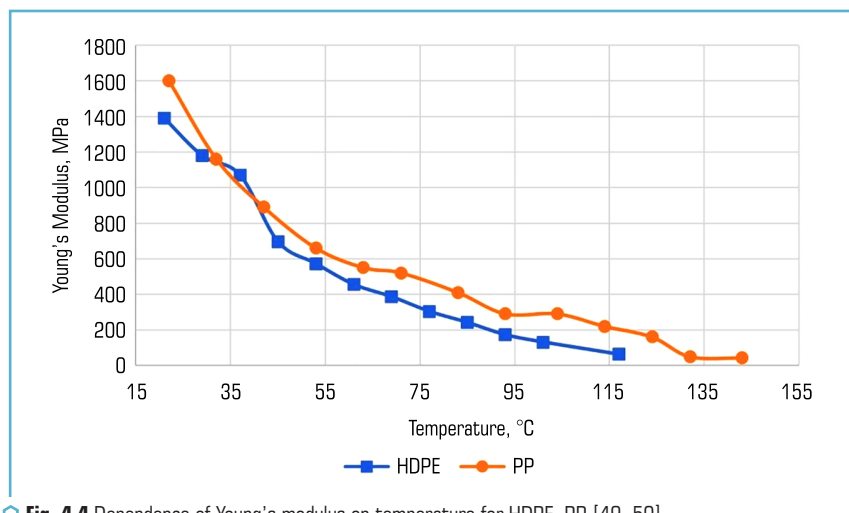


Fig. 4.4 Dependence of Young's modulus on temperature for HDPE, PP [49, 50]

However, when choosing a polymer as a structural material, one should focus not only on physical-mechanical and thermal properties, but also on the technology of manufacturing the product and the possibility of modifying the material. The authors [52] found that the injection molding technology leads to a significantly higher HDPE service life compared to blow molding or pressing. This is believed to be due to higher crystallinity and molecular orientation when injection molding is used.

When choosing materials for traditional LV bodies, they proceed from the need to reduce the mass of the "dry" structure, as well as technological requirements, corrosion resistance, cost, availability of materials, etc. But the main criterion, based on the principles of system design, is the criterion of the minimum weight of the structure. But for burned rockets, the mass of the structure is not passive, it is simultaneously the mass of fuel consumed during the operation of the rocket engine.

Thus, on the basis of the initial review of the literature on the complex of physical, mechanical and thermal properties of polyolefins, UHMWPE, PE-X, PP can be singled out as promising basic alternative construction materials for the manufacture of shells of autophagic missiles. At the same time, the need for an experimental study of the physical and mechanical properties of the selected polymers, taking into account the conditions of their further operation, is mandatory.

4.1.2 METHODOLOGY OF EXPERIMENTAL STUDIES OF THERMODYNAMIC PROCESSES DURING THE THERMAL DESTRUCTION OF POLYMER MATERIALS BY METHODS OF THERMAL ANALYSIS

Experimental studies of thermodynamic processes of thermodynamic processes are based on thermal analysis. Thermal analysis (TA) is a method of studying physicochemical and thermodynamic phenomena occurring in a substance under conditions of controlled heating of the external environment. This method allows to qualitatively and quantitatively study the processes of phase transformations, determine temperatures and thermal effects of phase transformations. Methods of thermal analysis are presented in detail, for example, in [53].

Thermal analysis methods were used for the research: differential thermal analysis (DTA), thermogravimetric (TG), differential thermogravimetric analysis (DTG), differential scanning calorimetry (DSC). Thermogravimetric analysis (TG) allows to determine the change in the mass of the sample under investigation during heating. DTA is based on measuring the temperature difference between the substance under investigation and an inert standard using a differential thermocouple. This makes it possible to detect thermal effects in the substance under investigation. The DSC method allows to measure changes in heat flow from temperature and directly determine the change in energy (enthalpy) in the process. The methods of thermogravimetric analysis allow to determine the change in mass during heating, and the DTG curve to determine the temperature of chemical reactions.

The schematic diagram of the simplest thermoanalytical device, which is used in almost all variants of thermal analysis, is shown in **Fig. 4.5**.

The thermal analyzer consists of high-precision scales with crucibles (usually platinum), which are placed in the chamber of a small electric furnace. A control thermocouple is located in the immediate vicinity of the sample, which measures the temperature with high accuracy. The furnace chamber may be filled with an inert gas to prevent oxidation or other undesirable reactions. The system is managed, and data processing is carried out by specialized software.

In this work, the experiments were performed on the basis of the center for collective use of scientific equipment "Innovative technologies in the rocket and space industry" at Oles Honchar Dnipro National University (Dnipro, Ukraine). A high-precision STA 6000 analyzer was used for the experiments, which allows simultaneous thermogravimetric, differential thermal analysis and differential scanning calorimetry. The device is equipped with a SaTurnA sensor, the compact heating furnace is characterized by an improved temperature control system, measurement accuracy and

rapid cooling. The general view of the analyzer is presented in **Fig. 4.6**. The device analyzes solid samples in the form of powder, crystals or granules. The object of the study were samples of high-density polyethylene, low-density polyethylene, and polypropylene, which were placed in the crucible of the analyzer in **Fig. 4.7**.

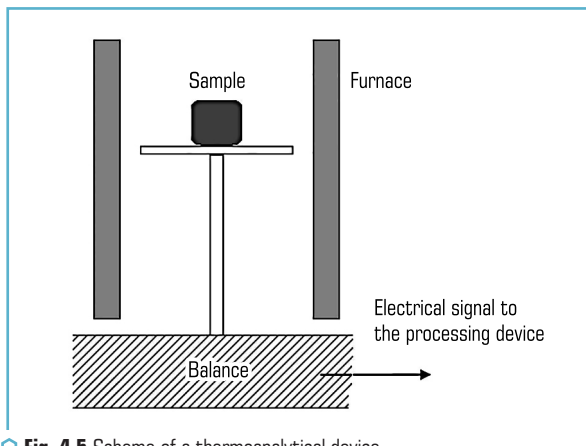


Fig. 4.5 Scheme of a thermoanalytical device

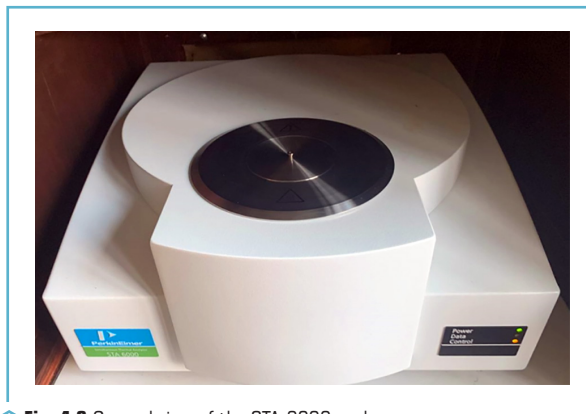


Fig. 4.6 General view of the STA-6000 analyzer

Heating took place at a constant rate in a neutral medium (argon). In the course of the experiment, thermograms were constructed on which DTA, TG, DSC curves were reflected. The nature of the curves reflects the processes occurring in polyethylene during its heating. Visualization

of such curves is a thermogram. The obtained curves are processed with the help of specialized software, which allows to determine the thermal effects of the relevant processes, temperatures that correspond to structural transformations and reflect changes in the mass of the investigated samples during heating.

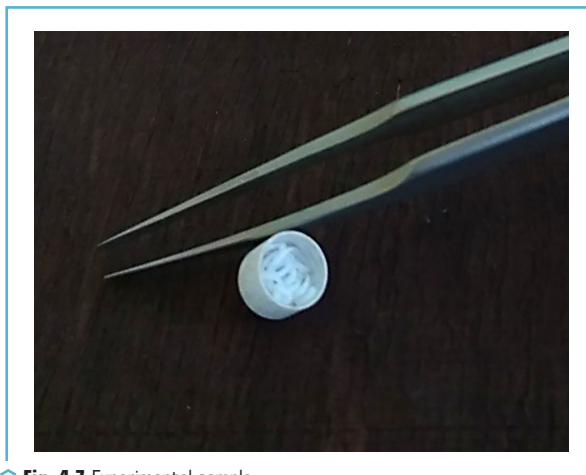


Fig. 4.7 Experimental sample

Methodologically, experimental research consists of the following successive stages:

- preparation of a sample of the substance under investigation: grinding, determination of initial parameters;
- preparation of the analyzer for work: zeroing of parameters, programming of research parameters: heating rate, temperature range, installation of the sample in the crucible in the furnace;
- conducting an experiment;
- processing of experimental thermograms obtained as a result of the experiment: determination of temperatures corresponding to transformations in the material, parameters of mass loss, thermal effects of phase transformations.

Conclusions about physical phenomena and their quantitative characteristics are made on the basis of the analysis of curves on thermograms, for example, **Fig. 4.8** schematically shows a typical view of TG and DSC curves.

Analysis of these curves allows determining the main parameters of thermodynamic processes. Temperature is plotted on the abscissa axis, and mass loss or heat flows are plotted on the ordinate axis. The TG curve usually has an initial section where the change in mass is insignificant and it is most often associated with the release of residual solvent or water from the sample, as well as a second (or more) section that is due to the thermal destruction of the sample under study.

The presence of peaks on the DSC curve indicates the effects of heat release or absorption, which is associated with phase transformations inside the material. The area of the figure bounded by the peak (**Fig. 4.8**) determines the thermal effect of this transformation.

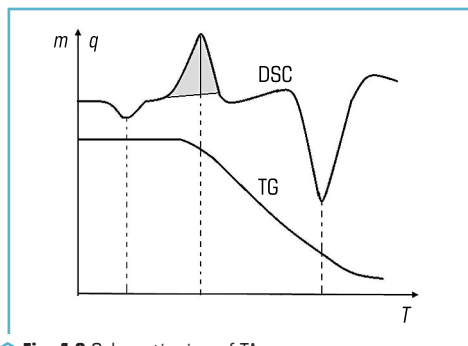


Fig. 4.8 Schematic view of TA curves

4.1.3 RESEARCH RESULTS OF THERMODYNAMIC PROCESSES OF DESTRUCTION OF POLYMERIC MATERIALS DURING HEATING

According to the methodology described above, research was carried out on the following materials: high molecular weight polyethylene, low molecular weight polyethylene, white polypropylene and gray polypropylene.

The research was conducted under the following conditions: at the beginning of the experiment, the furnace temperature was kept constant at 30 °C for 3–5 minutes, then the temperature was varied in the range from 30 °C to 600 °C at a rate of 10 °C/min. The system was filled with argon, which excluded the possibility of accidental oxidation of the materials under study. As a result of the experiments, the thermograms presented in **Fig. 4.9–4.12**.

Fig. 4.9 shows a thermogram obtained during heating of high molecular weight polyethylene.

The data in **Fig. 4.9** show that for polyethylene structural changes in the material began at a temperature of 136 °C (409 K). The thermogravimetric curve shows that the active mass loss of the sample began at a temperature of 251 °C (524 K). At a temperature of 500 °C (773 K), almost complete gasification of polyethylene took place, the rate of mass loss was 0.075 mg/°C.

Fig. 4.10 shows the thermogram obtained during the heating of polyethylene of low molecular weight polyethylene.

The data in **Fig. 4.10** show that the structural changes in the sample of low molecular weight polyethylene began at a temperature of 108 °C (381 K), which is 28 °C lower than the temperature value in the previous case. At the same time, the mass loss of low molecular weight

polyethylene begins at a temperature of 229 °C (502 K), which is 20 °C lower than for the previous sample. At a temperature of 498 °C (771 K), the mass loss was 97 % of the initial one, and at 593 °C (866 K), complete gasification of the sample occurred. The rate of mass loss was 0.098 mg/°C.

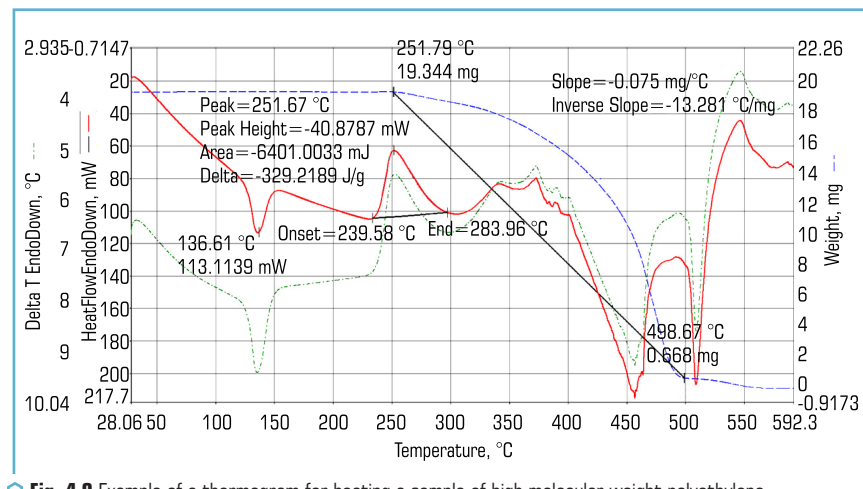


Fig. 4.9 Example of a thermogram for heating a sample of high molecular weight polyethylene

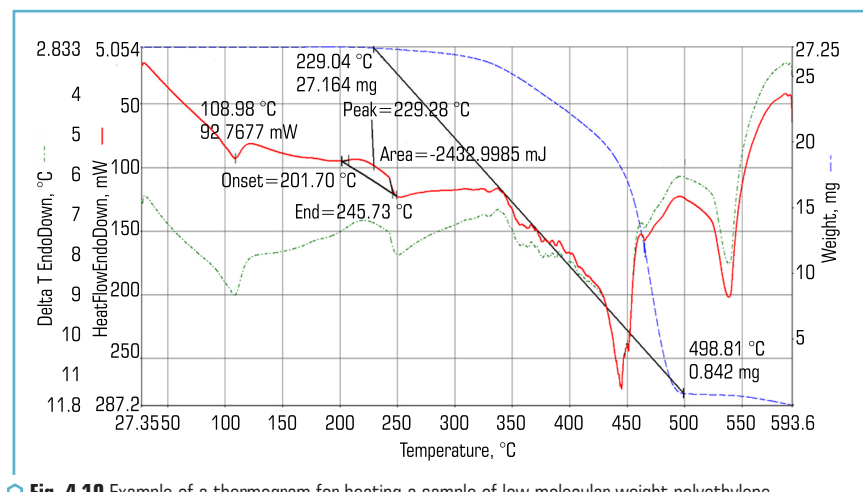


Fig. 4.10 Example of a thermogram for heating a sample of low molecular weight polyethylene

A comparison of two samples of polyethylene shows that from the point of view of using this polymer as a structural material for LV bodies, preference should be given to high molecular weight polyethylene, as it has greater heat resistance. It should be noted that, as was shown above, high molecular weight polyethylene also has higher strength and wear resistance.

Fig. 4.11 shows a thermogram obtained during heating of gray polypropylene.

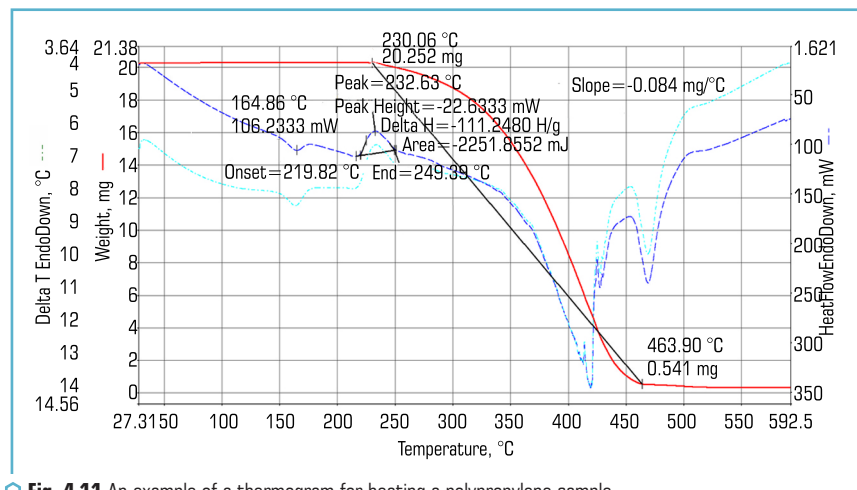


Fig. 4.11 An example of a thermogram for heating a polypropylene sample

For the considered sample of gray propylene, structural changes begin at a temperature of 164 °C (437 K), mass loss begins at a temperature of 230 °C (503 K), at a temperature of 463 °C (775 K), almost complete gasification of the sample occurred, the rate of mass loss was 0.084 mg/°C.

Fig. 4.12 presents the thermogram obtained during the heating of white polypropylene.

As can be seen from the data in **Fig. 4.12**, structural changes in the white polypropylene sample began at a temperature of 131 °C (408 K), mass loss began at a temperature of 258 °C (531 K), at a temperature of 500 °C (773 K), the sample lost 97 % of its mass, complete gasification occurred at 594 °C (867 K), the rate of mass loss was 0.112 mg/°C.

So, the results of experimental studies of selected samples of gray and white polypropylene show that polypropylene has greater heat resistance than polyethylene. In the considered case, white propylene showed better results in terms of heat resistance, while white propylene had higher values in terms of heat resistance, but also a higher rate of decomposition than the other samples.

Based on the obtained results, high molecular weight polyethylene and polypropylene (white) can be recommended for practical use as a structural material under the condition of heat

resistance. According to the DTA curves, the thermal effect of thermal destruction was determined as the area of the figures described by the peaks of the heat flow curves. So, based on the results of the experiments and the data of p. 4.1.1, the initial data (**Table 4.4**) were determined for further use during the mathematical modeling of heat and mass transfer processes both in engines and in the conditions of interaction of the polymer shell of the LV body with the high-speed flow of oncoming gas.

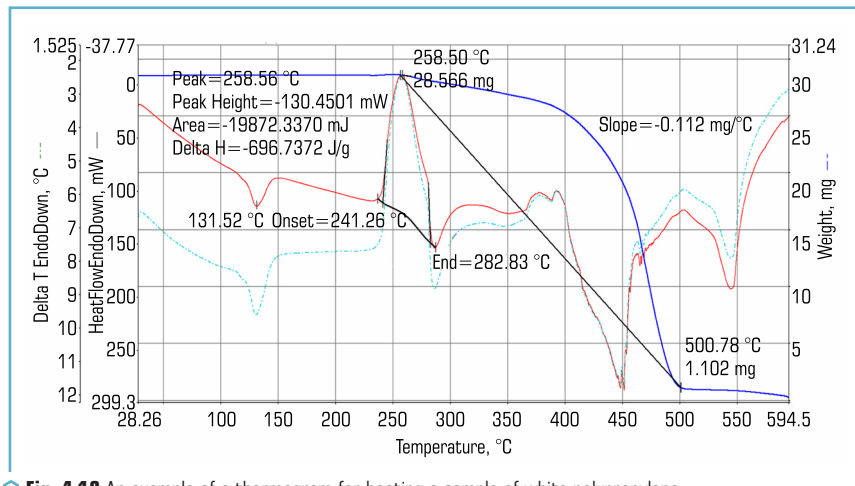


Fig. 4.12 An example of a thermogram for heating a sample of white polypropylene

Table 4.4 Research results

Material	High molecular weight polyethylene	Polypropylene
Density ρ , kg/m ³	930	920
Thermal conductivity coefficient λ , W/(m·K)	0.335	0.12
Heat capacity s , J/(kg·K)	$1.94 \cdot 10^3$	$2.5 \cdot 10^3$
Melting point, K	502	531
Full gasification point, K	866	867
The rate of mass loss during heating, mg/°C	0.098	0.112
Total thermal effect of thermal destruction, J/kg	$7\,173 \cdot 10^3$	$3\,380 \cdot 10^3$

4.2 ANALYTICAL STUDY OF THE DESTRUCTION RATE OF THERMOPLASTIC POLYMERS UNDER THE INFLUENCE OF HIGH-SPEED GAS FLOWS

4.2.1 PHYSICAL MODELS OF THERMAL DESTRUCTION OF THERMOPLASTIC MATERIALS UNDER THE INFLUENCE OF HIGH-TEMPERATURE AND HIGH-SPEED GAS FLOW

Polymers are high-molecular chemical compounds, the macromolecules of which are formed from a set of monomer units.

Polymer molecules are characterized by a large molecular mass, from several thousand to several million atomic mass units.

The dynamics of the destruction of polymers under thermal and dynamic influence mainly depends on their structure. Polymers with a linear structure do not lose their plastic properties when heated to the melting point, they are called thermoplastics. With a further increase in temperature, they melt, then the macromolecule chain gradually disintegrates into separate links. Due to the fact that the molecular weight of the final products is many times less than the weight of the polymer, these products are in the gas phase at the decomposition temperature.

Given the problem of using polymers as a fuel and the main structural material for the bodies of ultra-light LVs, the most important characteristics are thermal and heat resistance. Heat resistance characterizes the upper limit of the temperature range in which the polymer material can bear mechanical loads without changing its shape. Loss of heat resistance is caused by physical processes (transition of glassy polymers into a highly elastic state or melting of crystalline polymers). Thermal resistance characterizes the upper limit of working temperatures in those cases when the performance of the polymer is determined by resistance to chemical transformations (usually to the destruction of polymers in inert or oxidizing environments).

Recently, polymer materials have begun to be used quite actively in aerospace engineering along with traditional materials – metals. Mainly, polymers are used as part of new composite materials [54]. Polymer composites are used as structural materials for the creation of stabilizers, elements of jet engines, turbine blades, as well as in thermal protection systems, that is, elements that are of critical importance for the functioning of aerospace technology. Consequently, the issues of stability and strength of polymers, which are fundamental characteristics of solids, have attracted the attention of many researchers. These issues become especially important if polymer materials are used in conditions of high temperatures and interaction with high-speed flows of chemically active gases.

The problem of the destruction of materials from a theoretical point of view is quite complex and significantly non-linear. It is known [55] that there are three types of polymer failure: brittle, quasi-brittle, and non-brittle. Each type of destruction takes place in a certain temperature range. Models and approaches to the study of the mechanics of brittle and quasi-brittle failure of polymeric materials are considered in works [56, 57]. It should be noted that today, the theoretical

foundations of the mechanics of the destruction of polymeric materials are based on the theory of thermal fluctuation destruction, in which the temperature factor plays a leading role.

Under the conditions of operation of polymeric LVs, the main mechanisms of destruction of polymeric materials will be thermal degradation, destruction, and melting of the material mass. Thus, in the future, it is not possible to consider the processes of brittle and quasi-brittle destruction, given their secondary nature under the conditions of thermal loads in the combustion chamber of the polymeric LV engine or aerodynamic heating of the body. For LVs and spacecraft, the processes of thermal degradation occur under the influence of atmospheric oxygen, thermal loads are accompanied by the introduction of material mass. As a result of such influences, there is mass transfer from the surface and a change in the physical and mechanical properties of materials and erosion (reduction in durability) of the material.

Depending on the level of thermal and gas dynamic loads, several options for applying thermoplastic materials are implemented. At relatively high heat fluxes and low tangential stresses, mass transfer occurs mainly due to thermal decomposition of the material. At high heat fluxes and minor tangential stresses, mass transfer is caused by both thermochemical processes and material erosion. At high heat fluxes and high tangential stresses, thermal decomposition does not occur, since the temperature on the surface does not reach the value of the destruction temperature. The process of destruction, in this case, is caused only by erosion of the material. However, the specific values of the parameters determining one or another failure mode may differ for different thermoplastics.

The failure patterns that occur in practice depend on the scheme of use of the thermoplastic material. In the case of using polymer fillers in composite elements of thermal protection, the destruction process occurs as a result of physical and chemical transformations under the influence of convection and radiation heat flows brought to the surface, diffusion flows of chemically active components, as well as under the influence of gravity and friction. In this case, there is a certain self-regulation of the process – a change in the mass flow rate of the material under the condition of a change in the heat load. The destruction processes are accompanied by phase and chemical transformations. **Fig. 4.13** presents examples of schemes for applying the mass of a composite heat-insulating material with a polymer filler, which can be set depending on the level of heat load and the high-speed pressure of the gas flow.

Fig. 4.13, a shows a model of quasi-stationary destruction, when the polymer filler, which has a low temperature of thermal decomposition, is removed at the same speed as the refractory frame. At the same time, the front of the polymer filler is located at a certain depth from the surface of the coating, that is, in the region of lower temperatures.

Fig. 4.13, b shows the case when the filler has a sufficiently high thermal resistance and will be mechanically destroyed and carried away by the gas flow due to the influence of high-speed pressure. Such a case is more characteristic of organic sublimating materials.

In the case of making LV bodies from polymer materials, the destruction process occurs according to the model presented in **Fig. 4.14**.

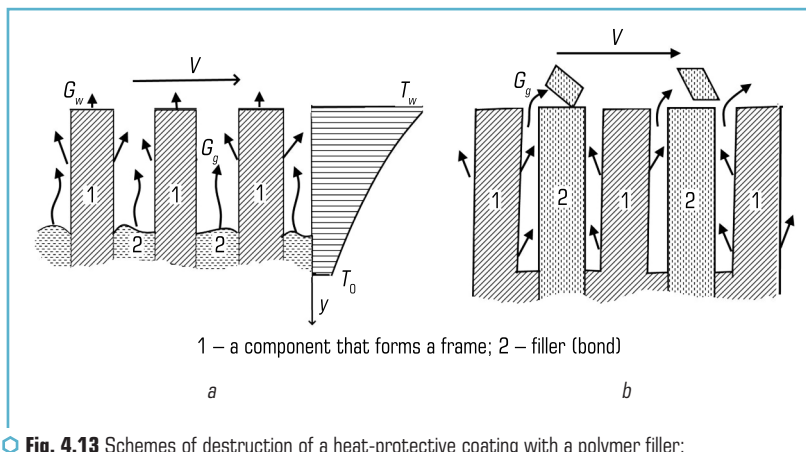


Fig. 4.13 Schemes of destruction of a heat-protective coating with a polymer filler:
a – a filler with high thermal resistance; *b* – a filler with low thermal resistance

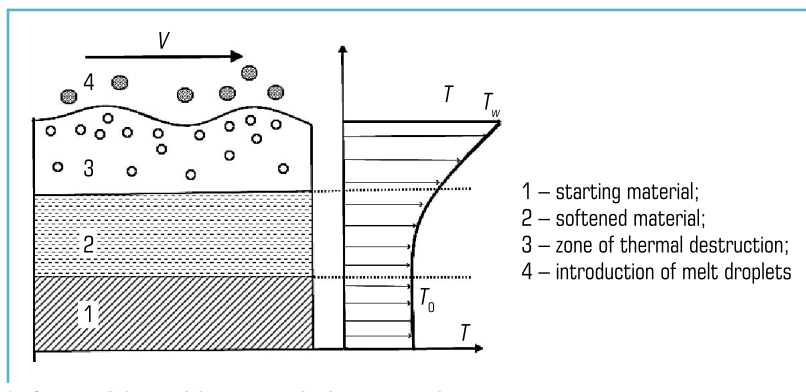


Fig. 4.14 Scheme of destruction of polymer material

Unlike sublimating materials, the transition to a gaseous state in thermoplastics does not occur on the surface, but in a layer of material of a certain thickness bordering the surface (zone 1 and 2 in **Fig. 4.14**). In zone 2, the softening of the material occurs, and in zone 3, the process of thermal destruction takes place. At high temperatures, a melt film can form directly on the surface and even waves can be formed, as shown in [58]. Such a film is very thin and is worn away in the form of drops 4 by a gas flow. In most cases, during the decomposition of polymers, the solid phase immediately turns into a gaseous state.

Therefore, a zone is formed in the middle of the material where it is necessary to take into account the absorption of heat due to the breaking of chemical bonds in the process of thermal

destruction. It should also be taken into account that part of the thermal energy is spent on heating the material to the corresponding destruction temperature. In zone 1 (**Fig. 4.14**), the temperature is low enough and thermal destruction processes do not occur.

The considered physical model of thermal destruction of polymer materials is the basis for building a mathematical model and determining the rate of destruction and mass removal.

In the conditions of the practical use of thermoplastic materials for the manufacture of polymer LV bodies, the phenomenon of polymer aging should be taken into account. This process depends on the flow of heat, oxygen, sunlight, ionizing radiation and has a significant impact on thermodynamic characteristics [59]. Aging of polymer systems is accompanied by the following thermodynamic processes:

- the formation of a surface layer, which has the value of surface tension, adsorption capacity, chemical potential and activation energy, the energy at which chemical transformations in the structure of the polymer begin, which differ from the main mass of the material;
- adsorption of moisture, gases and change in thermodynamic characteristics of the surface;
- diffusion of low molecular weight substances into the volume of the polymer;
- influence of the stress-strain state of the surface layer;
- the influence of a complex of climatic factors: temperature, which increases the total energy of the polymer and increases the mobility of macromolecule links in it, breaks low-energy bonds, and creates new spatial bonds; humidity, which affects thermodynamic and mechanical characteristics, plasticizes and reduces strength.

All these phenomena affect the thermodynamic characteristics of the surface and the ability of the surface to adsorb and enter into chemical interaction with atmospheric liquids and gases, create prerequisites for premature destruction of materials. Therefore, the introduction into practice of the use of polymer casings for LVs, which at the same time are combustible, requires the definition and development of regulations regarding the conditions of storage and operation of polymer casings.

4.2.2 DEVELOPMENT OF A METHOD FOR DETERMINING THE SPEED OF THERMAL DESTRUCTION OF THERMOPLASTIC MATERIALS UNDER THE INFLUENCE OF HIGH-TEMPERATURE AND HIGH-SPEED GAS FLOW

Let's determine the quantitative characteristics of the process of destruction of thermoplastic material under the influence of a high-temperature gas flow in accordance with the physical model adopted above. Let's suppose that the destruction process occurs without the formation of a melt film on the surface, and the solid phase of the polymer passes immediately to the gas phase, which is carried by the oncoming gas stream. Let's analyze the process of removal of thermoplastic material from the LV surface as a result of thermal influence from the standpoint of energy balance. The total thermal effect of destruction consists of the heat required to heat the material to the temperature of loss of heat resistance and the heat of sublimation

$$H = c_p(T_p - T_0) + \Delta Q, \quad (4.1)$$

where the values included in (4.1) are defined in clause 1 of this paper.

Let's assume that the entire mass of the polymer that is gasified during heating will be entrained by the oncoming gas flow, so the rate of mass loss will be equal to the entrained mass rate. For polymers, the rate of thermal destruction is generally determined by the kinetics of the decomposition process. The equation describing the decomposition rate has the form [60]:

$$-\frac{d\rho}{dt} = Kf(\rho), \quad (4.2)$$

where ρ – density; t – time; K – reaction rate constant that depends on temperature, $f(\rho)$ – function that K – characterizes the mechanism of decomposition of a substance and is usually given by the dependence $f(\rho) = \rho^n$, n – order of the reaction. The reaction rate constant is determined by the Arrhenius law:

$$K = B \exp\left(-\frac{E}{RT}\right), \quad (4.3)$$

where B – pre-exponential factor; E – activation energy; R – gas constant; T – temperature. So, taking into account (4.3), the expression (4.2) takes the form:

$$g = -\frac{d\rho}{dt} = B \exp\left(-\frac{E}{RT}\right) \rho. \quad (4.4)$$

If to assume the one-dimensionality of the heat propagation process in the material layer, the weak dependence of thermal conductivity on temperature. constant filling of cavities with melt formed as a result of thermal destruction in the thickness of the layer, then in the quasi-stationary mode the equation of heat transfer in the material has the form:

$$\lambda \frac{d^2T}{dy^2} + \rho c u_\infty \frac{dT}{dy} - q_v = 0, \quad (4.5)$$

where u_∞ – linear rate of mass removal, λ – thermal conductivity $q_v = B\Delta Q\rho \exp(-E/RT)$. Taking into account that the rate of destruction is determined by the law (4.4), let's determine the linear rate of mass loss is defined as:

$$u_\infty = \frac{G_\Sigma}{\rho} = \frac{\int_0^h g dy}{\rho} = \int_0^h B \exp\left(-\frac{E}{RT}\right) dy, \quad (4.6)$$

where G_Σ – mass flow rate, h – thickness of the material layer.

The first term of equation (4.5) describes the transfer of heat due to thermal conductivity, the second term of heat absorption due to heat capacity, the third term of heat absorption due to thermal destruction of the material. Knowing the temperature distribution, it is possible to calculate the rate of mass introduction, respectively, the rate of destruction according to the formula (4.6).

Equation (4.5) does not have an analytical solution in the presented form. If to assume that the second term of equation (4.1) can be neglected, then equation (4.5) can be written in the form:

$$\lambda \frac{d^2 T}{dy^2} - B \Delta Q \rho \exp\left(-\frac{E}{RT}\right) = 0. \quad (4.7)$$

In the case when a sufficiently thick flat layer of polymer material is considered, which decomposes at the surface temperature T_∞ , then the boundary conditions should be added to equation (4.7)

$$T|_{y=0} = T_\infty, \quad T|_{y \rightarrow \infty} \rightarrow T_0. \quad (4.8)$$

For the problem (4.7)–(4.8) in [61], a solution was obtained, according to which an approximate formula was proposed for calculating the mass rate of removal of polymer material from a unit area of a flat surface:

$$G_s = \frac{\sqrt{B \rho \lambda \frac{R}{E} \exp\left(-\frac{E}{RT_\infty}\right) T_\infty}}{\sqrt{H - \frac{1}{2} \Delta Q}}. \quad (4.9)$$

Expression (4.9) makes it possible to estimate the contribution of the mass of the polymer material during thermal destruction for the quasi-stationary regime. At the same time, during the LV passage of the atmospheric section of the trajectory, the thermal load conditions change significantly. In work [62], theoretical calculations of the trajectories of a rocket with a polyethylene body and thermal loads during passage through the lower layers of the atmosphere were performed. Let's evaluate the heat loads on the side surface of the LV polymer body according to the data [62], the methodology [63] and the parameters of the standard atmosphere [64].

Fig. 4.15 shows how the flight parameters change: altitude 3, Mach number 2, heat flow due to aerodynamic heating 1, as well as heat flow due to solar radiation 4 [65] in the atmospheric section of the flight of a polymer rocket with a diameter of 0.3 m and an initial overload of 1, 2.

As can be seen from **Fig. 4.15**, the maximum heat loads correspond to the height range of 20...60 km. Under the influence of intense heat flows, thermoplastic materials, including polyethylene and polypropylene can heat up, which leads to a decrease in strength characteristics and possible deformation of the body. When polymer shells are heated, a number of homogeneous and heterogeneous chemical reactions and phase transformations can begin, which are accompanied

by heat absorption and mass loss. Therefore, in mathematical modeling, additional terms in the energy equation describing processes of volumetric heat absorption should be taken into account.

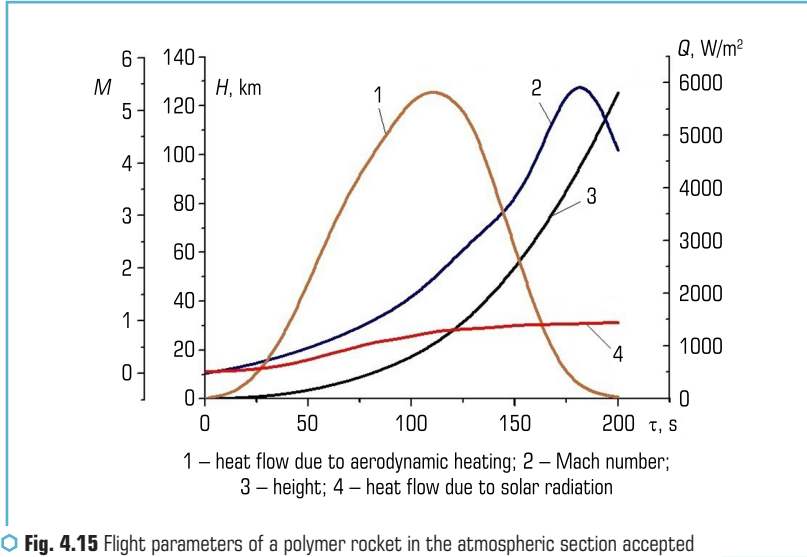


Fig. 4.15 Flight parameters of a polymer rocket in the atmospheric section accepted for calculation

The mathematical model of non-stationary heat transfer in the hull shell during movement on the atmospheric part of the trajectory in a one-dimensional formulation has the form:

$$c\rho \frac{\partial T}{\partial \tau} = \frac{1}{r} \frac{d}{dr} \left(\lambda r \frac{dT}{dr} \right) - q_i(r), \quad \tau > 0, R_1 \leq r \leq R_2, \quad (4.10)$$

$$T|_{t=0} = T_0, \quad (4.11)$$

$$\left. \frac{\partial T}{\partial r} \right|_{r=R_1} = 0, \quad \lambda \left. \frac{\partial T}{\partial r} \right|_{r=R_2} = -q(\tau), \quad (4.12)$$

where T_0 – initial temperature of the wall; R_1, R_2 – inner and outer radii of the body shell; c – heat capacity.

The source term in (4.10) is defined as in (4.5), and the right-hand sides of the second equality (4.12) are determined according to the heat flow function presented in **Fig. 4.15**.

Problem (4.10)–(4.12) was solved numerically. **Fig. 4.16, a** shows the results of calculating the temperature fields in the polyethylene cylindrical wall of the body during the LV movement along the trajectory described by the data in **Fig. 4.15**. The results of a similar calculation for a polypropylene wall are shown in **Fig. 4.16, b**.

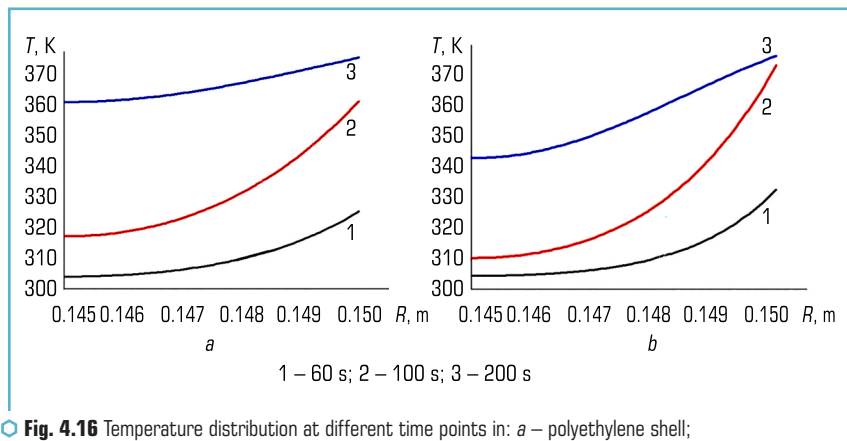


Fig. 4.16 Temperature distribution at different time points in: *a* – polyethylene shell; *b* – polypropylene shell

As can be seen from **Fig. 4.16**, the outer surface of the walls made of polypropylene heats up during flight in the atmosphere a little more than that of polyethylene. This is due to the lower thermal conductivity of polypropylene than polyethylene. The temperature of the outer surface of the case at the moment of time after 200 s (altitude 125.3 km) is 375 K for polyethylene and 419 K for polypropylene. Therefore, for both materials, the surface temperature remains lower than the temperature at which thermal destruction begins.

If the heat flows are large enough, and the zone of thermal destruction degenerates into a thin layer, then the destruction process will occur only on the surface of the material. It is possible to estimate mass transfer using the ratio used to estimate the process of ablation of materials [66]:

$$G_{\Sigma} = \frac{q_s}{H}. \quad (4.13)$$

In the case of the combustion process of polymer fuel, it is necessary to take into account the chemical interaction of the polymer surface with the gas flow. For this, it is necessary to take into account the additional heat flow due to the burning of the oxidizer, therefore:

$$q_{\Sigma} = q_s + G_o \Delta Q_{comb},$$

where G_o – mass flow of the oxidant per unit area, ΔQ_{comb} – heat of combustion of the polymer. The oxidant flow to the polymer surface due to diffusion is equal to

$$G_0 = \beta(C_{oo} - C_{ow}),$$

where β – mass transfer coefficient, C_o – oxidant concentration. Heat flow according to the Newton-Richmann law:

$$q_s = (\alpha / c_p)(I_{oo} - I_w),$$

where α – heat exchange coefficient, I – enthalpy. If it is supposed that $C_{ow} = 0$, and taking into account the principle of analogy between heat and mass transfer there is $\beta = \alpha / c_p$, then (4.13) it is possible to write

$$G_s = \frac{q_w}{H} \left(1 + \frac{C_{oo} \Delta Q_{comb}}{I_{oo} - I_w} \right). \quad (4.14)$$

ACKNOWLEDGEMENTS

The work was carried out within the framework of the project "Development of theoretical foundations for the creation of ultralight launch vehicles from polymeric materials", funded by the European Union's external assistance instrument under the European Union's Framework Programme for Research and Innovation Horizon 2020 (contract PH/12-2023).

CONFLICT OF INTEREST

The authors declare that they have no conflict of interest in relation to this research, whether financial, personal, authorship or otherwise, that could affect the research and its results presented in this paper.

REFERENCES

1. Kumar, S., Panda, A. K., Singh, R. K. (2011). A review on tertiary recycling of high-density polyethylene to fuel. Resources, Conservation and Recycling, 55 (11), 893–910. doi: <https://doi.org/10.1016/j.resconrec.2011.05.005>

2. Kumar Jha, K., Kannan, T. T. M. (2021). Recycling of plastic waste into fuel by pyrolysis – a review. *Materials Today: Proceedings*, 37, 3718–3720. doi: <https://doi.org/10.1016/j.matpr.2020.10.181>
3. Al-Salem, S. M., Chandrasekaran, S. R., Dutta, A., Sharma, B. K. (2021). Study of the fuel properties of extracted oils obtained from low and linear low density polyethylene pyrolysis. *Fuel*, 304, 121396. doi: <https://doi.org/10.1016/j.fuel.2021.121396>
4. Ito, S., Kamps, L., Nagata, H. (2021). Fuel Regression Characteristics in Hybrid Rockets Using Nitrous Oxide/High-Density Polyethylene. *Journal of Propulsion and Power*, 37 (2), 342–348. doi: <https://doi.org/10.2514/1.b37875>
5. Quero Granado, E., Hijlkema, J., Lestrade, J.-Y., Anthoine, J. (2021). Development and Validation of a 1.5-D Combustion Chamber Model for a Hybrid Rocket Engine Applied to a Cylindrical HDPE Chamber. *AIAA Propulsion and Energy 2021 Forum*, 3495. doi: <https://doi.org/10.2514/6.2021-3495>
6. Kositsyna, O. S., Dron, M. M., Yemets, V. V. (2020). The environmental impact assessment of emission from space launches: The promising propellants components selection. *Journal of Chemistry and Technologies*, 28 (2), 186–193. doi: <https://doi.org/10.15421/082020>
7. Yun, Y., Huh, J., Kim, Y., Heo, S., Kim, H., Kwon, S. (2021). Scale-Up Validation of Hydrogen Peroxide/High-Density Polyethylene Hybrid Rocket with Multiport Solid Fuel. *Journal of Spacecraft and Rockets*, 58 (2), 552–565. doi: <https://doi.org/10.2514/1.a34707>
8. Yemets, V., Dron, M., Dreus, A., Yemets, M., Pashkov, A. (2021). Heat flow in the gasification chamber of the polymer propelled autophage launch vehicle. *Proceedings of the 72nd International Astronautical Congress*. Dubai.
9. Kryzhanovskii, V. K., Burlov, V. V., Panimatchenko, A. D., Kryzhanovskaia, Iu. V. (2005). *Tekhnicheskie svoistva polimernykh materialov*. Saint-Petersburg: Professia, 248.
10. Spalding, M. A., Chatterjee, A. M. (Eds.) (2017). *Handbook of industrial polyethylene and technology: definitive guide to manufacturing, properties, processing, application and markets*. Hoboken: John Wiley & Sons, 1333. doi: <https://doi.org/10.1002/9781119159797>
11. Khattar, N., Jagriti, Ahlawat, V., Sharma, P., Berar, U., Diwan, P. K. (2023). Optimization of compression parameters of UHMWPE through thermal stability. *Materials Chemistry and Physics*, 307, 128220. doi: <https://doi.org/10.1016/j.matchemphys.2023.128220>
12. Balobanov, V., Verho, T., Heino, V., Ronkainen, H., Pelto, J. (2021). Micromechanical performance of high-density polyethylene: Experimental and modeling approaches for HDPE and its alumina-nanocomposites. *Polymer Testing*, 93, 106936. doi: <https://doi.org/10.1016/j.polymertesting.2020.106936>
13. Polietilen nizkogo davleniia: Nauchno-tekhnicheskie osnovy promyshlennogo sinteza (1980). Leningrad: Khimiia, 240.
14. Rechyskiy, O. N., Reshnova, S. F. (2018). *Khimiia vysokomolekuliarnykh spolk v skhemakh*. Kherson: Vyshemyrskiy V. S., 462.
15. Wypych, G. (2016). Copyright. *Handbook of Polymers*. Toronto: ChemTecPublishing, 706. doi: <https://doi.org/10.1016/B978-1-895198-92-8.50002-1>

16. Hassan Awad, A., El Gamasy, R., Abd El Wahab, A., Hazem Abdellatif, M. (2019). Mechanical and Physical Properties of PP and HDPE. *Engineering Science*, 4 (2), 34–42. doi: <https://doi.org/10.11648/j.es.20190402.12>
17. Wypych, G. (2016). Copyright. *Handbook of Polymers*. Toronto: ChemTecPublishing, 706. doi: <https://doi.org/10.1016/B978-1-895198-92-8.50002-1>
18. Dixit, D., Pal, R., Kapoor, G., Stabenau, M. (2016). Dixit D. 6 – Lightweight composite materials processing. *Woodhead Publishing Series in Composites Science and Engineering, Lightweight Ballistic Composites*. Woodhead Publishing, 157–216. doi: <https://doi.org/10.1016/b978-0-08-100406-7.00006-4>
19. Hartmann, B., Lee, G. F., Cole, R. F. (1986). Tensile yield in polyethylene. *Polymer Engineering & Science*, 26 (8), 554–559. doi: <https://doi.org/10.1002/pen.760260806>
20. Hartmann, B., Lee, G. F., Wong, W. (1987). Tensile yield in polypropylene. *Polymer Engineering & Science*, 27 (11), 823–828. doi: <https://doi.org/10.1002/pen.760271109>
21. DSTU B V.2.7-143:2007. Truby zi strukturovanoho polietylenu dlia merezh kholodnoho, hariachoho vodopostachannia ta opalennia. *Tekhnichni umovy (EN ISO 15875-2:2003, MOD) (2008)*. Derzhavne pidpriemstvo «Tsentr-SEPROteplomerezh».
22. Amjadi, M., Fatemi, A. (2020). Creep and fatigue behaviors of High-Density Polyethylene (HDPE): Effects of temperature, mean stress, frequency, and processing technique. *International Journal of Fatigue*, 141, 105871. doi: <https://doi.org/10.1016/j.ijfatigue.2020.105871>
23. Menczel, J. D., Prime, R. B. (2009). *Thermal analysis of polymers: fundamentals and applications*. John Wiley & Sons. doi: <https://doi.org/10.1002/9780470423837>
24. Waheedullah, S. G., Siakeng, R., Rasheed, M., Saba, N., Jawaid, M. (2018). The role of advanced polymer materials in aerospace. *Sustainable Composites for Aerospace Applications*. Woodhead Publishing, 19–34. doi: <https://doi.org/10.1016/b978-0-08-102131-6.00002-5>
25. Callister, W. D., Rethwisch, D. G. (2020). *Characteristics, applications, and processing of polymers in materials science and engineering*. Wiley, 523–576.
26. Bartenev, G. M., Zuyev, Y. S. (1968). *Strength and failure of visco-elastic materials*. Pergamon press, 419. doi: <https://doi.org/10.1016/c2013-0-05219-x>
27. Bucknall, C. B. (1978). *Fracture and failure of multiphase polymers and polymer composites*. Failure in Polymers. *Advances in Polymer Science*. Vol. 27. Springer, Berlin, Heidelberg. doi: https://doi.org/10.1007/3-540-08829-6_3
28. Shuvalov, V. A., Tokmak, N. A., Reznichenko, N. P. (2015). Degradation of spacecraft polymer films on long exposure to atomic oxygen flows and vacuum ultraviolet radiation. *Kosmocna Nauka & Tehnologija*, 21 (5 (96)), 57–68. doi: <https://doi.org/10.15407/knit2015.05.057>
29. Kuznetsov, G. V. (1999). Mekhanizm vysokotemperaturnogo razrusheniia termoplastichnykh polimernykh materialov v usloviakh intensivnogo teplovogo i gazodinamicheskogo vozdeistviia. *TVT*, 37 (1), 117–121.
30. Laganelli, A. L., Zempel, R. E. (1970). Observations of surface ablation patterns in subliming materials. *AIAA Journal*, 8 (9), 1709–1711. doi: <https://doi.org/10.2514/3.5973>

31. Celina, M., Linde, E., Brunson, D., Quintana, A., Giron, N. (2019). Overview of accelerated aging and polymer degradation kinetics for combined radiation-thermal environments. *Polymer Degradation and Stability*, 166, 353–378. doi: <https://doi.org/10.1016/j.polymdegrad-stab.2019.06.007>
32. Witkowski, A., Stec, A. A., Hull, T. R. (2016). Thermal Decomposition of Polymeric Materials. *SFPE Handbook of Fire Protection Engineering*. New York: Springer, 167–254. doi: https://doi.org/10.1007/978-1-4939-2565-0_7
33. Polezhaev, Iu. V., Iurevich, F. B. (1976). *Teplovaia zashchita*. Moscow: «Energia», 392.
34. Dreus, A., Yemets, V., Dron, M., Yemets, M., Golubek, A. (2021). A simulation of the thermal environment of a plastic body of a new type of launch vehicle at the atmospheric phase of the trajectory. *Aircraft Engineering and Aerospace Technology*, 94 (4), 505–514. doi: <https://doi.org/10.1108/aeat-04-2021-0100>
35. Dron, M., Dreus, A., Golubek, A., Abramovsky, Y. Ev. (2018). Investigation of aerodynamic heating of space debris object at reentry to earth atmosphere. *Proc. 69th International Conference IAC-18, A6.2*. Bremen.
36. Leslie, F. W., Justus, C. G. (2008). The NASA MSFC Earth global reference atmospheric model-2007 Version (No. NASA/TM--2008-215581).
37. Krasnov, N. F. (1976). *Aerodinamika. Ch. II – Metodi aerodinamicheskogo rascheta*. Moscow: Vysshaya shkola, 368.
38. Fahy, W. P., Chang, A., Wu, H., Koo, J. H. (2021). Recent Developments of Ablative Thermal Protection Systems for Atmospheric Entry. *AIAA Scitech 2021 Forum*, 1474. doi: <https://doi.org/10.2514/6.2021-1474>

INNOVATIVE MATERIALS AND TECHNOLOGIES IN FUNCTIONAL ENGINEERING SYSTEMS

Sergiy Luniov, Yuliia Udovytska, Vitalii Kashytskyi, Mykola Khvyshchun, Yurii Koval,
Sergiy Moroz, Maryna Zhaldak, Olena Mokrousova, Anna Bondarieva, Nina Merezhko,
Taras Karavaiev, Halyna Mykhailova, Valentyna Halushko, Sergiy Kolesnichenko,
Kostiantyn Polianskyi, Oleksandr Slipych, Denis Uvarov, Oksana Kliui, Mykola Dron',
Andrii Dreus, Ludmila Dubovik, Olena Kositsyna

Collective monograph

Technical editor I. Prudius
Desktop publishing T. Serhiienko
Cover photo Copyright © 2023 Canva

TECHNOLOGY CENTER PC
Published in December 2023
Enlisting the subject of publishing No. 4452 – 10.12.2012
Address: Shatylova dacha str., 4, Kharkiv, Ukraine, 61165
